Fall 2017

A computational investigation of patient factors contributing to contact stress abnormalities in the dysplastic hip joint

Holly Dominique Thomas
University of Iowa

A COMPUTATIONAL INVESTIGATION OF PATIENT FACTORS CONTRIBUTING TO CONTACT STRESS ABNORMALITIES IN THE DYSPLASTIC HIP JOINT

by

Holly Dominique Thomas

A thesis submitted in partial fulfillment
of the requirements for the Master of Science
degree in Biomedical Engineering in the
Graduate College of
The University of Iowa

December 2017

Thesis Supervisor: Assistant Professor Jessica E. Goetz

Graduate College
The University of Iowa
Iowa City, Iowa

CERTIFICATE OF APPROVAL

_____

MASTER'S THESIS

_____

This is to certify that the Master's thesis of

Holly Dominique Thomas

has been approved by the Examining Committee for
the thesis requirement for the Master of Science degree
in Biomedical Engineering at the December 2017 graduation.

Thesis Committee: _____
Jessica E. Goetz, Thesis Supervisor

_____
Donald D. Anderson

_____
Nicole M. Grosland

_____
David G. Wilder

_____
Michael C. Willey

ACKNOWLEDGEMENTS

First and foremost, I would like to thank my research advisor, Dr. Jessica Goetz, for her continued guidance and support that has been crucial to my development as a researcher. Furthermore, I would like to thank her and Dr. Don Anderson for being open to taking me on as a transfer graduate student. I would like to thank the other members of my thesis committee, Drs. Don Anderson, Nicole Grosland, David Wilder, and Michael Willey, for their guidance and perspectives on this work. I would like to thank the other students and faculty members in the Orthopedic Biomechanics Laboratory, with a special thanks to Kevin Dibbern and Dr. Andrew Kern for their advice and guidance on this project. Funding for this work was provided by the NIH NIAMS Program Grant P50 AR055533 and an OREF Career Development Grant. Additionally, I would like to thank Dr. Jodi Prosise, my close friend and mentor, for her constant support and guidance in my academic and life endeavors. Finally, I would like to thank my family, fiancé, and friends for their love and support during this journey and always.

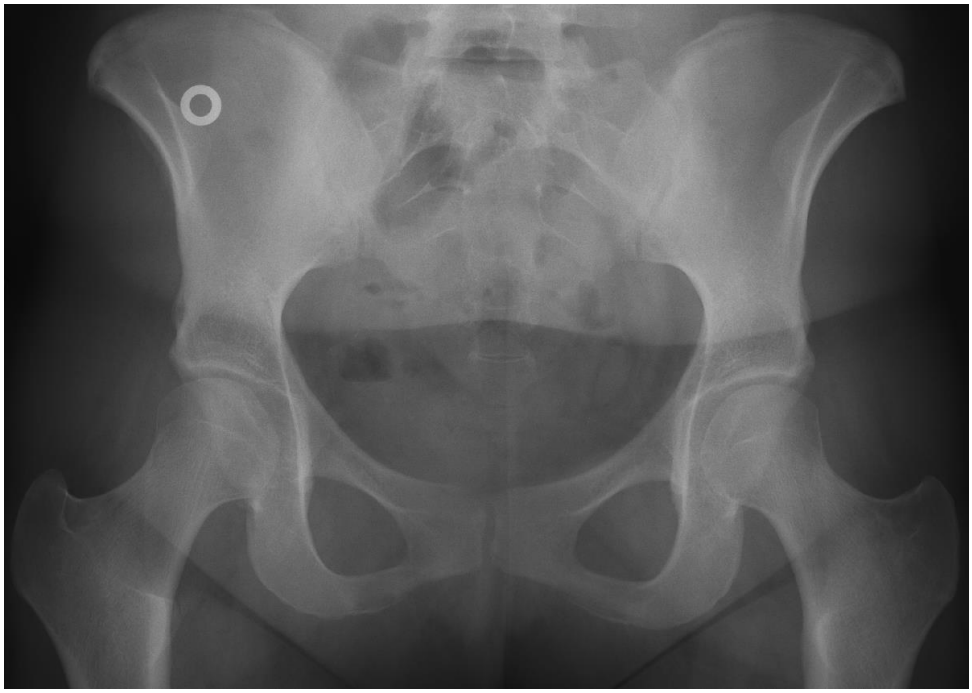

ABSTRACT

Acetabular dysplasia, a deformity characterized by the presence of a shallow acetabulum inadequately covering the femoral head, alters force transfer through a joint, causing early-onset hip pain and degeneration. Dysplasia is often treated surgically with a periacetabular osteotomy (PAO), which permits multiplanar acetabular reorientation to stabilize the joint and alleviate pain. PAO alters joint mechanics, including contact stress, which can be assessed via computational methods.

This work sought to enhance a discrete element analysis (DEA) model for assessment of the dysplastic hip. The primary focus was on understanding how the gait parameters used to load a DEA model affect the computed contact stress. Several additional studies focused on understanding specific anatomic and demographic factors contributing to the contact stress evaluation were also performed.

Implementation of a dysplastic gait pattern to load the DEA models resulted in more cases with improved contact stress and clinical measures after PAO, which concurred with clinical findings. Patient demographics and acetabular and femoral geometry all affected the computed contact stress distributions, emphasizing the importance of proper cohort categorization prior to interpretation of DEA-calculated contact stress. These results indicate that accurate modeling of the particular deformity in this cohort likely requires evaluation of both functional and anatomic differences.

These studies improve the ability to realistically model and characterize dysplastic hip contact mechanics. DEA is a valuable tool for assessing contact stress in dysplastic joints, which has the potential to improve patient outcomes by guiding clinicians in non-operative treatment, pre-operative PAO planning, and evaluating intraoperative success.

PUBLIC ABSTRACT

Hip dysplasia is a deformity of the pelvic bone that results in a mechanically unstable hip joint. This can be painful and lead to development of arthritis at a young age. Treatment may involve surgery to change how the hip socket is positioned and oriented in the pelvis to improve hip stability and decrease the damaging, painful stresses on the hip socket. Success of this realignment is largely determined by the ability of the surgeon to determine hip function in 3D from 2D X-ray images that can be obtained during surgery. Computational modeling offers the opportunity for analysis of joint mechanical function in 3D, which provides a much more realistic assessment of the mechanical changes after surgery.

The purpose of this work was to develop the best method for using a specific type of computational modeling to evaluate changes in the joint mechanics of dysplastic hips before and after corrective surgery. This involved an investigation of model loading parameters and patient factors that contribute to the computed contact stress. As anticipated, loading the computational models with a gait pattern that is more typical of patients with hip dysplasia produced mechanical changes that agreed well with clinical assumptions. Patient age, weight, and hip joint geometry all had an effect on the joint mechanics computed for the models, indicating the importance of properly categorizing patients based on this information before attempting to interpret mechanics data.

These studies have improved the ability to perform realistic computational modeling and interpret the resulting data for patients with hip dysplasia. This technique has the potential to improve patient selection for surgery and pre-operative planning for optimum realignment, which subsequently can improve clinical outcomes.

TABLE OF CONTENTS

LIST OF FIGURES

CHAPTER 1: INTRODUCTION

1.1 The Hip Joint

1.1.1 Normal Anatomy & Joint Loading

The hip joint is a ball-and-socket joint formed by the articulation between the concave acetabulum and the convex femoral head that provides load-bearing support for the human body (Figure 1). The articulating surfaces of the acetabulum and femoral head are covered by hyaline cartilage [1]. The labrum, a wedge-shaped cartilage ring surrounding the outer edge of the acetabulum, deepens the acetabular socket and increases the intra-articular fluid pressurization, thereby limiting the stresses on the articular cartilage of the joint [2-6] (Figure 2).

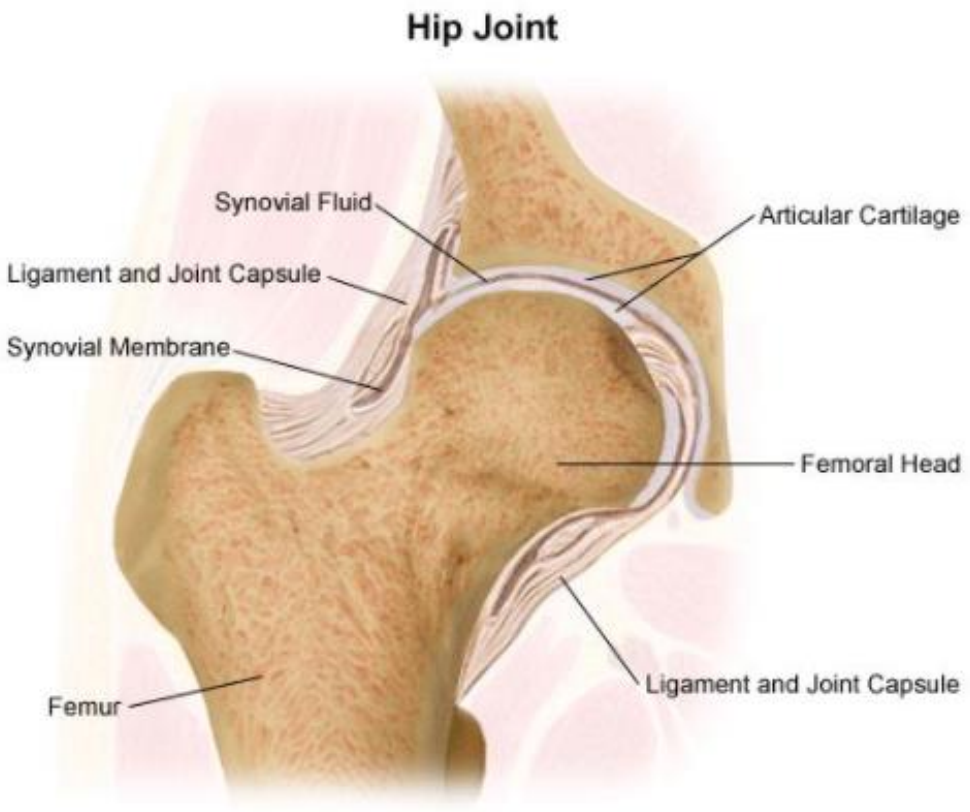

Figure 1. Anatomy of the normal hip joint [7].

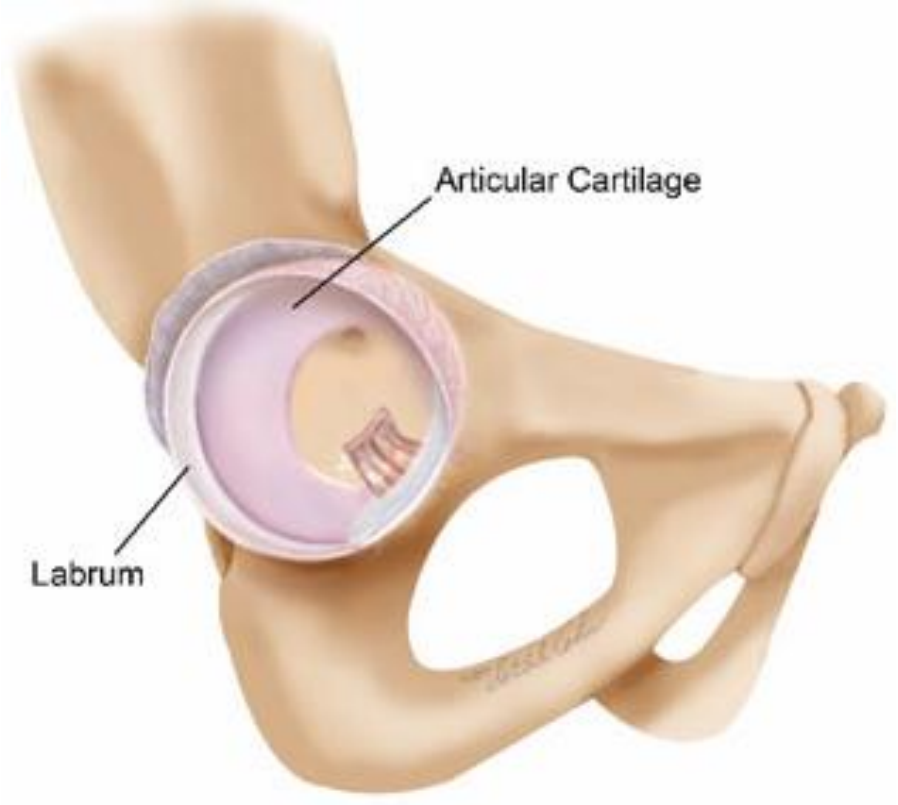

Figure 2. The fibrocartilaginous labrum surrounds the periphery of the acetabulum to provide additional support and stability [8].

The structure of the hip joint is designed to serve as a support system for the head, arms, and trunk of the human body. Its arrangement permits flexion/extension, abduction/adduction, and internal/external rotation of the femur relative to the pelvis in the sagittal, frontal, and transverse planes, respectively. Normal range of motion for the hip joint is approximately 90-125° of flexion and 10-30° of extension, depending on flexion or extension of the knee. Hip range of motion also typically includes 45-50° of abduction and 20-30° of adduction relative to a standing position [1]. When the hip is flexed, up to 70° of internal rotation and 90° of external rotation can be achieved. However, when the joint is extended, tension in the soft tissues limits the degree of available internal and external rotation considerably [9].

The forces through the hip joint can vary significantly depending on the activity being performed. In a normal walking gait cycle, anterior and medial forces equivalent to an individual's body weight, and superior forces of nearly four times body weight, are achieved shortly after heel-strike, concurrent with toe-off of the contralateral limb [10]. Stair climbing has been shown to result in peak forces of 2.5 times body weight [11], and during stumbling, peak forces can reach nearly eight times body weight [12]. The geometry of the acetabulum and its articular cartilage is designed to support such large forces by optimizing the joint loading distribution [13, 14]. Additionally, intra-articular fluid pressurization [4] increases joint lubrication and limits the cartilage stresses that otherwise could result in frictional cartilage wear. However, without proper support from a stable joint, cartilage degeneration can occur [15, 16].

1.1.2 Acetabular Dysplasia & Joint Loading Alterations

Hip dysplasia is a deformity characterized by a shallow acetabulum inadequately covering the femoral head, flattening of the femoral head, and possible shortening of the femoral neck [17-20] (Figure 3). For dysplastic hips to withstand normal walking loading, the abductor muscles must increase their force generation along a more vertically oriented line of action, which leads to increased hip contact forces directed near the edge of the acetabular socket [21]. These increased forces combined with a decreased weight-bearing surface area results in increased cartilage contact stresses that, with prolonged exposure, have been shown to have detrimental effects on the hip joint. Dysplastic hips have been found to have 26% less contact area and 23% greater contact pressures than normal hips [22], and much more of this force is loaded along the acetabular rim in dysplasia patients

[23]. Such altered mechanics can result in further joint damage, including labrum hypertrophy and tears, articular cartilage degeneration, and early osteoarthritis development [24-26]. In one study, nearly 50% of total hip arthroplasty patients under 50 years of age had radiographic evidence of hip dysplasia, further indicating the need for early dysplasia diagnosis and treatment [27].

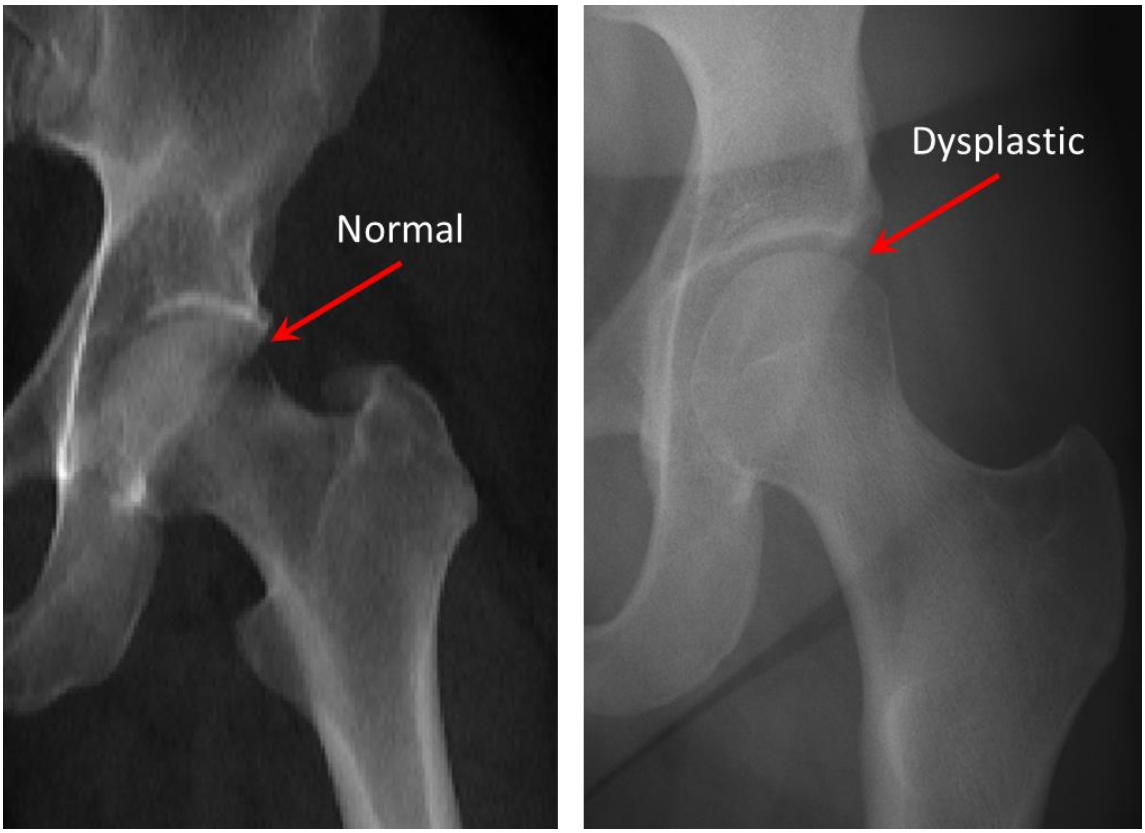

Figure 3. (Left) Orthographic projection of a normal hip joint generated from CT images. (Right) X-ray image of a dysplastic hip joint with a shallow acetabulum, inadequate coverage of the femoral head, and femoral head flattening.

If the diagnosis of hip dysplasia is made during infancy, where it is known as developmental dysplasia of the hip (DDH), treatments such as the Pavlik harness and osteotomies can be utilized to stabilize the hip joint during its development [17, 22, 23]. Mostert *et al.* showed that the Pavlik harness, which is a brace that holds the hips and

knees up with the legs apart to keep the hip joint aligned and secure during development, was 97% effective at restoring normal hip development in stable dysplastic hips, but its efficacy in more severe dysplasia cases dropped to 50% due to difficulty in maintaining normal femoral head position [28]. Another study found the survival rate of Salter innominate osteotomies (a surgical technique in which a complete osteotomy of the ilium is performed to permit acetabulum reorientation, and a bone graft is used to maintain the reorientation) to be 90% after 35.3 years [29]. These results indicate these treatment techniques have good long-term results when performed early enough to restore the normal configuration of the hip joint. However, in many cases, the deformity of the acetabulum in infancy is subtle, which delays diagnosis until after skeletal maturity [30]. This has resulted in a young adult patient population with radiographic acetabular dysplasia, with the prevalence varying from 3.6% to 12.8% [31, 32].

Once a patient comes into the clinic as a result of chronic hip pain, dysplasia is diagnosed largely based on radiographic measurements, the most common of which is Wiberg's lateral center edge angle (LCEA) [33]. Wiberg defined the LCEA on a supine AP radiograph as the angle between a vertical line through the center of the femoral head and a line from the center of the femoral head to the lateral edge of the acetabular sourcil (Figure 4). A LCEA of less than 20° typically defines a dysplastic hip, with smaller angles indicating less coverage of the femoral head and greater deformity. LCEAs of 20°-25° are considered borderline dysplasia, and angles greater than 25° are viewed as normal [34, 35].

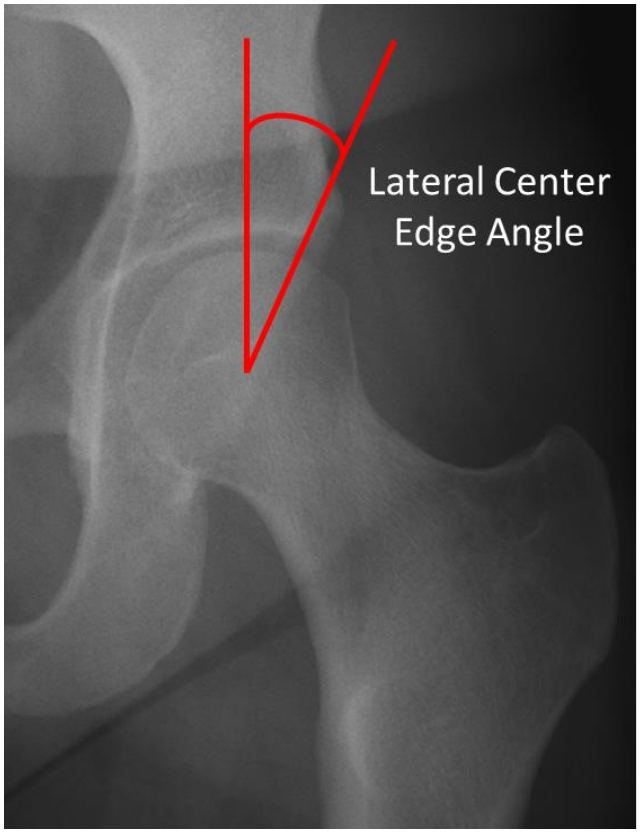

Figure 4. X-ray image of a dysplastic hip illustrating the lateral center edge angle measurement as defined by Wiberg [33]. Note the edge of the sourcil in this case is not the lateral edge of the bone.

In addition to the LCEA, several other radiographic measurements can be made to describe the severity of dysplasia. The anterior center edge angle of Lequesne is measured on a false lateral view as the angle between a vertical line through the center of the femoral head and a line from the center of the femoral head to the anterior edge of the acetabular sourcil [36]. The Tönnis angle, or acetabular index, defines the weight-bearing surface angle as the angle between a horizontal line and a line from the medial to lateral edges of the acetabular sourcil [37]. The extrusion index defines the femoral head undercoverage as a percentage of the total horizontal femoral head diameter [38]. These radiographic angles are all used to quantify some aspect of acetabular coverage, but the

accuracy of these measures is largely variable depending on the anatomic landmarks selected, quality of the x-ray, and expertise of the surgeon making the measurement.

The categorical measures of the crossover sign and posterior wall sign are utilized to describe acetabular version. The crossover sign is a positive/negative discriminator in which positive means that the anterior wall crosses over the posterior wall on an AP radiograph, indicating acetabular retroversion [39]. Similarly, a positive posterior wall sign means that the outline of the posterior acetabular rim lies medial of the hip center, indicating a retroverted acetabulum [39]. However, while these measures differentiate between an anteverted and a retroverted acetabulum, they do not describe the severity of version deformities. A quantitative measurement that accurately describes the functional acetabular environment would provide a more consistent methodology for assessing the presence and severity of dysplasia.

To reduce joint pain and compensate for the joint instability caused by a dysplastic deformity, patients often alter their gait pattern. Numerous studies have investigated the differences in gait between dysplastic patients and normal individuals and concluded that dysplasia changes hip kinematics and kinetics during gait [40-46]. However, the specific changes described have been somewhat contradictory and based on patient age, severity of the deformity, and measurement technique utilized (e.g. motion capture, musculoskeletal models). For instance, numerous studies found that dysplasia patients have lower peak hip extension during stance phase of gait [40, 44], but Pedersen *et al.* showed a lack of a significant difference in extension [42], indicating a lack of consensus in previous findings. While a variety of studies have concluded that dysplasia changes hip kinematics and kinetics during gait, only two of these studies investigated

differences in the hip joint forces in dysplastic patients compared to normal individuals. Skalshoi *et al.* found that dysplastic patients had greater superior and anterior forces near toe-off [45], whereas Harris *et al.* described greater medial forces as the major difference from healthy controls [46]. These alterations indicate that dysplasia patients generate greater push-off forces and prevent femoral subluxation by increasing medially directed forces. The common conclusion in all of these studies was that patients with hip dysplasia adjust their movement patterns at the hip, which is likely done as a strategy to decrease pain or feelings of instability.

1.1.3 Contact Stress Contributes to Osteoarthritis Development

Mavčič, *et al.* used a 3D mathematical model to determine contact stress in the hip during one-legged stance and found that dysplastic hips (n = 58) were exposed to higher peak and cumulative contact stresses than normal hips (n = 48), and the cumulative contact stress measure was superior to the LCEA for predicting osteoarthritis development [26]. A finite element study in dysplastic and impinging hip joints found that locations of high von Mises stresses were associated with areas of observable damage to the acetabular cartilage and labrum [47]. This is not surprising given that the decreased contact area and joint instability in dysplasia subjects the hip joint to elevated contact stresses, which have been linked with an increased risk of osteoarthritis development [48, 49]. A cross-sectional study of 2,232 women and 1,336 men randomly selected for a longitudinal, general health survey found that hip dysplasia was significantly associated with hip osteoarthritis [32].

Osteoarthritis describes cartilage loss and progression of joint degeneration. Patients with osteoarthritis often have severe functional limitations and joint inflammation, stiffness, and pain. Most often, it is the severity of these symptoms that leads a patient to seek surgical treatment. The younger patients (e.g. patients in their thirties) desire a surgical treatment that will provide them with a functional hip for many decades, whereas the older patients mostly want something that will alleviate their osteoarthritis pain. Osteoarthritis diagnoses make up ~70% of patients undergoing total hip arthroplasty (THA) [50]. And while 85% of older THA patients may still have a functioning hip replacement after 20 years [51], revisions are often necessary to address recurrent symptoms. However, the need for an invasive THA can potentially be postponed by correcting the mechanical joint environment to reduce damaging contact stress.

1.2 Periacetabular Osteotomy

Numerous surgical techniques have been utilized to treat hip dysplasia, all with the intent of increasing femoral head coverage with the goals of increasing stability through joint center medialization and decreasing contact stress and hip pain. Such techniques include innominate, double, and triple osteotomies [52-58]. In an innominate osteotomy, a full-thickness bone graft is removed from the anterior portion of the iliac crest and trimmed into a wedge shape. A complete osteotomy of the ilium permits forward, downward, and outward rotation of the acetabulum, and the wedge-shaped graft is inserted into the osteotomy site to maintain the new acetabular position [52] (Figure 5).

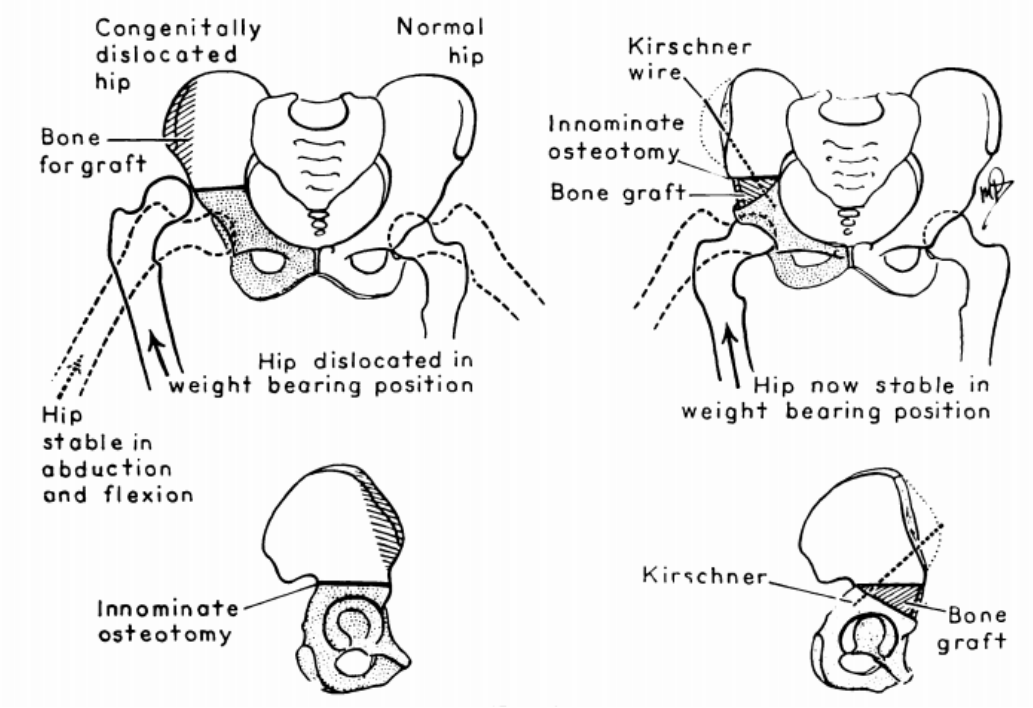

Figure 5. Illustration of an innominate osteotomy. A portion of the iliac crest is removed and trimmed into a wedge-shaped bone graft. The acetabulum and femur are rotated into a stable weight-bearing position, and the bone graft is positioned in the osteotomy site to maintain acetabular reorientation. Image taken from Salter [52].

In a double osteotomy, the innominate osteotomy is performed first and followed by an additional pubic osteotomy to increase acetabular rotation and femoral coverage [53]. The triple osteotomy further expands upon the double osteotomy; the ischium is osteotomized from a dorsal incision behind the hip joint, and then the patient is turned to permit medial and lateral incisions for the double osteotomy [56, 57]. However, such methodologies involve multiple incisions, complete osteotomy of the hemipelvis, and removal of a portion of the pelvis to maintain acetabular rotation, which is highly difficult due to muscle and ligament insertions, risk of vascular impairment to the acetabulum, and the resulting asymmetry of the pelvis [59, 60]. To circumvent such limitations, a somewhat newer approach to treating hip dysplasia in young adults was implemented by

the orthopaedic surgeon Reinhold Ganz, MD in 1984 [59]. His technique is also a triple osteotomy technique, now more commonly known as a periacetabular osteotomy (PAO). The surgery is accomplished through a single incision and does not require a bone graft, which simplifies the procedure and maintains the shape of the pelvis. These advantages have led to the PAO becoming the most common treatment for adult dysplasia. It involves an incomplete osteotomy of the ischium, a complete osteotomy of the pubis, and a two-component osteotomy of the ilium [59] (Figure 6).

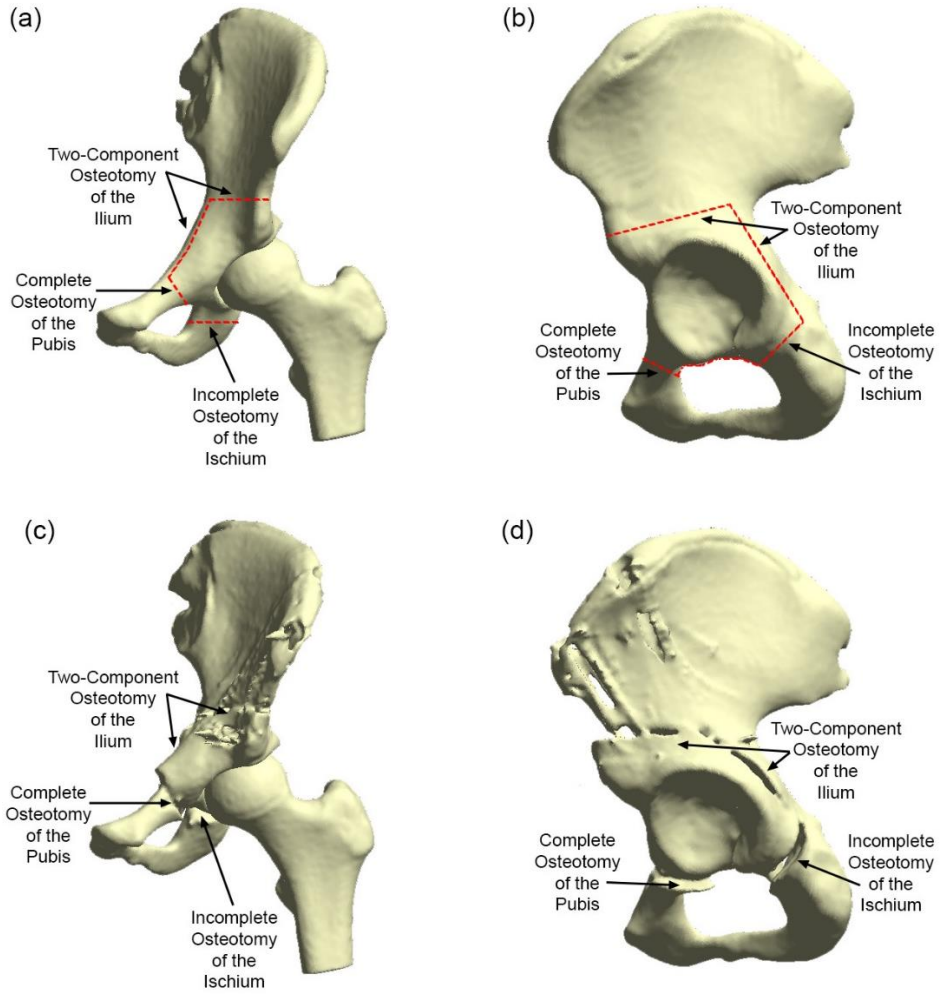

Figure 6. Illustration of a periacetabular osteotomy. Pre-operative coronal (a) and sagittal (b) pelvic views show the numerous osteotomies performed around the acetabulum to free it for corrective realignment. Post-operative coronal (c) and sagittal (d) images show the improved coverage of the femoral head following acetabular reorientation.

The advantages of the PAO procedure over previous techniques are numerous: (1) only one surgical incision is required; (2) the surgeon has the ability to reorient the acetabulum in all directions, including medial and lateral rotation; (3) blood supply to the acetabulum is preserved; (4) the posterior column of the hemipelvis remains intact, permitting immediate post-operative limb use without external fixation; and (5) the unaltered pelvic shape eliminates potential complications during future childbirth in female patients [59]. Studies on PAO patient outcomes have also indicated better clinical results over other osteotomy types in patients of adolescent or adult age. Salter and Dubos reported good or excellent results after an average of 5.5 years in 56.7% of patients who underwent innominate osteotomy between ages four and ten years [61]. In contrast, an investigation of adult patients who underwent PAO at an average age of 29.3 ± 11.6 years found survivorship of 60% (41 hips) in 58 patients (68 hips) after 20-year followup [62]. Haidar, *et al.* found that 8.1% of 37 hips developed avascular necrosis when treated with an innominate osteotomy [63], whereas Ganz *et al.* demonstrated no evidence of vascular impairment in a series of 75 hips that underwent PAO [59]. Radiographic severity of pre-existing osteoarthritis was found to progress in only 5% of 123 PAO cases after 4 years [64]. While the optimal treatment strategy likely varies based on patient age, dysplasia severity, and surgeon experience with the various techniques, these studies illustrate that the PAO procedure is an effective technique for adult dysplasia patients that minimizes the risk of impairing surrounding tissues and vascularization and limits osteoarthritis progression.

1.3 Periacetabular Osteotomy-Induced Changes in Joint Mechanics

As previously discussed, the objective of the PAO procedure is to improve the joint mechanics of the dysplastic hip and alleviate associated pain. Many previous studies have assessed these changes in joint mechanics after PAO via experimental techniques, mathematical models, and clinical outcome measures. Mechlenburg, *et al.* used a stereologic technique to systematically measure the projected acetabular margins on the femoral head to determine their contribution to the load-bearing acetabular area. They compared 6 dysplastic hips with spherical femoral heads to 6 healthy controls and showed that PAO increased the average contact area of the femoral head by nearly 50%, resulting in a post-operative contact area similar to that of normal hips [65]. However, they did not control for age between the cohorts (dysplastic: 33 (26-39) years; normal: 52 (27-77) years), which could significantly affect the size and shape of the load-bearing area. Additionally, the mean femoral head radius was 2.2 cm in both groups, and as the measurements were made solely on the femoral head geometry, they may not be accurately representing the differences in acetabular coverage between normal and dysplastic individuals. Iglic, *et al.* developed a mathematical model to estimate the stress on the articular joint surface based on the post-operative changes in weight-bearing surface area and center of hip joint rotation. With this model, they showed that improving lateral coverage of the femoral head decreased stress on the articular surface by 44%, and medializing the hip joint center of rotation decreased this stress by an additional 15% [66]. However, this mathematical model assumed that the femoral head can be represented by a sphere and the acetabulum can be represented by a spherical shell, both of which may not be accurate assumptions, especially in severe dysplastic deformations.

Moreover, only mediolateral changes in center of rotation were investigated, thereby neglecting any effects of anteroposterior and/or superoinferior movement.

Orthopaedic surgeons use a variety of patient-reported outcome measures to assess pain and functional outcomes following PAO. In a study of 25 patients, the Harris Hip Score (HHS), which is a metric of pain, function, presence of deformity, and range of motion, increased on average from 78.08 pre-operatively to 95.36 one year after PAO, indicating improved function, range of motion, and pain [67]. Another study of 87 hips found a decrease in WOMAC pain scores from 8.7 to 3 after an average of 4.9 years [68]. This combination of studies describes improved contact area, decreased stress, and improved outcomes after PAO, which agrees with the clinical assumption that PAO improves hip joint mechanics.

1.3.1 Finite Element Analysis

In addition to experimental techniques, mathematical models, and clinical outcome measures, computational modeling enables assessment of joint mechanics through stress analysis. Finite element analysis (FEA) is the computational technique most commonly utilized for stress analyses in orthopaedic biomechanics problems. FEA involves subdividing two-dimensional or three-dimensional geometry into smaller elements to create a mesh over the surface or within the volumetric geometry. Each individual element can be assigned material properties and boundary conditions that govern stiffness matrices. Complex differential equations are simultaneously solved for nodal force equilibrium [69].

The development of FEA has enabled calculation of internal stresses and strains in models of complex human anatomy [69]. Additionally, it has been utilized as a methodology for computing stresses between contacting joint bodies. FEA modeling has been a substantial area of computational research; a Pubmed search on FEA for biomechanics produces over 2,000 results. Furthermore, the large majority of FEA biomechanics studies have been conducted in the hip joint, with a similar Pubmed search finding more than 1,100 articles on FEA in the hip joint, which includes both native mechanics and altered mechanics due to deformity or arthroplasty. Such studies have greatly improved the general knowledge of native hip joint mechanics and the potential problems arising after joint modification or replacement.

While FEA computational models have been beneficial in understanding joint mechanics, there are numerous limitations to their use in general and for studies of hip dysplasia in particular. FEA modeling is a very time-consuming, labor-intensive process, especially with regard to anatomic modeling. FEA requires the geometry to be discretized completely, making the mesh generation process for an irregular bony structure highly complex. Furthermore, problems can arise with computational convergence, leading to a time-consuming iterative process of mesh refinement until a converged computational solution is reached. As a result, a wide variety of simplifications of the geometry and material properties are often implemented. These may include: modeling cortical and cancellous bone as a homogenous structure; assuming bones to be rigid structures rather than deformable bodies; assuming cartilage to be isotropic, hyperelastic, and incompressible rather than biphasic and poroelastic; and overly smoothed, spherical cartilage surfaces with constant thickness [70, 71]. However, such simplifications to the

hip joint geometry have been shown to greatly affect the quality of the computed solution. Anderson, *et al.* showed that models utilizing spherical hip joint geometry and smoothed articular cartilage surfaces underestimated peak and average contact pressures by 50% and 25%, and the assumption of rigid bones resulted in higher calculated pressures than the use of deformable bones [70].

Even after an accurate mesh has been generated, the computation time to reach a FEA solution can take hours or even days [48, 72]. Such mesh and computation complexity has limited most FEA studies to small numbers of patients [73, 74]. For conditions such as hip dysplasia, where the deformity type and severity can vary greatly, obtaining an accurate understanding of the joint mechanics requires larger samples sizes that include multiple patients with similar deformities. Thus, a computational modeling technique that is free from extreme computational complexity and permits accurate stress analysis of larger sample sizes would be much better suited for dysplasia cohorts.

1.3.2 Discrete Element Analysis

Discrete element analysis (DEA) is an alternative computational technique with greatly simplified computational complexity compared to FEA. DEA, also known as a rigid body spring model, represents contacting surfaces as rigid bodies separated by a bed of compressive springs [75] (Figure 7). When a load or displacement is applied to one or all of the bodies in the model, the resulting spring deformation is utilized to solve for the spring forces and the contact stresses between the bodies. The contact stress calculations can be performed using a variety of computational techniques, including the minimum energy principle [75, 76] and a Newton-Raphson iterative solver [72, 77].

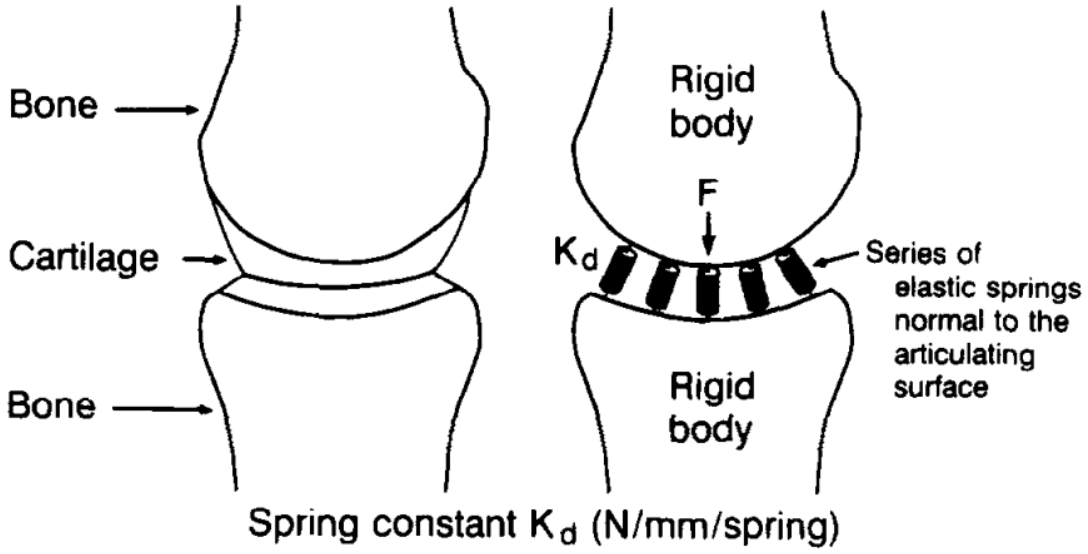

Figure 7. Conceptual diagram of rigid body spring modeling. Cartilage surfaces are modeled as beds of elastic, compressive springs bonded to underlying rigid bony surfaces. When a load or displacement is applied, the spring deformation permits calculation of the stress between the bodies. Image taken from Schuind *et al.* [75].

Even though it is a simplified modeling strategy, DEA has been shown to correlate well with FEA results, indicating that it produces accurate stress calculations. Li, *et al.* compared DEA predictions in the ankle to other numerical and computational techniques and found that DEA predicted only 5% higher peak contact stresses [78]. Another study in the ankle illustrated that DEA-computed maximum contact stresses were within 0.85±0.64 MPa of FEA-computed stresses and within 19% of experimentally measured stresses [79]. A direct comparison of FEA and DEA in a cadaveric hip showed that DEA predicted slightly higher peak (9.8-13.6 MPa) and average (3.0-3.7 MPa) contact stresses than FEA (6.2-9.8 and 2.0-2.5 MPa, respectively) and but only 3.7-9.7% lower contact areas than FEA [72].

There are however several limitations of utilizing DEA for contact stress computations in articular joints. DEA assumes that one of the contacting surfaces does not move relative to the other during load application. Additionally, there is no deformation of the contacting surfaces due to load application as there would be in FEA. Due to DEA's use of compressive springs rather than continuum elements to model cartilage, cartilage thickness variations must be represented implicitly as variations in the spring lengths and deformations [80]. Similarly, DEA does not provide an explicit method for implementing muscle forces, meaning that all aspects of loading (i.e. joint reaction forces, muscle forces, etc.) must be incorporated as a single load application. Muscle attachments can be represented as additional springs acting along the muscle line of action, and the spring stiffness is selected based on the material properties of the muscle, but no muscle force can be generated separately from other loading forces. It is highly difficult to model poroelasticity and other complex material properties with DEA, which typically causes cartilage to be modeled as an isotropic linear elastic surface. Perhaps the strongest limitation is that DEA is only able to provide information on the contact stress distributions and the associated reaction forces; it cannot predict internal tissue stresses or strains [81].

Despite these limitations, modeling with DEA can be very advantageous. DEA's computational time is greatly reduced from FEA due to the absence of a complex mesh generation procedure that is subject to refinement and convergence complications. DEA's reduced simulation complexity eliminates the need to solve complex differential equations. A direction comparison between DEA and FEA models of the hip joint has previously illustrated that DEA solutions could be achieved in ~7 seconds on a standard

computer, compared to ~65 minutes on a computing cluster for FEA [72]. This is independent of the increased time required for mesh development for FEA that is unnecessary in DEA. The reduced complexity and computational time of DEA permits evaluation of much larger patient cohorts than previous FEA studies, which is crucial for establishing direct relationships between changes in contact stress and patient outcomes.

While radiographic measures have been the "gold standard" for assessing dysplasia, measurement accuracy varies depending on the exact anatomic landmarks utilized, patient orientation during imaging, and experience of the surgeon performing the measurement. An accurate prediction of contact stress distributions within the joint has the potential to provide a more rigorous evaluation of the whole joint environment, which may be able to explain why some hip dysplasia patients have historically had less than ideal outcomes after a PAO. Future assessment of a large cohort of dysplasia patients with a variety of deformity types (e.g. lateral coverage deficiency, acetabular version, etc.) using DEA will permit development of meaningful correlations between changes in contact stress and patient outcomes. With this information, pre-operative surgical planning can be improved to include contact stress optimization at the hip joint, which may lead to improved clinical outcomes.

1.3.3 Previous Work & Rationale

To evaluate the accuracy of DEA for contact stress assessment in the hip joint, a validation study was conducted by members of the Orthopaedic Biomechanics Laboratory at the University of Iowa [77]. This study investigated the accuracy of a custom DEA methodology that had previously been validated in the ankle [79] for use in

the hip. In that work, two intact cadaveric hip specimens were subjected to static loading experiments in a variety of positions representing instances within a walking gait cycle. Contact stresses were physically measured with Tekscan sensors [82] and compared on a point-by-point basis with DEA-calculated stresses. Peak contact stresses computed using DEA were within an average of 0.5 MPa (range: 0.2-0.8 MPa) of the Tekscan stresses [77]. Correlations between the DEA-computed contact stress distributions and Tekscan-measured distributions ranged from 0.93-0.99, indicating excellent agreement between the two techniques over the entire contact area [77]. Those results indicated that this custom DEA methodology can accurately predict contact stresses in the hip joint.

Following validation of the custom DEA methodology, an initial series of nineteen patients was retrospectively selected for DEA assessment from a larger cohort of patients who underwent PAO by a single orthopaedic surgeon (Todd McKinley MD) at the University of Iowa Hospitals & Clinics between 2007 and 2009. Pre- and post-operative CT scans had been obtained for all patients, and the femoral, pelvic, and spinal geometry was segmented using a custom semi-automatic technique [83]. These patient-specific models were then smoothed and aligned to the coordinate system defined by Bergmann *et al.* [11]. The acetabular and femoral cartilage was approximated by a 1-mm uniform projection of the subchondral bone surfaces into the joint space and smoothed using a previously developed custom smoothing algorithm [84]. The resultant DEA models, consisting of bone and cartilage surfaces, were loaded using forces and rotations measured from instrumented total hip patients during a walking gait cycle. Applied loading data were scaled according to the individual patient's body weight [11]. Computation of the contact stress distributions was completed using the custom DEA

methodology, and pre- to post-operative changes in maximum contact stress were correlated with changes in VAS, WOMAC, and SF-36 patient-reported outcome scores. Changes in VAS pain scores significantly correlated with changes in maximum contact stress ($R^2 = 0.6024$, $p < 0.001$). Changes in SF-36 quality-of-life scores correlated well with changes in maximum contact stress ($R^2 = 0.5239$, $p = 0.012$), and changes in WOMAC functional scores correlated moderately with changes in maximum contact stress ($R^2 = 0.373$, $p = 0.046$) [85].

While the cadaveric validation work supported the use of DEA to assess changes in the dysplastic hip joint following PAO, there were several limitations to note in the application of the methodology to the PAO patients studied in the previous work. Those results illustrated poor agreement between contact mechanics and outcome scores [85]. Upon further analysis, it was noted that the gait data used to load the DEA models [11], while having high measurement reliability and frequent use in the field of orthopaedic research, may not be representative of dysplastic patient joint loading and could be altering the computed contact stress. It was thought that through improving the fidelity of the DEA modeling, a better understanding of the dysplastic joint environment could be obtained.

While the forces and rotations used to load the DEA models represent a valid gait pattern, the subjects in the Bergmann study were much older and slower than the typical PAO patient. Therefore, this pattern may not be representative of true dysplastic loading and could be unintentionally altering the computed contact stress. It was hypothesized that loading the dysplastic hip models with a gait pattern measured in dysplasia patients

would produce more realistic contact stress computations that more closely agree with clinical expectations of improved joint mechanics and outcome scores after PAO.

In addition to modeling parameters, it is also probable that numerous patient factors could affect the interpretation of the contact stress computations. Deformities of the acetabulum and femoral head make dysplastic hips very different from normal hips, and they would be hypothesized to have greater DEA-computed contact stress than normal hips. The shallow nature of the acetabulum in dysplastic hips typically produces a lateralized center of hip rotation, which is assumed to be medialized after PAO. Thus, it is hypothesized that a decrease in contact stress would be correlated with medialization of the center of rotation. Deformities of the femoral neck (e.g. cam deformities) also create non-ideal contact surfaces that, if not addressed, can lead to increased risk of impingement following PAO, which could result in an increased contact stress and poor patient outcomes. Additionally, young adults tend to have better outcomes following PAO than older adults, but the reasons for such differences and their relationship to joint mechanics are not well known.

It was thought that further investigation of modeling parameters and patient factors would provide a better understanding of which/how these factors influence DEA-computed contact stress in dysplastic patients. Based on identification of influential patient factors, the large PAO cohort can be broken down into smaller, meaningful groups before performing DEA analysis to provide more accurate relationships between computational results and patient-reported outcomes. Such knowledge could prove to be clinically relevant in pre-operative PAO planning to improve patient outcomes.

1.4 Purpose of this Work

The objective of this thesis is to understand how modeling parameters and gait loading of dysplastic models, as well as patient-specific demographics and anatomic variations, influence the joint mechanics that are computed with DEA. The long-term objective of this line of work is to relate these biomechanical data with clinical measures of treatment success (i.e. radiographic measurements, patient-reported outcomes). Understanding how an individual patient's deformity is affecting the contact mechanics of their hip joint is crucial in determining the best possible correction for alleviating damaging stress and patient pain. Creating a computational model that replicates a sufficiently realistic joint environment is imperative for achieving this goal.

CHAPTER 2: METHODS

In this thesis, the influence of modeling parameters utilized for articular cartilage surface generation, hip joint loading patterns, as well as patient-specific demographics and anatomic variations on the DEA-computed joint mechanics in pre- and post-operative dysplastic hips was investigated. Our research team has access to a large database of 139 PAO cases treated by a single orthopaedic surgeon (Todd McKinley MD) at the University of Iowa Hospitals and Clinics between 2002 and 2010. These patients were an average age of 30.1 years (12-54 years) and weighed an average of 81.0 kg (43.9-153.9 kg) at the time of operation. Clinical evaluation for each patient consisted of some combination of pre- and post-operative patient-reported outcome scores. Importantly, this database contains pre- and post-operative CT imaging for every patient, making it possible to analyze the changes in joint mechanics due to acetabular reorientation. In this thesis, sub-samples of patients were selected from this database under Institutional Review Board approval for DEA assessment. The knowledge obtained from this work will enable more realistic DEA modeling of the three-dimensional joint environment present in hip dysplasia patients.

2.1 DEA Model Creation

Creation of the three-dimensional hip models began with segmentation of femoral, pelvic, and spinal bone geometry from pre- and post-operative CT scans using a semi-automated watershed-based program previously developed in MATLAB (Mathworks, Natick, MA) by members of our laboratory [86]. The watershed analysis views the CT image data as a topographical map, in which basins (i.e. bones) are

separated by ridgelines (i.e. high-intensity cortical bone). The segmentation algorithm first separates the bony geometry from the image dataset, and then a watershed algorithm fills the bony regions until another cortical bone edge is reached based on a threshold attenuation value between cortical surfaces [86]. This watershed-based algorithm is highly effective at differentiating cortical bone from the surrounding soft tissues in the CT images using perceptible differences in attenuation values. However, the high porosity of cancellous bone can lead to lower attenuation values that are comparable to those of soft tissues. Additionally, in dysplastic hips, joint space narrowing or femoral head subluxation may occur, bringing the bones into direct or nearly direct contact, resulting in a lack of attenuation value differences between bony surfaces (Figure 8). This can make automatic discrimination between the superior edge of the femoral head and the inferior edge of the acetabulum difficult.

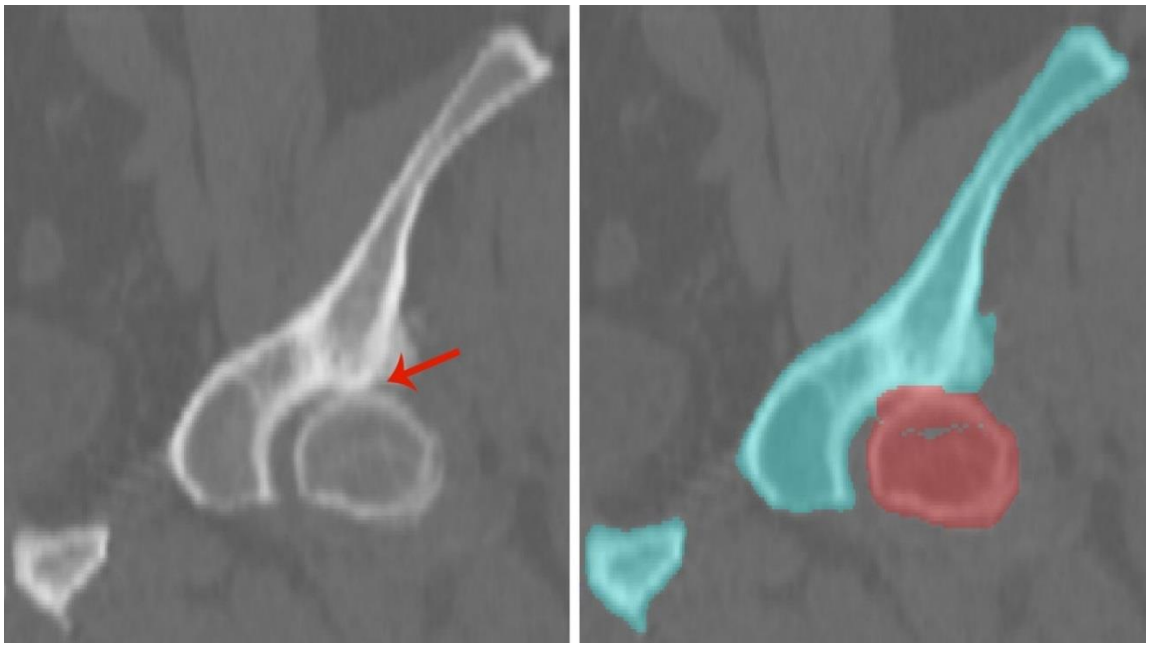

Figure 8. Coronal CT image of a dysplastic hip with a narrowed joint space (left). The attenuation values at this location are similar, making it difficult for the automated algorithm to accurately identify the bone edges in its segmentation (right).

To ensure accurate segmentation, the automatically generated segmentations were overlaid on the corresponding CT scans in ITK-Snap, and any minor errors in edge definition or holes in cancellous bone were manually corrected (Figure 9). An investigation of interobserver and intraobserver variability associated with this manual step of segmentation was performed in a pre-operative dysplastic hip. Comparison between three segmenters over three non-consecutive days illustrated an average percent difference in the computed contact stress of 7.8% (0.2%-18.3%). An average percent difference in the computed contact stress of 9.3% (2.4%-18.0%) was associated with variability in manual segmentation performed by the author of this thesis on three non-consecutive days. These results indicate a minimal effect of variability in manual segmentation on the resulting contact stress calculation.

Once segmentation was complete, each individual bone data set was transformed into a triangulated surface and exported from ITK-Snap as an STL model. These STL models were then imported into Geomagic Design X (3D Systems, Inc., Rock Hill, SC), where the triangulated surfaces were smoothed to create a more realistic representation of the bony geometry. Patient-specific anatomic landmarks were identified on the finalized models and used to align the models to the Bergmann coordinate system [11] for load application. Repeating the smoothing and alignment process on the same dysplastic hip segmentation on three non-consecutive days found an average percent difference in the computed contact stress of 5.9% (1.1%-15.3%), indicating a minimal effect of variability in these manual processes on the resulting contact stress.

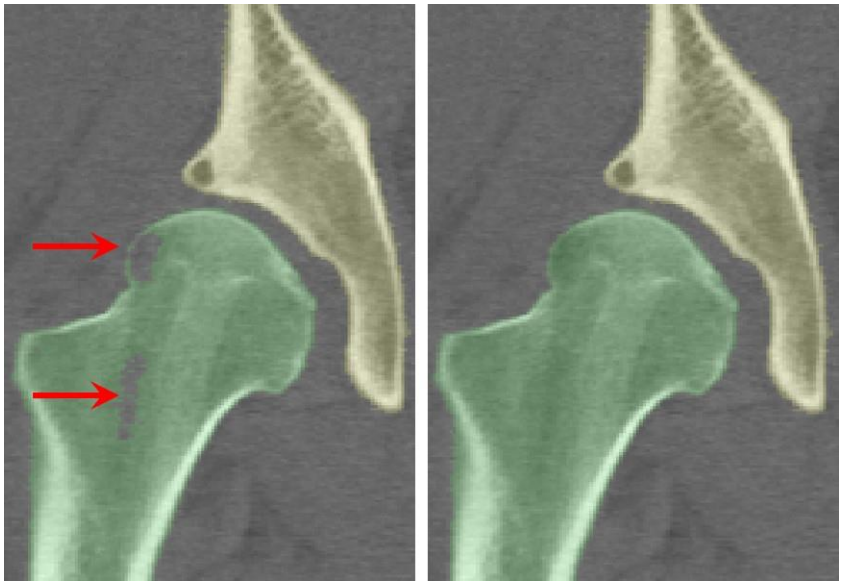

Figure 9. Visualization of the pelvic CT scan in ITK-Snap. The watershed algorithm accurately distinguishes between the bony geometries, and each bone is segmented as a different color. However, some holes in the segmentation (as indicated by arrows) remain due to similar attenuation values between the cancellous bone and soft tissues (left). Minimal manual intervention is required to obtain a complete and accurate segmentation (right).

2.2 Cartilage Surface Generation

This database of PAO patients is unique in that it contains pre- and post-operative CT scans for each patient, making it possible to generate surface models of each patient's bony anatomy before and after PAO. While CT scans are sufficient for understanding bony deformity and segmenting bony geometry, without the use of an intra-articular contrast agent, they do not enable visualization of articular cartilage surfaces. As cartilage surfaces are necessary for performing DEA analysis on dysplasia patients, the articular cartilage must be approximated based on the bony geometry. The methodology for this cartilage approximation was developed previously in MATLAB and involves uniformly projecting the segmented subchondral bone of the femoral head and acetabulum a user-specified distance [84], here 1 mm.

However, the subchondral bone surface is not a smooth delineation between bone and cartilage, and this uniform-thickness projection creates a cartilage surface with the same surface irregularities as the bone-cartilage interface. This irregular surface can create points of very high contact stress that are not representative of the true contact stress distribution. To eliminate these confounding stresses, a smoothing technique was implemented to smooth the incongruent projection and create a nearly spherical articular surface. This surface smoothing algorithm was developed previously in MATLAB and iteratively repositions each vertex towards the average distance of its connected neighbors until the surface approaches sphericity [84]. It was found that five smoothing iterations created an articular cartilage representation approaching a nearly spherical surface (Figure 10) [85]. The distance from this spherical cartilage surface to the subchondral bone varies over the joint surface and produces a non-uniform cartilage thickness, which has been shown by previous studies to be a more realistic cartilage representation [87-90]. This cartilage generation and smoothing methodology has been validated in cadaveric specimens and produces accurate contact stress computations in the intact hip joint [77]. The realistic cartilage representation and accuracy of the resulting contact stress distributions support the use of this projection and smoothing technique to create the CT-based articular cartilage surfaces for the dysplastic hip models in this work.

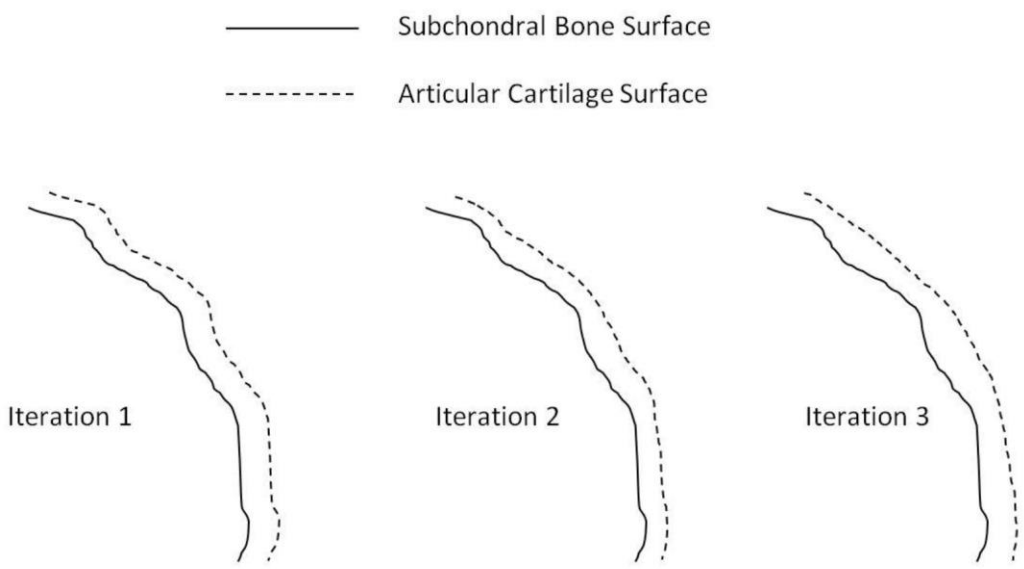

Figure 10. Pictorial representation of the surface smoothing algorithm. As the number of iterations increases, the articular cartilage surface approaches sphericity with varying cartilage thickness. A total of 5 iterations was found to generate realistic articular cartilage surfaces that produce accurate contact stress distributions. Image taken from Townsend [85].

2.3 Material Properties and Cartilage Thickness

Selecting parameters that accurately represent cartilage stiffness and thickness in the hip joint, in conjunction with applying appropriate loading conditions is crucial to developing a realistic computational model. In the previous work [85], a cartilage modulus of 8 MPa and a Poisson's ratio of 0.42 were selected based on values reported in the literature for average cartilage modulus when loading at rates similar to walking [91, 92]. A uniform cartilage thickness of 1 mm was selected based on the mean acetabular and femoral cartilage thicknesses of the two cadaveric specimens studied [85].

To explore the effects of these modeling parameters on contact stress calculations, a parametric variation of cartilage thickness and Young's modulus for one of the intact

specimen models from the previous validation study [77] was performed. Projected cartilage thickness values of 1.0 mm, 1.3 mm, 1.5 mm, and 2.0 mm, and Young's modulus values of 6 MPa, 7 MPa, 8 MPa, 9 MPa, and 10 MPa, were investigated, resulting in a total of 20 combinations of these parameters (Figure 11). Static loadings of 1000N were applied, and DEA computation of contact measures was performed. The contact stress distributions for all 16 combinations of parameters were correlated on a point-by-point basis to the physical Tekscan measurements obtained from the validation study [77] (Figure 11).

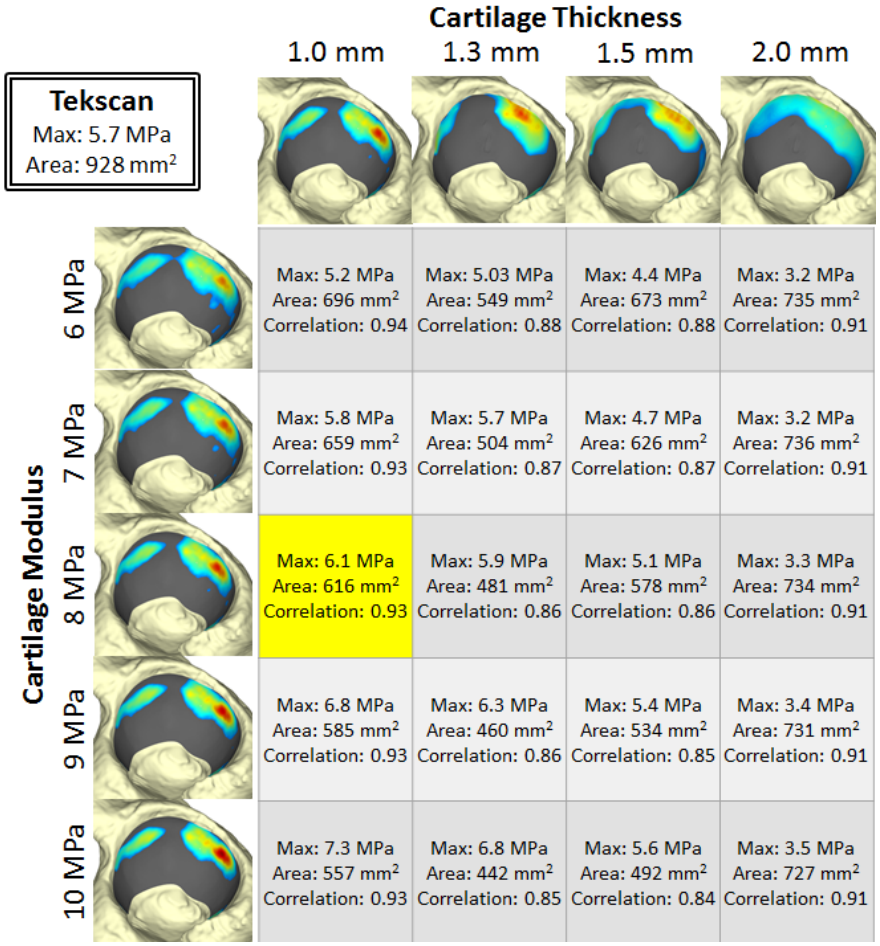

Figure 11. Parametric variation of cartilage thickness and cartilage modulus in a DEA model of a cadaver hip indicates that the originally selected parameters (cartilage thickness of 1 mm and cartilage modulus of 8 MPa) produce contact results that correlate well with physical measurements.

As the cartilage thickness was increased from 1 mm to 2 mm, the computed maximum contact stress and correlation with Tekscan measurements both decreased. Additionally, the location of the acetabular contact patch moved superiorly with increasing cartilage thickness. This may indicate that thicker cartilage does not permit the femoral head to sit adequately within the acetabular socket, resulting in a contact pattern suggestive of femoral subluxation.

As the cartilage modulus was increased to 9 and 10 MPa, the maximum contact stress increased, indicating that a stiffer cartilage does not permit as much deformation and experiences higher contact stresses. In comparison, decreasing the cartilage modulus to 6 and 7 MPa decreased the contact stress, indicating that a softer cartilage that permits greater deformation is not subjected to as high of contact stresses. While changing the cartilage modulus changes the stiffness of the articular surfaces, it does not change the cartilage geometry. Only the amount of allowable deformation, and not the pattern of contact between the two articular surfaces, was affected. Therefore, there was no meaningful change in correlation with Tekscan measurements. The results of this parametric variation in cartilage thickness and cartilage modulus indicated that the originally selected parameters (cartilage thickness of 1 mm and cartilage modulus of 8 MPa) agree with material properties reported in the literature [91, 92] and produce contact results that correlate well with physical measurements [77], making them valid parameters to use in our DEA methodology.

2.4 Hip Joint Loading & Alignment

Upon creating patient-specific hip models, boundary and loading conditions for these models were defined. It was decided that modeling the entire stance phase of walking gait, rather than a single pose, was critical to understanding how variations in dysplastic deformity affect the mechanics of the hip joint. For example, a severely retroverted acetabulum would likely cause the most pain and contact stress near heel-strike, whereas a severe lack of lateral coverage would result in high contact stress and risk of subluxation near midstance. Modeling the entire stance phase of walking gait would provide a broader understanding of how variations in dysplastic deformity under an applied loading pattern affect the contact stress distributions.

2.4.1 Previously Implemented Joint Loading & Alignment

Initially, the gait data from Bergmann, *et al.* [11] was utilized for loading the dysplastic hip models. In Bergmann's study, kinematic and kinetic measurements were obtained during a variety of activities of daily living in four subjects of ages 51-76 years who received instrumented total hip prostheses for treatment of osteoarthritis. This data set has the most extensive kinematic and kinetic gait data currently available, and the high reliability of instrumented total hip measurements has led to frequent use of this data set in computational modeling studies of the hip [93-96]. Hence, this gait pattern was believed to be the most logical starting point for use with our models.

The Bergmann gait data consists of kinematic and kinetic measurements taken at 201 time intervals representative of one gait cycle. These measurements were obtained directly from the total hip replacement for each subject, and the averages across all trials

for every subject were used to calculate an average/representative set of kinematics and kinetics. Toe-off occurred near 60% of the full step cycle (heel-strike to heel-strike), so the first 130 data points describe hip rotations, forces, and moments while the foot is in stance phase (i.e. heel-strike to toe-off of the foot). This set of 130 data points was discretized into 13 evenly distributed sets of forces and rotations to facilitate 13 discrete loadings encompassing the stance phase of gait for our models. The average hip contact forces in each of the X-, Y-, and Z-directions are shown in Figure 12. These subjects had a maximum vertical force of nearly 250% BW shortly after heel-strike, with a corresponding peak in medial force.

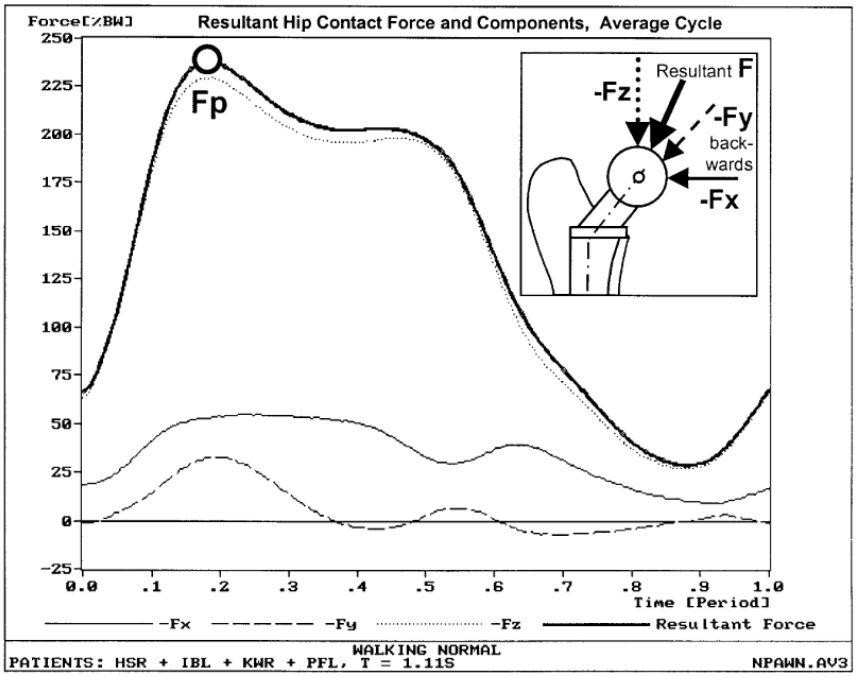

Figure 12. Average hip contact force of all subjects and its components. Toe-off occurred near 60% of the gait cycle, so the first 60% of the data was utilized to represent stance phase of gait. F_x, F_y, and F_z correspond to forces in the medial, anterior, and superior directions, respectively. Fp indicates the maximum force from the resultant of F_x, F_y, and F_z. Image taken from Bergmann *et al.* [11].

To facilitate application of the Bergmann forces and rotations in our models, the hip models generated from the CT scans needed to be positioned in the same orientation as the bones for the Bergmann data calculation. However, during a CT scan, the patient must be lying inside the CT scanner, which places the hip joint in a position other than in its normal anatomic orientation. Additionally, hip joint rotation in the supine position can vary between patients. Thus, the segmented hip models are in a variety of orientations that do not correspond to standing, walking, or any other functional position. To apply the Bergmann forces and rotations to load the DEA models, the hip models must be reoriented to the same coordinate system in which those forces and rotations are defined.

The Bergmann pelvic coordinate system (Figure 13) defines the origin as the center of the left acetabulum. The X-axis is defined as the line connecting the centers of both acetabula, with the positive direction pointing medially. The Z-axis is perpendicular to the X-axis and is defined as a vertical line through the center of the L5-S1 vertebral body. The Y-axis is perpendicular to both the X- and Z-axes and points anteriorly.

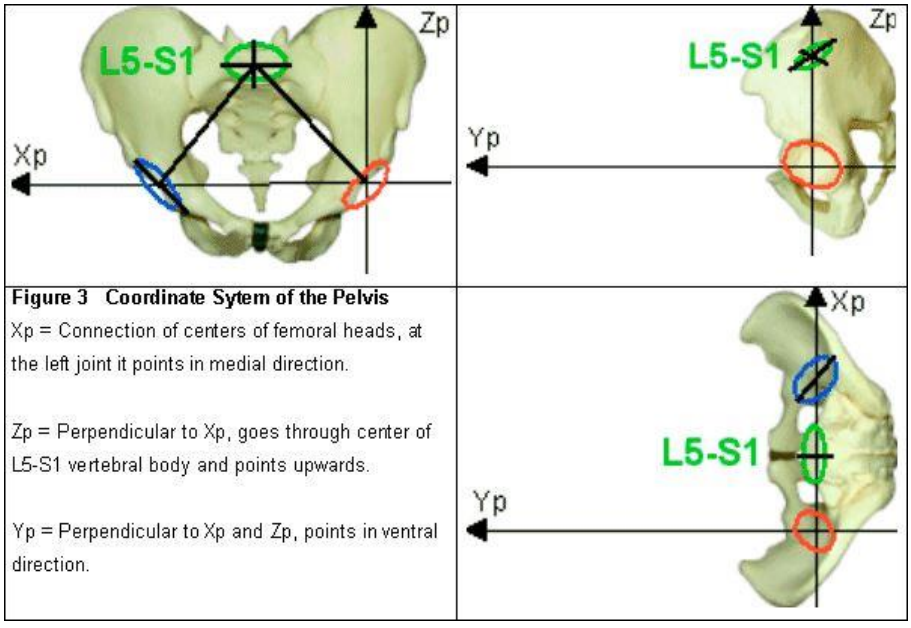

Figure 13. The pelvic coordinate system as defined by Bergmann, *et al.* [11].

Similarly, the Bergmann femoral coordinate system (Figure 14) defines the origin as the center of the left femoral head. The X-axis is defined as the line connecting the centers of both condyles, with the positive direction pointing medially. The Z-axis is perpendicular to the X-axis and is defined as a vertical line through the center of the femoral shaft. The Y-axis is perpendicular to both the X- and Z-axes and points in the anterior direction.

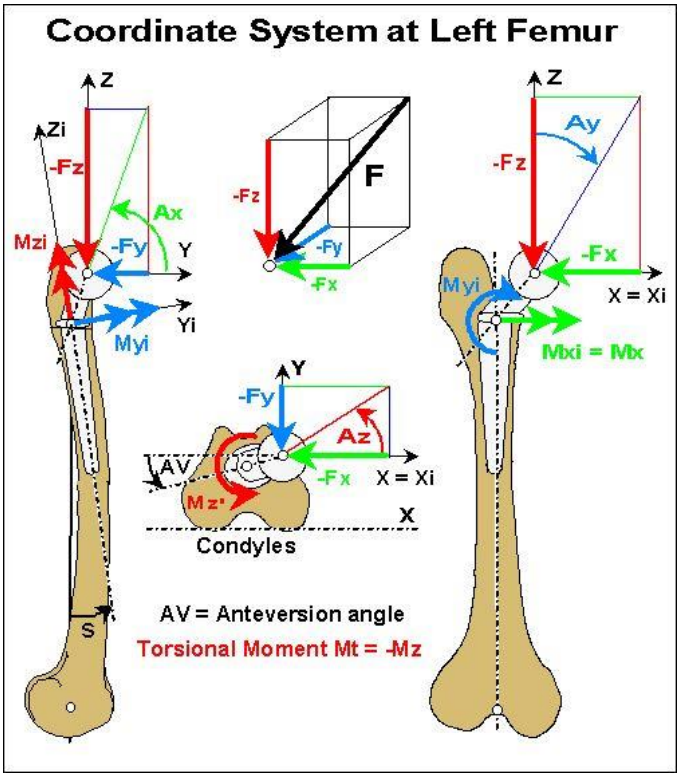

Figure 14. The femoral coordinate system as defined by Bergmann, *et al.* [11].

Each patient-specific dysplastic hip model was reoriented to the Bergmann pelvic coordinate system. First, the pelvis was imported into Geomagic Design X, and patient-specific anatomic landmarks were identified and used to align the pelvis to the Bergmann coordinate system. A reference femur that had been previously aligned to the Bergmann femoral coordinate system based on bony landmarks was imported into Geomagic Design

X, and the patient-specific femur model was translated and rotated to so as to overlay the reference femur. The centers of the patient-specific acetabulum and femoral head were identified by fitting spheres to the articular cartilage of both geometries, and the patient-specific models were translated such that the centers of both spheres were aligned to the origin. After this process was completed, the patient-specific model was properly aligned. The Bergmann forces and rotations were scaled based on the patient's body mass and applied to the model.

While the Bergmann-derived gait loading is a highly utilized data set, there are some limitations to using this gait pattern in a dysplasia cohort. The subjects in the Bergmann study ranged from 51-76 years of age, which is much older than typical PAO patients, who can range from young teens to an average of 30 years old. Even the oldest PAO patients are not in the same age range as the Bergmann subjects. Additionally, the Bergmann subjects received their instrumented total hip replacements for osteoarthritic changes and not as a treatment for dysplasia. Therefore, these subjects presumably would have altered their gait to alleviate osteoarthritis pain [97, 98].

The advanced ages of and the osteoarthritic changes in these patients resulted in a normal walking speed of 1.09 m/s, which is much slower than 1.35 m/s typical of a younger healthy individual [10]. Walking speed has been shown to significantly affect stride time, hip abduction/adduction angle, and overall stability [99, 100]. A slower walking speed in combination with a longer stride time can decrease force transfer through the hip joint. To improve comparability with younger, faster walking individuals, the Bergmann data implemented to load the DEA models was the data collected for the patients "fast" walking speed (average walking speed of 1.46 m/s). However, this pattern

may be less reliable and did not eliminate gait alternations due to osteoarthritis. When taking these factors into consideration, it is probable that the Bergmann gait pattern is not particularly representative of gait in a dysplasia patient. Young dysplasia patients are typically much more active than elderly, arthritic patients, making it much more likely that they would generate more force that could cause damaging contact stresses on an already unstable hip joint.

2.4.2 Dysplastic Gait Pattern

It was essential to implement alternative loading patterns and assess the effects that the loading pattern had on the computed contact stresses. Like arthritic patients, dysplasia patients also have an altered walking gait to alleviate pain, but also to minimize the risk of subluxation or possible dislocation of the hip joint. Therefore, it was pertinent to compare how such gait modifications differ from the originally modeled Bergmann data. In a study by Skalshoi, *et al.* [45], 3D motion capture of gait in 32 hip dysplasia patients was analyzed with inverse kinematics and static optimization in OpenSim 3.2 modeling software [101] to obtain joint angles and contact forces (Figure 15). These dysplastic subjects had vertical joint reaction forces of approximately 300% BW shortly after heel-strike and 315% BW near toe-off, compared to the 250% BW shortly after heel-strike and 160% BW near toe-off for patients in the Bergmann cohort. For the work in this thesis, data from the Skalshoi, *et al.* study were discretized into 13 evenly distributed steps during the stance phase of gait and directly compared with the Bergmann data.

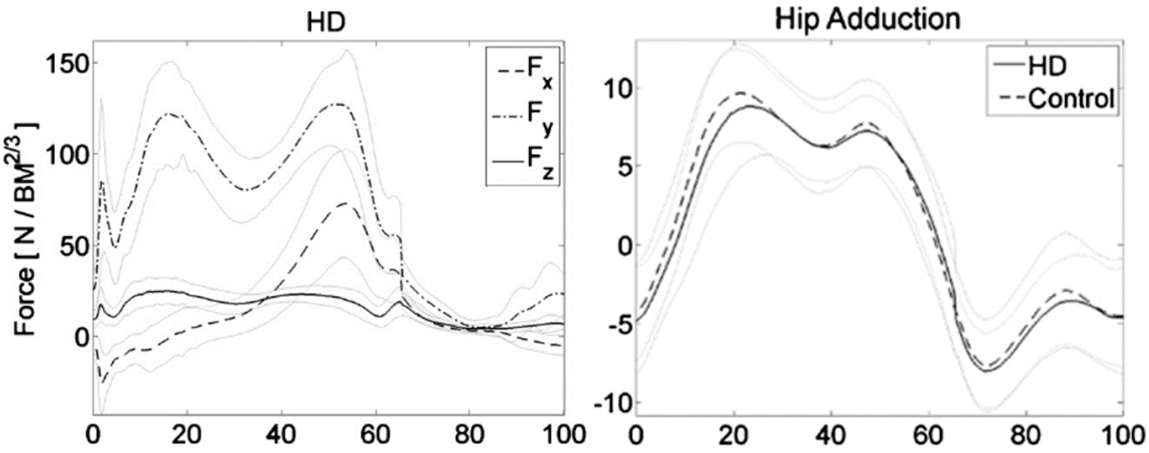

Figure 15. Average hip joint contact forces and hip adduction during gait in dysplasia patients. Adapted from Skalshoi, *et al.* [45].

The hip forces and rotations in the Skalshoi, *et al.* study were reported with respect to a pelvis anatomic reference frame (Figure 16), which is a different coordinate system than the Bergmann system. Since this gait pattern was being applied to hip models previously aligned to the Bergmann coordinate system, appropriate rigid transformations were needed in order to apply this alternative loading pattern. Rotations and translations needed to convert the pelvis anatomic reference frame to the Bergmann coordinate reference frame were calculated for each hip model and then applied to the average forces and rotations reported by Skalshoi, *et al.* to obtain forces and rotations that could be applied to a hip in the Bergmann reference frame. Again, applied forces were scaled based on the patient's body mass, and the forces and rotations were applied to the DEA model.

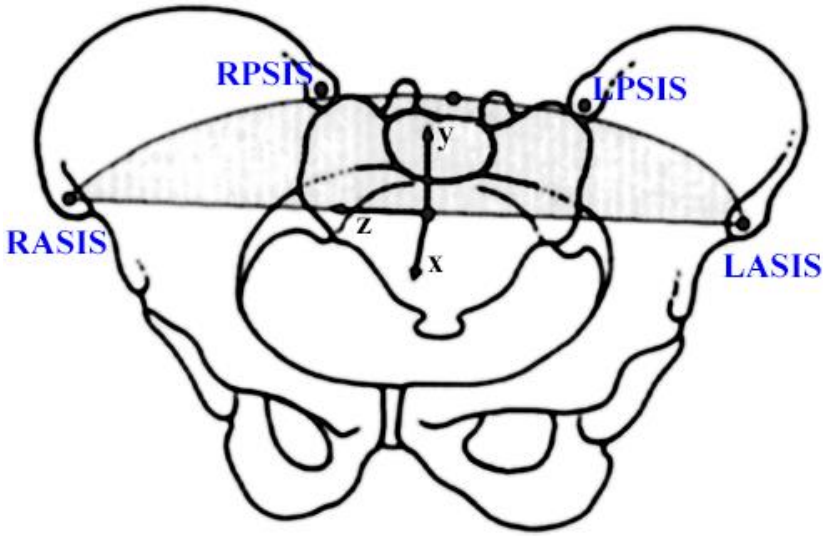

Figure 16. Definition of the anatomic landmarks and axes in the pelvic anatomic reference frame. Image adapted from Cappozzo *et al.* [102].

Graphs of the average forces and rotations with respect to the Bergmann coordinate frame for the thirty dysplastic patients in this study, as well as lines indicating ± one standard deviation, are shown in Figure 17. Important differences exist between the Bergmann and dysplastic gait patterns, namely the 150% BW increase in superior force near toe-off in the dysplastic gait. Greater forces near toe-off may result from an increase in walking speed or increase in push-off force, both of which may be related to the younger ages of this dysplasia cohort (median 34 years old). There is also a much greater adduction force near toe-off of the dysplastic patients, which may be related to an attempt to decrease pain and increase stability. However, as these forces and rotations were measured in 32 dysplasia patients, this data should provide a more realistic gait pattern for loading our dysplastic hip models.

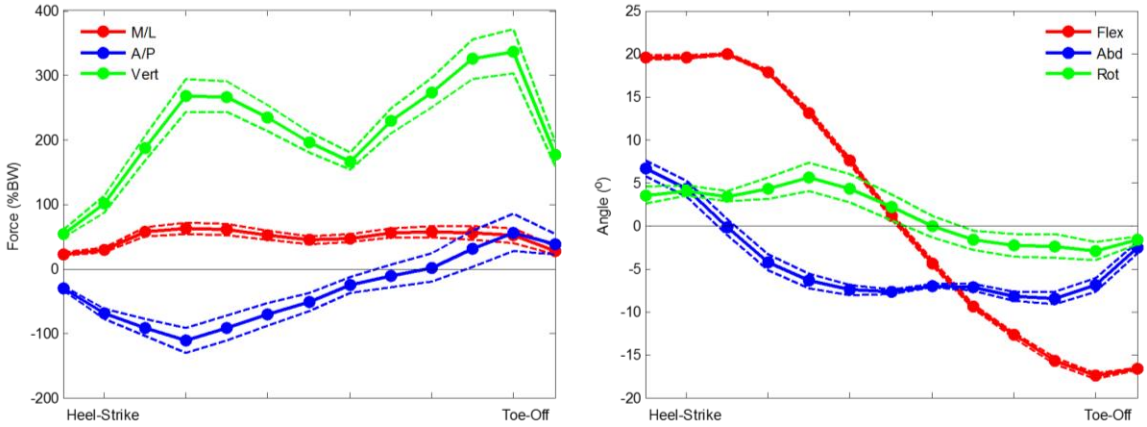

Figure 17. Average forces and rotations for the thirty dysplastic patients after rigid transformation from the pelvic anatomic frame to the Bergmann coordinate frame. Dashed lines indicate ±1 SD for the corresponding colored average of the thirty patients.

2.4.3 Normal Gait Pattern

In addition to comparing the Bergmann gait pattern with a dysplastic gait pattern, it was also essential to compare both patterns with a gait pattern in healthy individuals of typical PAO patient age. This allows direct comparison of how the slower walking speed and advanced ages in the Bergmann data, and the gait modifications due to presence of dysplastic deformity in young, active individuals, affect the forces and rotations during walking gait, and thus, the resulting contact stress distributions. Normal hip forces and rotations were selected from studies by the Pandy research group [10, 103] in which they used dynamic optimization techniques to assess 3D motion capture data from five healthy male subjects 26±3 years of age with an average walking speed of 1.35 m/s (Figure 18). For application in this thesis, and for direct comparison to the Bergmann and dysplastic gait patterns, data from these studies were discretized into the same 13 evenly distributed increments spanning the stance phase of gait. The data in these studies were reported in the orientation of the femur relative to the pelvis, and as this was the same orientation as

the Bergmann coordinate system, no rigid transformations needed to be applied before scaling the forces according to patient's body mass and loading the hip models with the normal gait pattern.

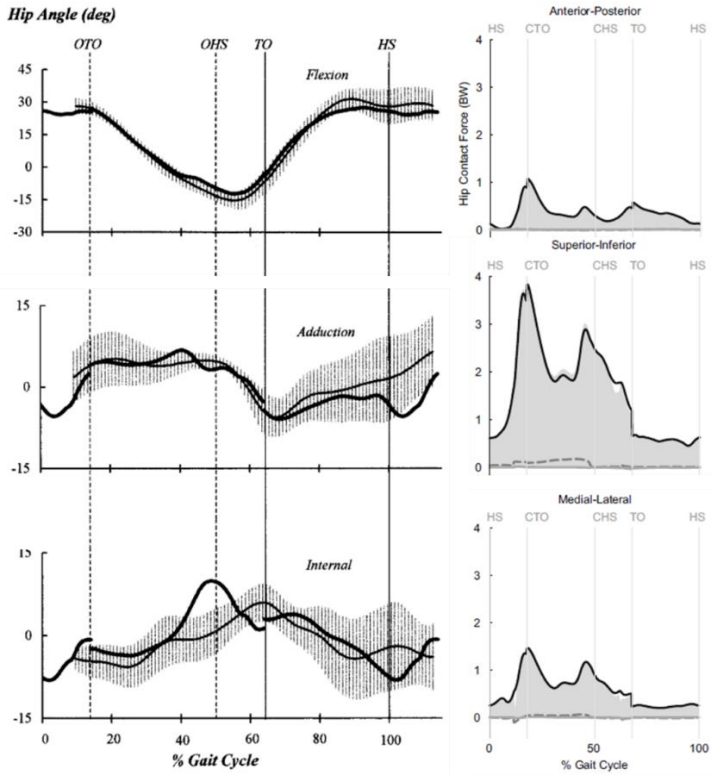

Figure 18. Average hip angles [103] and hip contact forces [10] in healthy individuals.

In comparison to the Bergmann gait pattern, healthy individuals had much greater peak forces shortly after heel-strike, greater extension near toe-off, and greater internal rotation (Figure 19). In comparison to the dysplastic gait pattern, the healthy individuals had a greater superior force near heel-strike but smaller superior force near toe-off; greater medial and anterior forces; greater extension throughout the majority of stance; and greater abduction near toe-off (Figure 19). In summary, there are noticeable differences in the forces and rotations between all three gait patterns, which may have significant effects on the resulting computed joint contact stress.

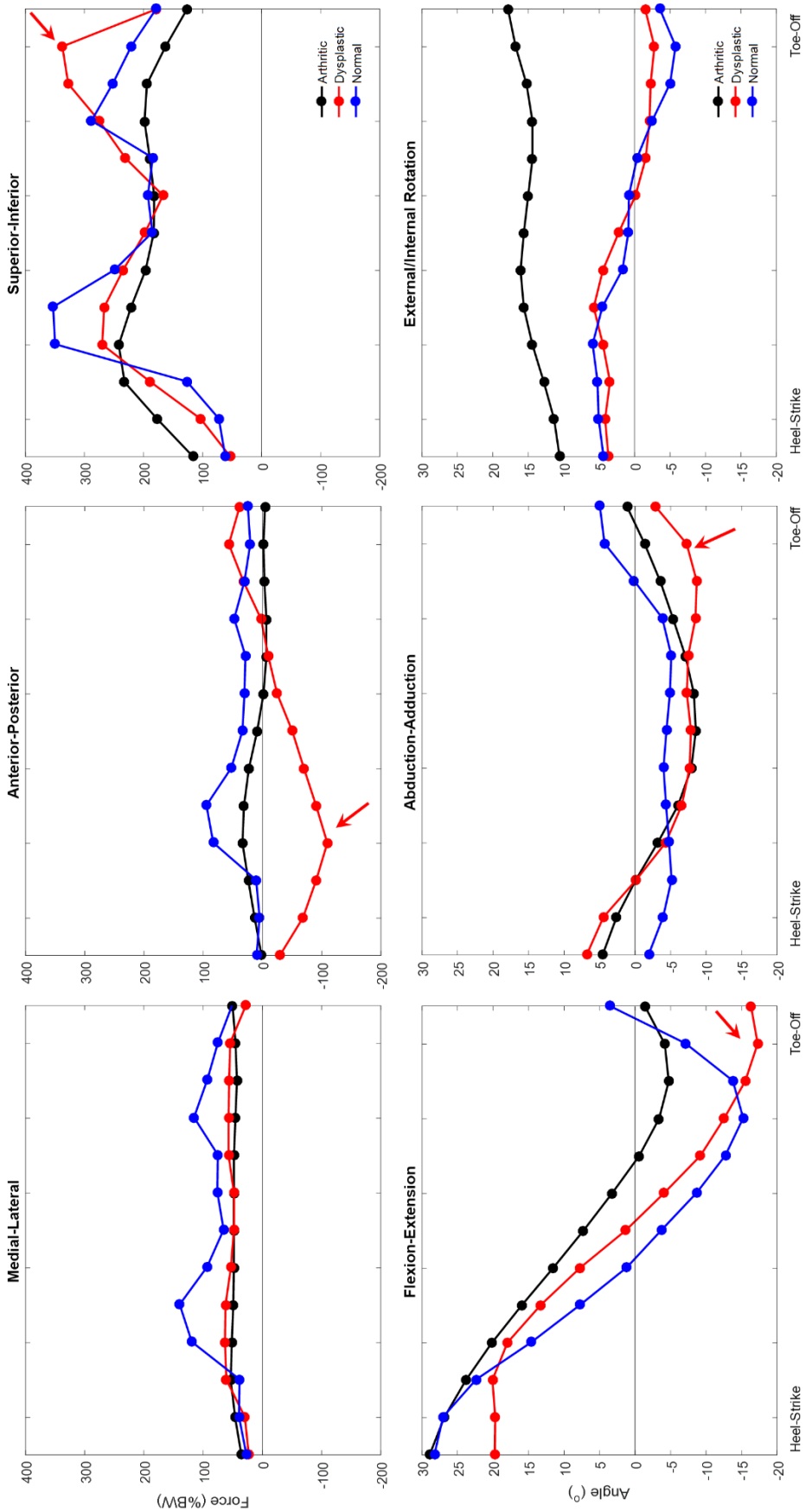

Figure 19. Hip contact forces and rotations during stance phase of gait for all three gait patterns.

2.4.4 Boundary Conditions

For boundary conditions, initial femoral position was mandated by the prescribed positions of the gait cycle loading. Femoral translation was constrained in all directions, but the pelvis was free to translate in all directions until convergence was reached. The user-prescribed forces, which were defined by the various applied gait cycles, are used as a comparison to the contact forces computed later in the DEA algorithm.

2.5 DEA Algorithm

Computation of contact stress in the hip joint upon application of each of the three different gait cycles was completed using a DEA technique previously developed in MATLAB by Andrew Kern, PhD [83]. This method consists of two rigid contact surfaces connected by a bed of compressive springs representing locations of potential contact. The DEA algorithm requires the user to input (1) two properly aligned, triangulated cartilage surfaces between which contact is to be determined, (2) the associated thickness and material properties of these cartilage surfaces, (3) the forces and rotations to be applied to these surfaces, (4) model termination constraints, and (5) any additional desired model constraints (e.g. linear springs to represent muscle attachments).

Contact is determined through a progression of iterative static solutions. Initially, the cartilage surfaces are moved out of any physical contact by translating the acetabular cartilage superiorly until no interaction is occurring between the cartilage surfaces. Each DEA iteration begins with no connecting springs between the cartilage surfaces to represent contact. For each increment of the gait cycle, forces and rotations in all three directions are applied to the femur, and any contact between the femoral and acetabular

cartilage due to these prescribed loadings must be determined. Triangular faces on the two cartilage surfaces that have become in contact with one another due to the change in loading are determined through use of a ray casting algorithm. Essentially, a ray is cast normal to each face on the acetabular cartilage surface toward the acetabular subchondral bone. If this ray intersects the femoral cartilage surface, then the femoral cartilage surface has translated inside of the acetabular cartilage, indicating that the two cartilage surfaces are now in contact at the location of that triangular face (Figure 20). A linear spring is then created from the centroid of the triangular face on the acetabular cartilage surface to the centroid of the triangular face on the femoral cartilage surface. If the ray does not intersect the femoral cartilage surface, then the femoral cartilage surface has not translated inside of the acetabular cartilage, and the two cartilage surfaces are not considered to be in contact at the location of that triangular face. In this instance, no linear springs are created between the centroid of the acetabular cartilage face and the centroid of the femoral cartilage face.

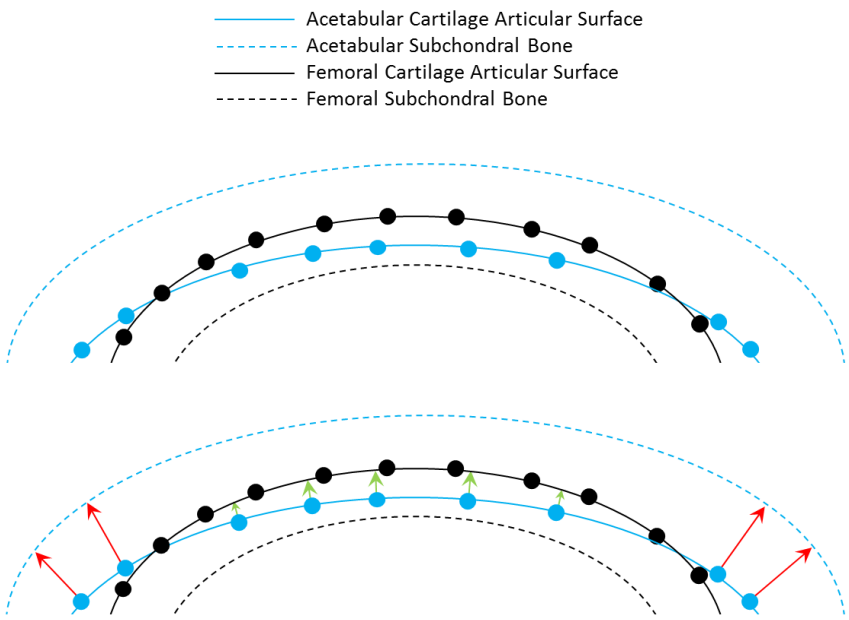

Figure 20. Cartoon of the ray casting technique used in the DEA algorithm. (Top) Points indicate faces on the acetabular (solid blue line) and femoral (solid black line) cartilage surfaces at which contact will be determined. The associated subchondral bone surfaces are shown in dashed lines. (Bottom) A ray is cast from each face on the acetabular cartilage surface until it intersects another surface. If the ray contacts the femoral cartilage, the two cartilage surfaces are considered to be in contact at that location (green arrows). A linear spring is created normal to the acetabular cartilage face, with the length of the casted ray representing the spring deformation. If the ray does not contact the femoral cartilage, the two cartilage surfaces are not considered to be in contact at that location (red arrows), and no springs are created.

The length of these linear springs represents the spring deformation, which can then be related to the contact stress within each contacting face using the following equation:

$$p = \frac{(1-v)E}{(1+v)(1-2v)}\frac{d}{h}$$

where p is the resulting contact stress; v is the Poisson's ratio of the cartilage; E is the Young's modulus of the cartilage; d is the spring deformation; and h is the cartilage thickness.

Following calculation of the contact forces based on the linear spring deformations, the DEA algorithm iterates through a load control calculation (Figure 21). In this algorithm, the current contact stress distributions are calculated based on the spring deformations and used to compute the contact forces in the current model. A Newton's method iterative scheme then compares the current contact forces with the total applied forces defined by the user. If the current contact forces are not within the defined tolerance of the user-prescribed forces, then a rigid transform is applied to the displacement of the contacting surfaces based on a Newton-Raphson method. If the values of the computed forces have oscillated over the user-prescribed force values, then the step-size of the translation is decreased by half, and the contacting surfaces are translated towards equilibrium. Otherwise, the step-size of the translation is maintained, and the contacting surfaces are translated towards equilibrium. After the rigid transform is applied, the spring deformations, contact stress, and contact forces are updated. Once the contact forces are within the defined tolerance of the user-prescribed forces, the DEA model is considered to have converged, and the contact stress distribution is output for the current gait pose. Each set of prescribed forces and rotations for each of the 13 gait poses is treated as a separate consecutive model in which the entire iterative scheme begins again from scratch. After the contact stress distributions for all 13 gait poses have been determined, the DEA calculations are complete. This iterative process was completed for all 30 dysplastic DEA models with each of the three different gait loading patterns applied to every model to determine the changes in contact stress resulting from gait modifications.

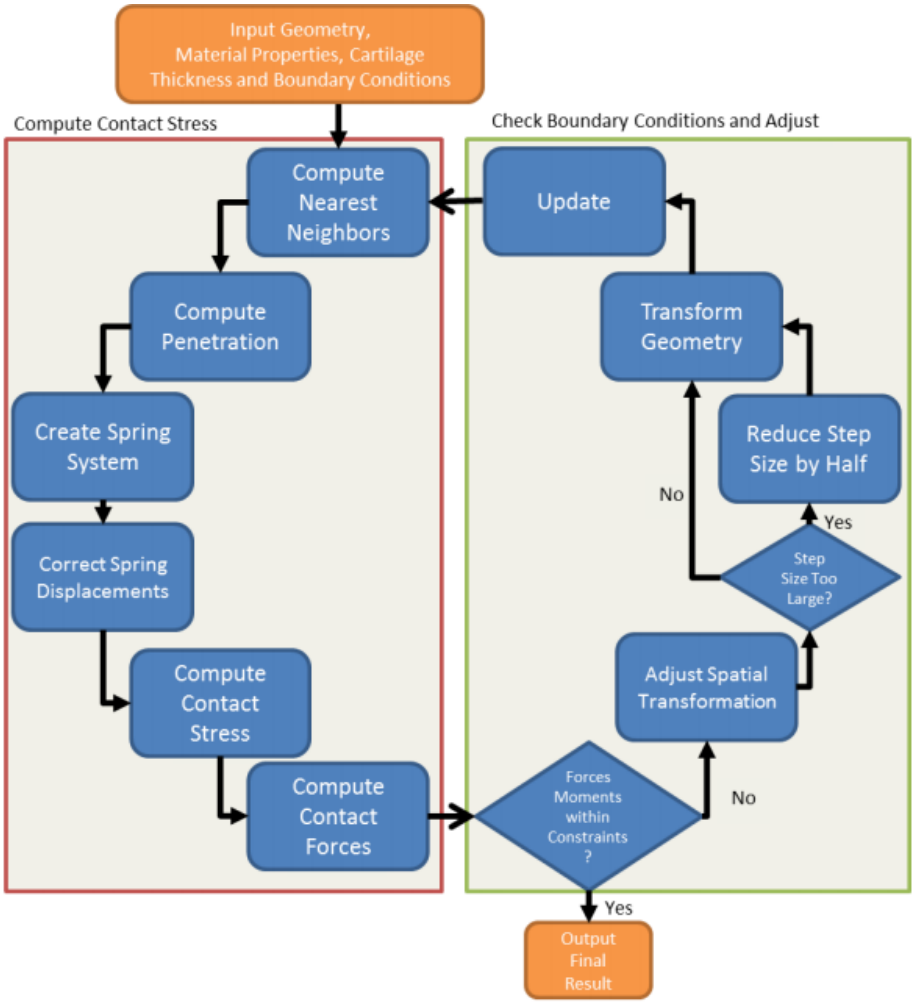

Figure 21. Flowchart of DEA algorithm used to iteratively compute contact stress distributions. Patient-specific geometries, material properties, and appropriate boundary conditions serve as inputs, and a Newton's iterative scheme computes the contact stress using a load control algorithm until a prescribed tolerance has been met. Image taken from Kern [83].

2.6 Clinical Measures of Patient Outcomes

The future goal of this overall line of investigation is to accurately model the three-dimensional joint environment in dysplasia patients and relate the DEA-computed contact stress results with patient-reported outcomes. To assess how DEA-calculated contact stress distributions relate to short-term patient-reported outcomes, VAS, WOMAC, and SF-36 outcome measures were extracted for each of the dysplasia patients

in our analysis before PAO and at an average of 2.5±1.9 years following PAO. As detailed above (section 1.3.3 Previous Work & Rationale), the VAS pain score evaluates a patient's hip pain on a scale of 0-10, with a higher score indicating more severe pain. The WOMAC score evaluates three categories: pain, stiffness, and function. Each category is scored on a scale of 0-100, with higher scores indicating less disability. The average of these three categorical scores determined the overall WOMAC score for correlation to contact stress measures. The SF-36 measures eight scaled quality-of-life factors: physical functioning, social functioning, physical role limitations, emotional role limitations, vitality, bodily pain, general mental health, and general health perceptions. Each scaled score is a weighted sum of the questions regarding each quality-of-life factor. Total scores range from 0-100, with higher scores indicating less disability. For each patient-reported outcome measure, pre- and post-operative contact stress results were correlated with pre- and post-operative outcome scores to determine relevant correlations. Meaningful relationships between biomechanical and outcome measures could assist orthopaedic surgeons in pre-operative PAO planning to further improve patient outcomes.

2.7 Patient Factors Influencing Contact Stress Interpretation

In addition to investigating how various modeling parameters (i.e. material properties, gait loading patterns) influence the DEA-computed joint mechanics, it was also of interest to understand how patient demographics and anatomic variations affect the computed contact stress distributions. Such patient factors may be important in the interpretation of the computed contact stress and assessment of PAO cohorts in general.

2.7.1 Acetabular Center of Rotation

It is important to understand how the multiplanar correction of the acetabulum affects contact stress results. Previous studies have assessed how the increase in center-edge angle affects the hip joint contact stress, but this radiographic measurement only quantifies single-plane acetabular repositioning [104, 105]. It is possible that a multiplanar correction may be performed even in instances where it is not intended. For instance, a dysplastic hip that is only insufficient in lateral coverage should not be corrected with anteversion, as this could likely lead to impingement. Therefore, it is important to understand how lateral and version corrections, or combinations of both corrections, influence the joint mechanics and clinical outcomes.

To investigate the effects of lateral and version corrections on the computed contact stress, 15 patients who were indicated primarily for correction of lateral coverage insufficiencies were pulled from the thirty cases analyzed above. All models were loaded with the dysplastic gait cycle [45] and assessed using the DEA methodology to obtain pre- and post-operative contact measures. Using Geomagic Design X, a sphere was fit to the acetabular cartilage geometry in each pre-operative model. The center of this sphere represented the pre-operative acetabular center of rotation. The non-acetabular portion of the pelvic geometry from the post-operative model was aligned to the pre-operative model (Figure 22), and the sphere-fitting technique was repeated to determine the post-operative center of rotation. Changes in mediolateral, anteroposterior, and superoinferior positions of the acetabular center of rotation relative to the Bergmann coordinate system were calculated and correlated with changes in DEA-calculated contact measures.

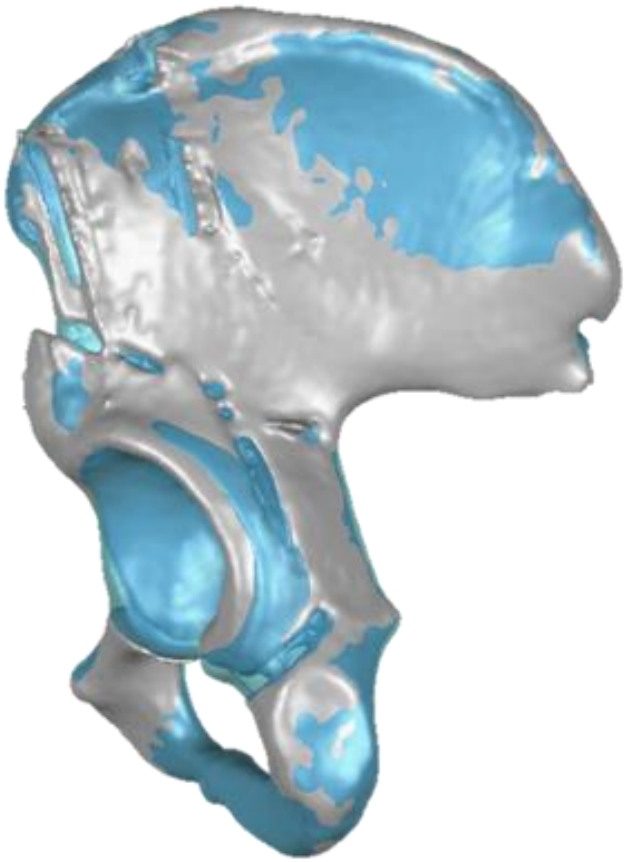

Figure 22. Post-operative patient model (grey) aligned to and overlaid on the corresponding pre-operative model (transparent blue) illustrates the change in acetabular orientation following PAO.

2.7.2 Effects of Femoral Deformity

One limitation of our PAO cohort is that the patients were not separately assessed for femoral deformities, such as cam deformities. Therefore, it was unknown whether these patients had strictly dysplastic hips or a combination of dysplastic-impingement deformity that may not have been fully addressed by acetabular reorientation. Unaddressed femoral deformities may contribute to less than ideal patient outcomes, undermining of the success of the dysplasia treatment.

An advantage of having a heterogeneous PAO group with pre- and post-operative contact stress assessments is that this biomechanical information could be used to further explore the effects of concurrent femoral deformities. To investigate the possibility of unaddressed cam deformities affecting the joint contact stress and patient outcomes, 20 PAO patients with post-operative increases in maximum contact stress were compared to 20 patients with decreased maximum contact stress.

For these 40 patients, the pre-operative CT scan views were reoriented in 3D Slicer to obtain a view parallel to the femoral neck axis and passing through the center of the femoral head [106] (Figure 23). These orientations permitted assessment of the α-angle for cam deformity. A custom analysis routine was written in MATLAB to allow the user to accurately compute the α-angle based on the definition by Nötzli *et al.* [106] (Figure 23). The α-angle describes the angle between a vector parallel to the femoral neck axis passing through the center of the femoral head and a vector from the center of the femoral head to the anterior location where the femoral head deviates from sphericity. An orthopedic resident (Elizabeth Scott, MD) measured the α-angle three times per patient using this MATLAB algorithm. For each patient, the average of these three trials was computed and then compared to the change in maximum contact stress following PAO. Two-tailed student's t-tests and chi-squared tests were used to determine significance, set to $p<0.05$, of the relationship of α-angle to DEA-computed contact stress.

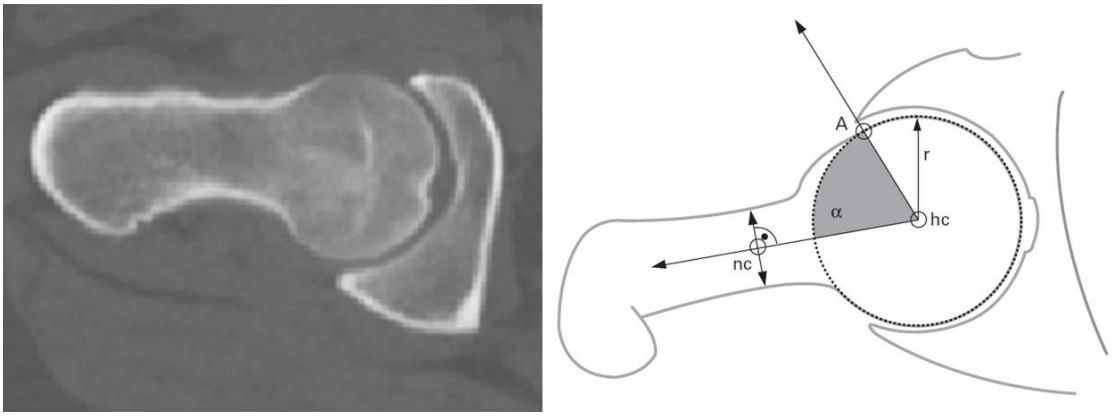

Figure 23. (Left) Reoriented pre-operative CT scan for assessing cam deformity. The plane is parallel to the femoral neck axis and passing through the center of the femoral head. (Right) α-angle measurement as defined by Nötzli et al. [106]. Briefly, a sphere is fit to the femoral head, and the sphere center is identified. A vector is drawn parallel to the femoral neck axis and passing through the center of the femoral head. Another vector is created from the center of the femoral head to the anterior location where the femoral head deviates from sphericity. The angle between these two vectors is the α-angle. A MATLAB algorithm permitted accurate identification of the vectors and α-angle.

2.7.3 Effects of Patient Age

Another advantage of our heterogenous PAO cohort is the large age range of the patients. Typical PAO patients are young, active individuals, ranging from their teens to early thirties [64, 107]. The average patient age for our cohort was 30.1 years, which agrees with the typical age range, but patients were as young as 12 years and ranged to a maximum age of 54 years. This wide range of patient ages in our PAO cohort, in combination with the pre- and post-operative contact stress assessments, could be used to further explore the effects of patient age.

Young adults are the typical candidates for PAO, as it is an elective surgery meant to alleviate pain and prevent joint degeneration. While older patients can undergo PAOs to delay total hip arthroplasty, there is likely already damage to the articular cartilage, making clinical outcomes less predictable. It is unclear how the age of the patient affects

the hip joint anatomy and mechanics and, therefore, the expected clinical outcomes. Understanding this relationship between patient age and joint mechanics would demonstrate whether all the PAO patients can be considered as one large cohort, or if the cohort should be divided into age brackets before evaluating the contact stress correlations with patient-reported outcomes.

To investigate the effects of patient age on the computed contact stress, 30 PAO patients were selected to obtain equal groups of patients based on age (less than 30 years old and greater than 30 years old) (Figure 24). Each patient's pre- and post-operative hip models were loaded with a dysplastic gait pattern [45] and analyzed using the DEA methodology to determine maximum contact stress and average contact area. To assess the level of acetabular deformity, a sphere was fit to each patient's acetabulum using a custom MATLAB program. For each acetabular vertex that did not lie on the sphere, the error between the sphere radius and the distance to the vertex was calculated. These errors were used to compute the total root-mean-square deviation (RMSD) from sphericity for the acetabulum. Relationships between contact measures, patient age and weight, and acetabular sphericity were investigated. Univariate relationships were evaluated with linear regressions, and multivariate relationships and interactions were assessed using SAS 9.4 (SAS Institute Inc, Cary, NC).

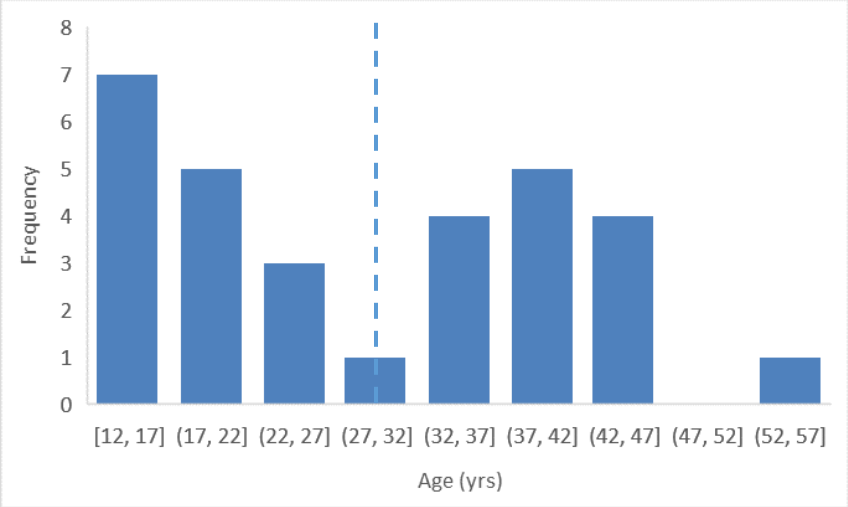

Figure 24. Histogram of patient age distribution in the 30 PAO cases. The dashed line indicates a cutoff value of 30 years to separate the two groups.

2.7.4 Comparison to the Healthy Hip Joint

In addition to understanding how patient demographics and anatomic variations affect the contact stress at the hip joint, it is also important to compare the computed contact measures in dysplastic hips to those of normal hip joints. While previous findings have indicated contact stress differences between normal and dysplastic hip joints [108, 109], comparisons of contact stress between normal and post-operative dysplastic hips have not been thoroughly investigated. The clinical assumption is that acetabular reorientation returns the dysplastic hip to a more normal articulation, thereby reducing the contact stress, but there is a lack of computational data to support this. The unique presence of post-operative CT imaging in our PAO cohort enables the post-operative contact stress computations in dysplastic hips necessary to investigate this assumption.

For this study, patient-specific hip models were created from CT scans of ten trauma patients without acetabular dysplasia, hip pain, or injury (average age = 31.3±9.2 years; average weight = 103.7±26.6 kg). The DEA methodology implementing the

Bergmann gait loading data was used to compute the contact stress during stance phase of walking gait. The contact stress results were then compared to the contact stress results of pre- and post-operative DEA calculations for ten dysplastic patients with an average age of 30.3±7.6 years and an average weight of 97.3±26.0 kg. These ten pre- and post-operative dysplastic models were also aligned to the Bergmann coordinate system and loaded with the Bergmann gait pattern to eliminate any differences in contact stress due to gait loading. The dysplastic patients were matched to the normal patients based on age, weight, and BMI. This matching scheme ensured that any differences in contact stress would result from anatomic variations between normal and dysplastic hips rather than age and weight differences. Differences between normal and dysplastic hip models are illustrated in Figure 25.

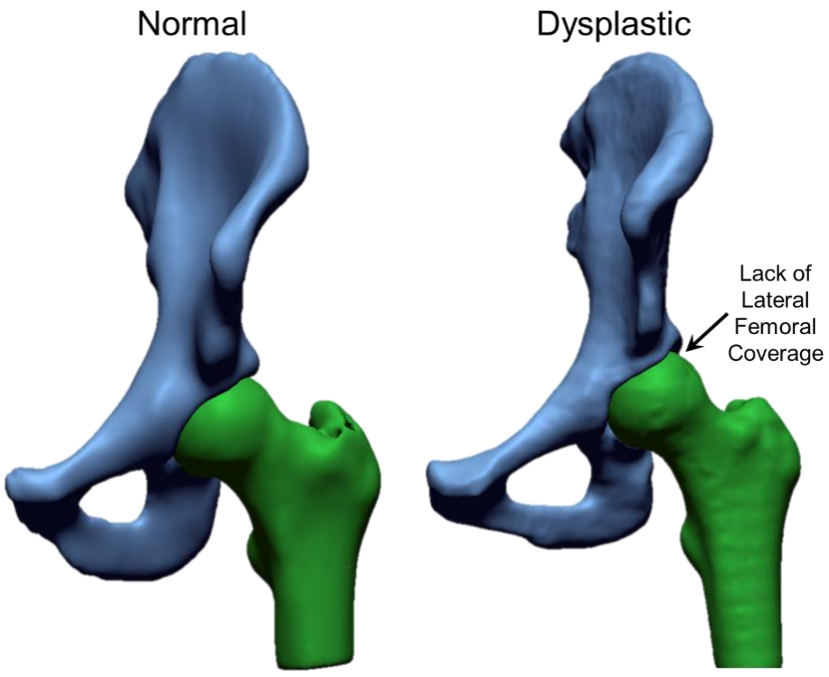

Figure 25. A normal hip model (left) compared to an age-, weight-, and BMI-matched dysplastic hip model (right) used for comparison of computed contact stress. The normal hip model has much greater acetabular coverage of the femoral head than the dysplastic hip model.

In summary, this body of work focused primarily on understanding the influence of hip joint loading patterns on the DEA-computed joint mechanics in pre- and post-operative dysplastic hips. Several illustrative studies of modeling parameters, patient-specific demographics, and anatomic variations were also conducted using this methodology with the objective of identifying factors that may contribute to the resulting contact stress distributions and the relationship to patient-reported outcomes.

CHAPTER 3: RESULTS

3.1 Influence of Gait Loading Pattern on Calculated Contact Stress and Relationship with Patient-Reported Outcomes

Notable kinematic and kinetic differences existed between the three gait patterns utilized in this work (Figure 19). Particularly, the dysplastic gait pattern subjected the models to much greater vertical reaction forces near toe-off compared to the arthritic and normal gait patterns. Subjecting the models to such different loading patterns altered the manner in which the forces were distributed across the hip joint, and thus, affected the DEA-computed contact stress.

DEA models loaded with the dysplastic gait pattern had a pre-operative maximum contact stress of 10.5±0.5 MPa, which was significantly (p=0.012) greater than the pre-operative maximum contact stress of 9.2±0.4 MPa when loading models with the normal gait pattern (Figure 27). DEA models loaded with the dysplastic gait pattern also had higher pre-operative maximum contact stress than models loaded with the arthritic gait pattern (7.4±0.4 MPa), but this difference was not quite significant (p=0.051; Figure 26). The maximum contact stress for pre-operative models loaded with the dysplastic gait pattern was higher than that computed in 25 (83%) of the pre-operative models loaded with the normal gait pattern. However, the maximum contact stress for pre-operative models loaded with the dysplastic gait pattern was only higher than that computed in 19 (63%) of the pre-operative models loaded with the arthritic gait pattern, which could explain the difference in significance levels. Additionally, the pre-operative maximum contact stress occurred at different stance positions depending on the gait pattern applied. While the maximum contact stress occurred shortly after heel-strike in models loaded

with the arthritic and normal gait patterns, the maximum contact stress shifted toward toe-off when implementing dysplastic loading, which corresponds with the increased superior loading near toe-off with dysplastic gait.

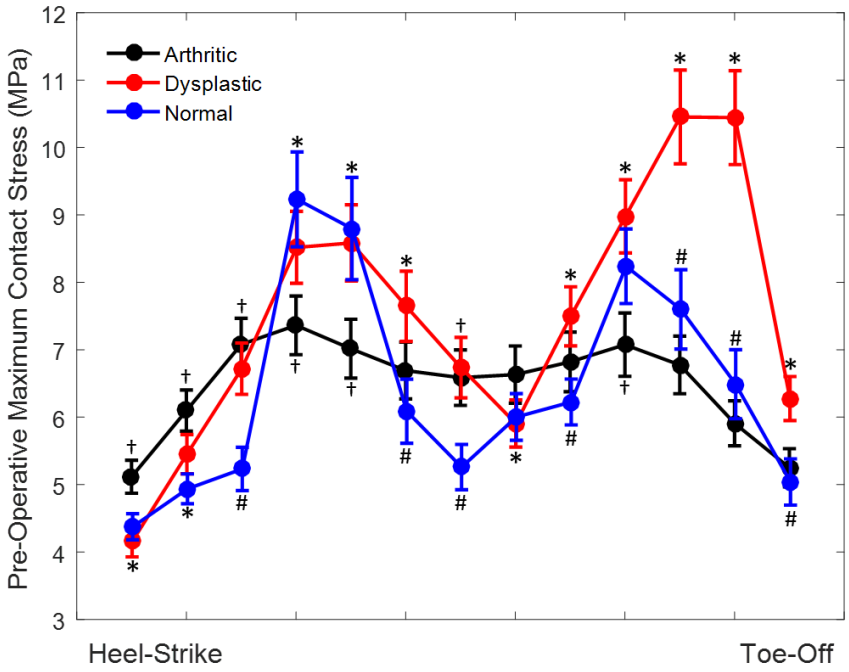

Figure 26. DEA models loaded with the dysplastic gait pattern experienced a pre-operative maximum contact stress near toe-off, whereas the models loaded with normal or arthritic gait patterns experienced a maximum contact stress shortly after heel-strike. Force and rotation differences between gait patterns alter the maximum contact stress magnitude and its time position during stance phase of gait. *dysplastic vs. arthritic, $p<0.05$. #dysplastic vs. normal, $p<0.05$. †arthritic vs. normal, $p<0.05$.

Models loaded with dysplastic gait had a pre-operative mean contact area of 814 mm^2, which was not significantly different (p=0.11 and p=0.073) from the mean contact areas of 787 mm^2 and 865 mm^2 for models utilizing arthritic and normal gaits, respectively (Figure 27). This lack of significant difference indicates that the increased contact stresses result from differences in applied forces and how they are transferred across the joint.

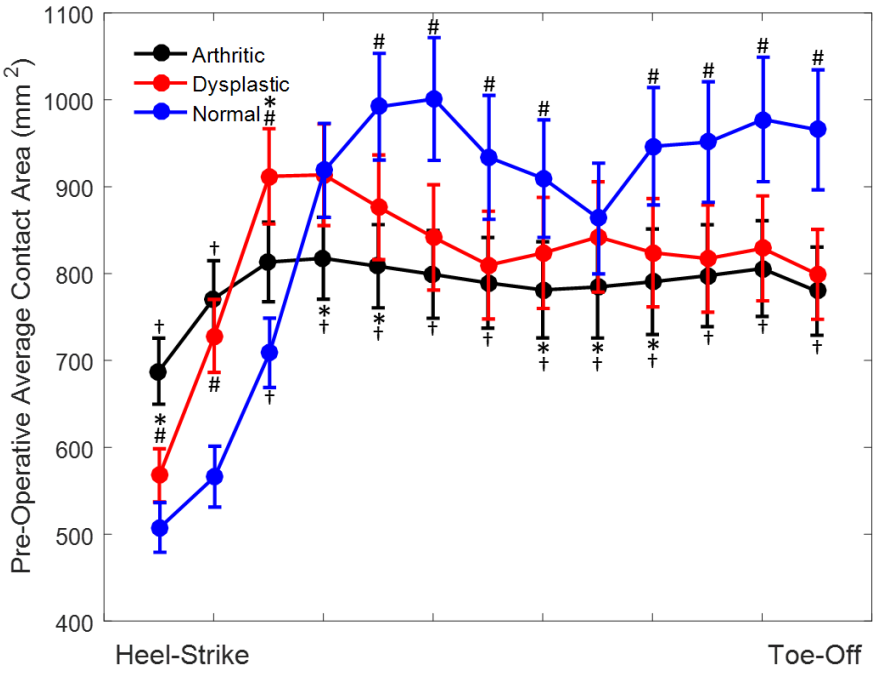

Figure 27. All three gait patterns used to load the DEA models produced the lowest contact area at heel-strike, with the normal gait producing the lowest contact area. The greatest contact area occurred closer to midstance, with the normal gait producing the greatest area. The arthritic gait pattern produced the lowest contact area throughout the majority of stance. While significant differences in contact area between the gait pattern exist at various timepoints, the average contact area over the entire stance phase of gait was not significantly different between gait patterns. *dysplastic vs. arthritic, $p<0.05$. #dysplastic vs. normal, $p<0.05$. †arthritic vs. normal, $p<0.05$.

Following PAO, DEA models loaded with the dysplastic gait pattern had an average decrease in maximum contact stress of 0.7±0.4 MPa, which is significantly ($p<0.001$) different from increases of 0.5±0.6 MPa and 1.3±0.6 MPa when utilizing the arthritic and normal gait patterns, respectively (Figure 28). An example of the differences in contact stress distributions between gait cycle loadings is shown in Figure 29.

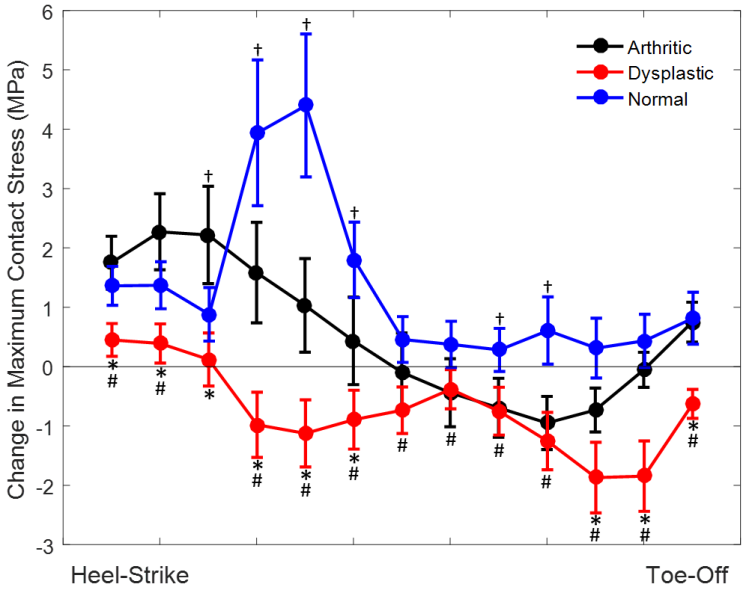

Figure 28. DEA models loaded with the dysplastic gait pattern had an average decrease in maximum contact stress after PAO, which was significantly ($p<0.001$) different from the increases in maximum contact stress for models loaded with arthritic and normal gait patterns. The arthritic gait pattern increased the contact stress near heel-strike but decreased the contact stress shortly before toe-off. The normal gait pattern produced a large increase in contact stress at steps 4 and 5 of the gait cycle. *dysplastic vs. arthritic, $p<0.05$. $^{\#}$dysplastic vs. normal, $p<0.05$. †arthritic vs. normal, $p<0.05$.

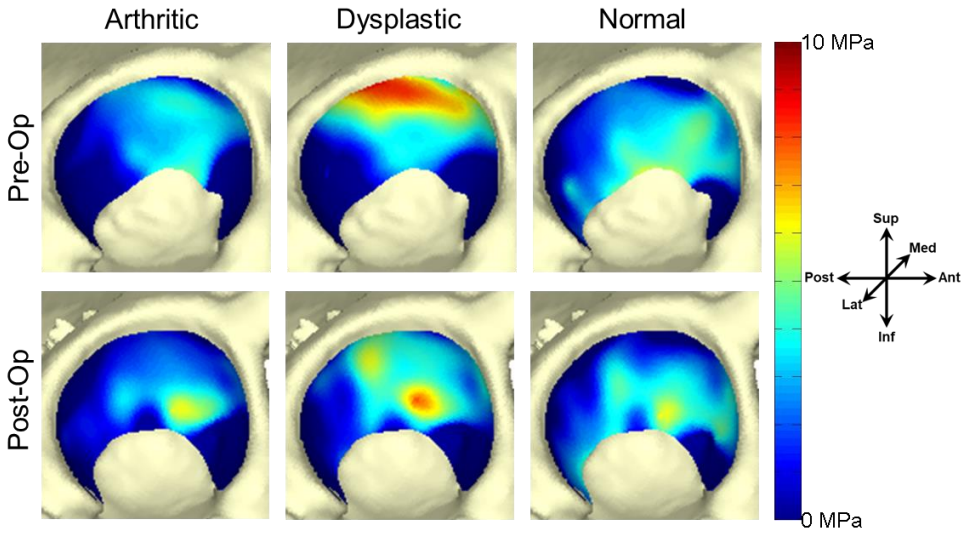

Figure 29. Pre- and post-operative contact stress distributions computed with all three gait patterns in a single dysplastic patient overlaid on the corresponding hip models. Dark blue color indicates no contact between the acetabular and femoral cartilage surfaces at that location. Loading this patient's DEA models with the dysplastic gait pattern resulted in decreased and medialized maximum contact stress after PAO, indicating improved joint mechanics.

Models loaded with the dysplastic gait pattern had an average decrease in contact area of 15 mm^2 compared to average decreases of 29 mm^2 (p=0.33) and 126 mm^2 (p<0.001) when utilizing the arthritic and normal gaits, respectively (Figure 30). This is counterintuitive to the clinical expectation that PAO improves the contact area of the hip joint to reduce pain and contact stress. However, in these thirty patients, only 14 (47%) hips had a post-operative increase in average contact area when loaded with the dysplastic gait pattern. Similarly, when loaded with the arthritic and normal gait patterns, only 12 (40%) and 5 (17%) hips, respectively, had an increase in average contact area.

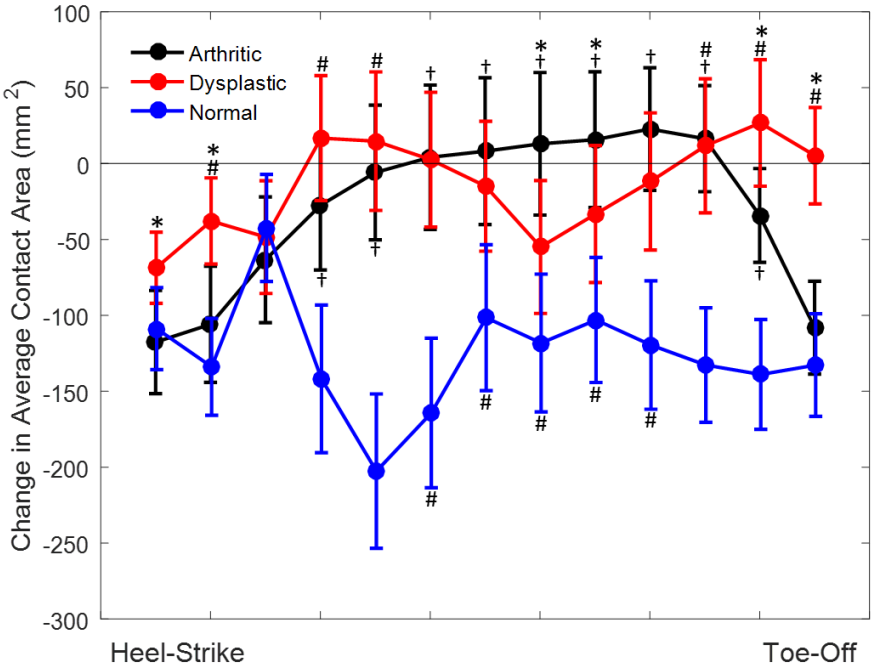

Figure 30. DEA models loaded with the dysplastic gait pattern had a greater average contact area than models loaded with arthritic and normal gaits. The dysplastic gait pattern increased the contact area near toe-off, which should assist in counteracting the high contact stresses at that location. The arthritic gait increased contact area near midstance but greatly decreased contact area at heel-strike and toe-off. The normal gait produced a decrease in contact area at every position during stance phase of gait. *dysplastic vs. arthritic, p<0.05. #dysplastic vs. normal, p<0.05. †arthritic vs. normal, p<0.05.

In addition to investigating the effect of gait pattern on the DEA-calculated contact stress and area, these contact measures were correlated to radiographic measures and patient-reported outcome scores. Accurate knowledge of the relationship between contact measures and patient-reported outcomes has the potential to assist orthopaedic surgeons in pre-operative PAO planning, which can lead to further improved patient outcomes. Models loaded with the dysplastic gait pattern had an improved correlation between the change in maximum contact stress and change in lateral center edge angle ($R^2 = 0.385$) compared to models loaded with arthritic and normal gaits (Figure 31; $R^2 = 0.147$ and $R^2 = 0.038$, respectively). Similarly, implementing the dysplastic gait loading also improved the correlation of the change in maximum contact stress with the change in Tönnis angle (Figure 31; $R^2 = 0.296$) and the change in extrusion index (Figure 31; $R^2 = 0.227$).

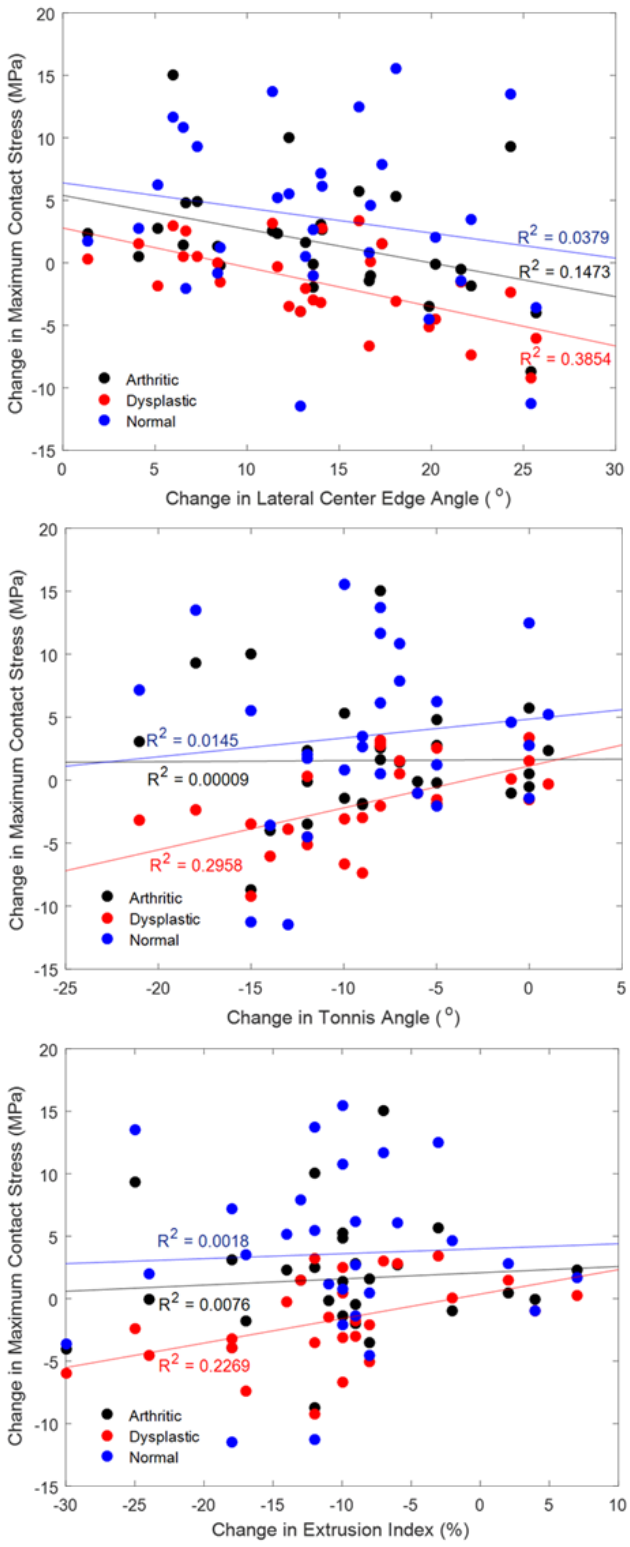

Figure 31. The correlations between the change in DEA-calculated maximum contact stress and the change in lateral center edge angle (left), change in Tönnis angle (middle), and change in extrusion index from radiographic measurements all improve when loading DEA models with dysplastic gait.

Models loaded with the dysplastic gait pattern had an improved correlation between pre-operative maximum contact stress and pre-operative VAS pain score (R^2 = 0.082) compared to models loaded with arthritic and normal gaits (Figure 32; R^2 = 0.006 and R^2 = 0.018, respectively). No meaningful correlations were found between post-operative maximum contact stress and post-operative VAS pain score for any of the gait patterns (highest R^2 = 0.0028). While no strong correlations were found between the change in maximum contact stress and the change in VAS score, more PAO cases had the expected clinical results of decreased stress and decreased pain (indicated by green quadrant outline) when loading models with the dysplastic gait pattern (Figure 33). Similarly, for cases that had both pre- and post-operative WOMAC and SF-36 outcome scores, more cases had decreased stress and increased function and increased quality-of-life when loading DEA models with the dysplastic gait pattern (Figure 33).

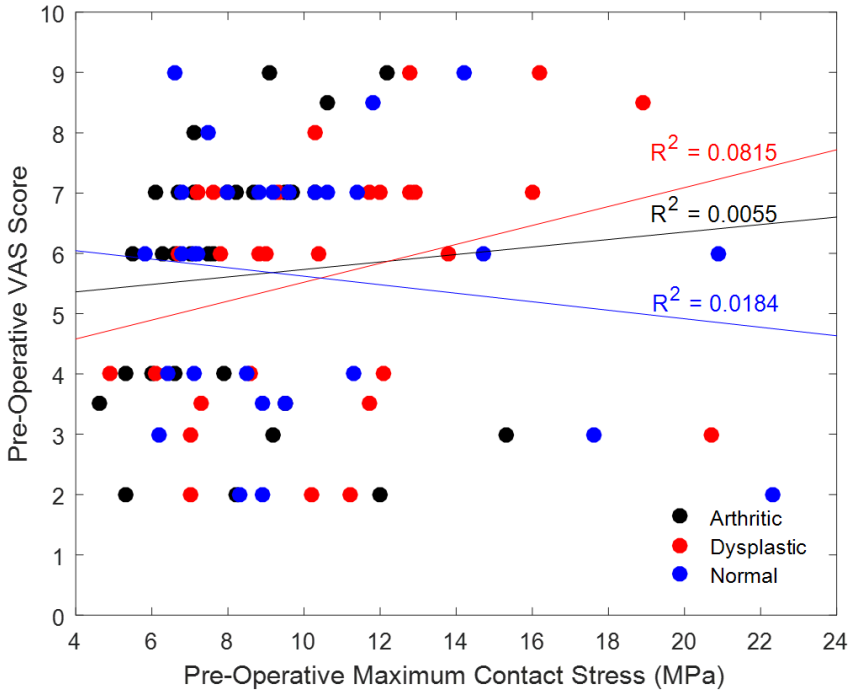

Figure 32. The correlation between pre-operative maximum contact stress and pre-operative VAS pain score improves when loading DEA models with the dysplastic gait pattern.

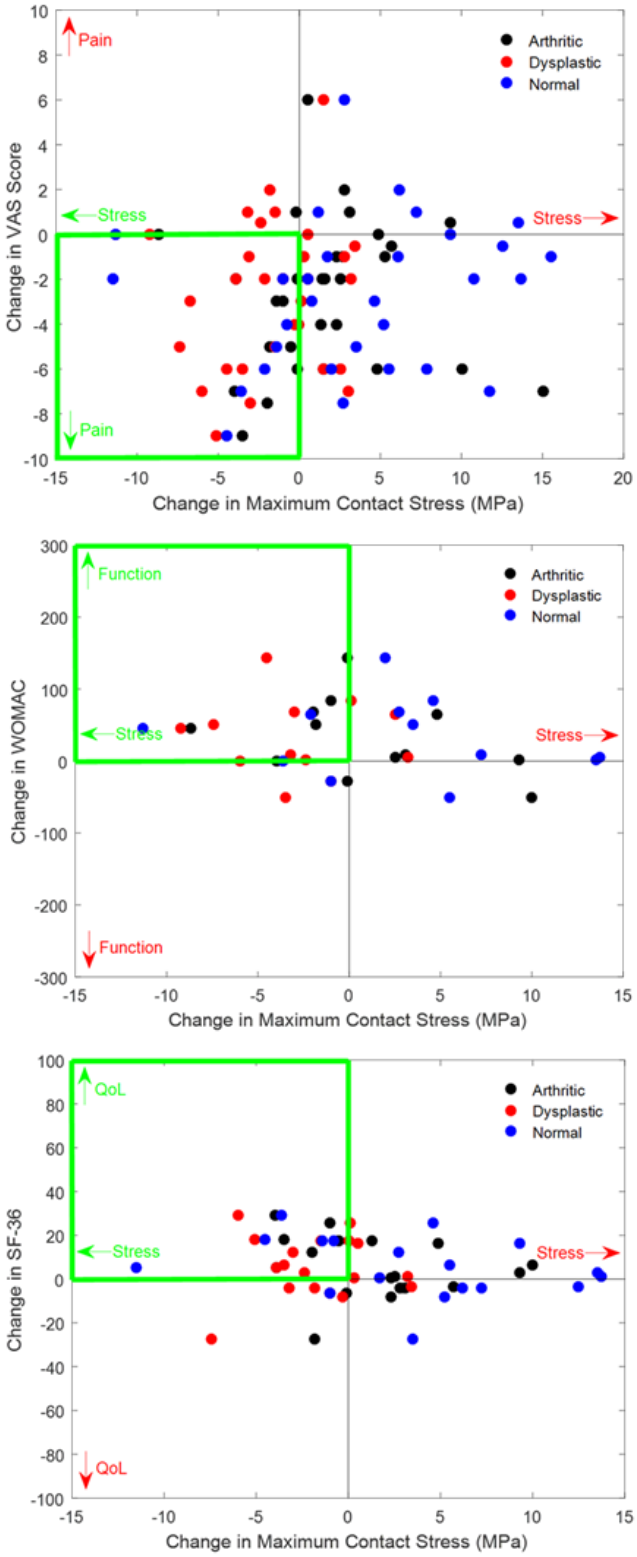

Figure 33. More patient models are within the "ideal quadrant" (green box), indicating improved patient-reported outcomes after PAO, when loaded with dysplastic gait. Vertical axes include all possible values for changes in patient-reported outcomes scores.

3.2 Contact Stress Correlation to Acetabular Center of Rotation

In addition to investigating how the gait pattern used to load the dysplastic models influences the DEA-computed joint mechanics, it was also of interest to understand the effects of anatomic variations and patient demographics on the computed contact stress. To investigate how alterations to the acetabular center of rotation affect contact stress, a sphere-fitting technique was used to identify the acetabular center of rotation in 15 pre- and post-operative hip models of patients indicated to have only lateral coverage deformities. Changes in mediolateral, anteroposterior, and superoinferior positions of the acetabular center of rotation were calculated and correlated with changes in DEA-calculated contact measures.

The average maximum pre-operative contact stress for these 15 PAO patients was 10.6±0.6 MPa, which was significantly (p=0.0028) greater than the average maximum post-operative contact stress of 8.2±0.5 MPa (Figure 34). Average contact area was not significantly different from pre-operative values after a PAO (713 mm^2 vs 759 mm^2).

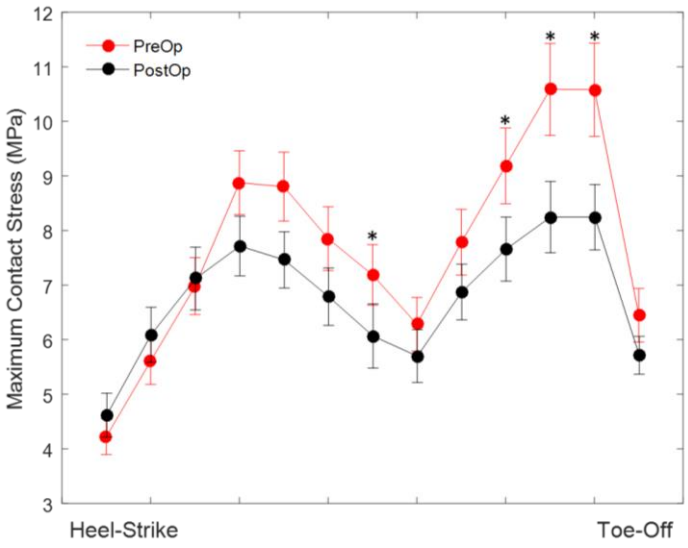

Figure 34. The average maximum contact stress decreased significantly (p=0.0028) following PAO. * pre-op vs. post-op, p<0.05.

Following deformity correction with PAO, the acetabular center of rotation moved an average of 4 mm both medially and anteriorly, which was significantly different (p<0.001) from the pre-operative location in both directions. The average acetabular center of rotation also moved 0.2 mm inferiorly, but this change was not significant (Figure 35).

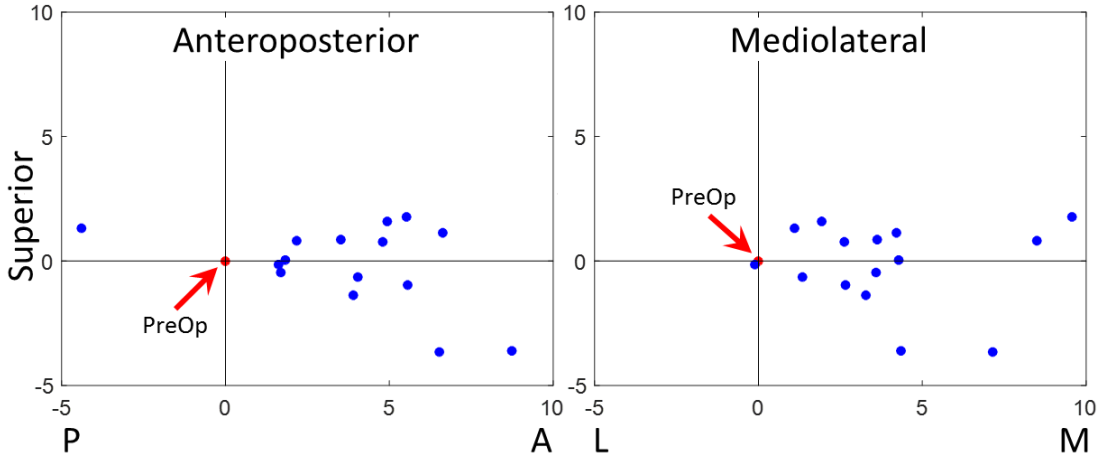

Figure 35. All pre-operative hips were aligned at the origin (indicated in red). Change in medial, anterior, and superior positions of the acetabular center of rotation are represented for each of the 15 cases. On average, the acetabular center of rotation moved 4 mm medially (p<0.001), 4 mm anteriorly (p<0.001), and 0.2 mm inferiorly.

Post-operative medialization of the acetabular center of rotation was negatively correlated (R^2 = 0.296) with maximum post-operative contact stress. Post-operative movement of the acetabular center of rotation anteriorly was also associated with decreasing the maximum contact stress (R^2 = 0.018); however, this low correlation was not considered meaningful in comparison to the much higher correlation between medialization and contact stress (Figure 36). This difference between the effect of medial and anterior movement on the resulting contact stress is also illustrated in the representative contact stress distributions (Figure 37).

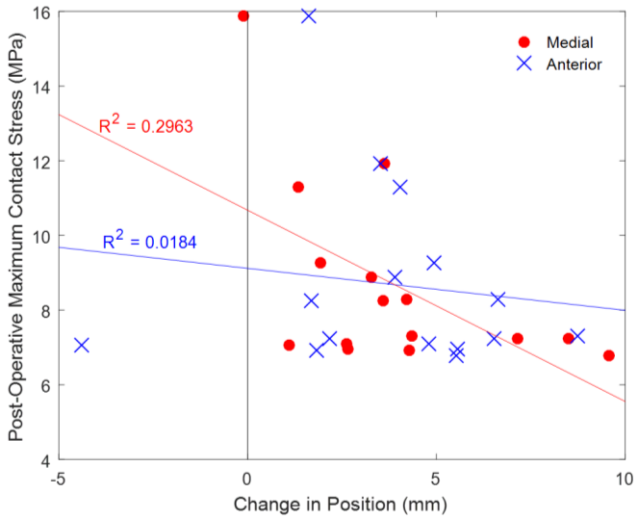

Figure 36. Changes in medial and anterior position of the acetabular center of rotation were compared with post-operative maximum contact stress. A positive change in position indicates a more medialized (red) or anteriorized (blue) center of rotation. Change in medialization of the acetabular center of rotation negatively correlates with the change in maximum post-operative contact stress. Anteriorization of the center of rotation does not appear to relate to changes in contact stress.

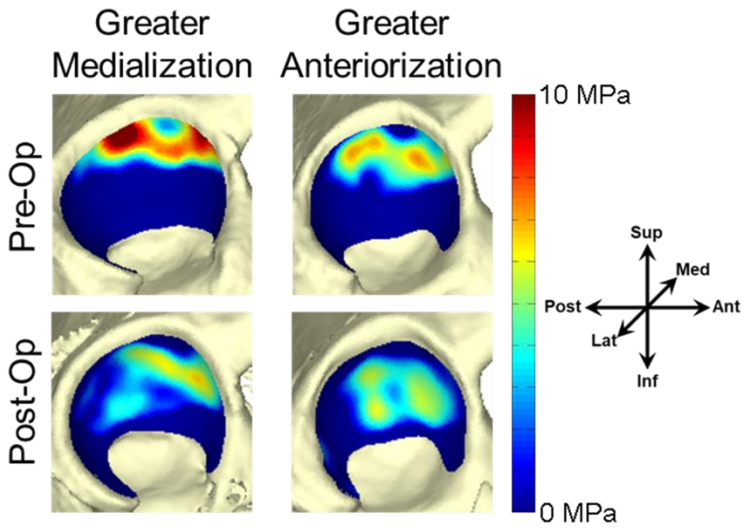

Figure 37. Pre- and post-operative contact stress distributions overlaid on the corresponding hip models for two dysplastic patients. (Left) A hip model with greater medialization than anterior movement of the center of rotation. (Right) A hip model with greater anterior movement than medialization of the center of rotation. Dark blue color indicates no contact between the acetabular and femoral cartilage surfaces at that location. The hip model with greater medialization had a much greater reduction in contact stress after PAO. Greater anterior movement did not have a large effect on the contact stress following PAO.

The relationship between acetabular center of rotation and VAS pain score was also investigated to determine if this biomechanical information should be included in a surgeon's pre-operative planning routine to improve patient outcomes. The average VAS pain score also decreased significantly (p<0.001) post-operatively from 5.7±0.5 to 2.4±0.6, but this did not correlate with acetabular center of rotation.

3.3 Contact Stress Correlation to Femoral Deformity

The patients in our heterogeneous PAO cohort were not separately assessed for femoral deformities, and the presence of such deformities may contribute to less than ideal patient outcomes. To investigate whether the presence of femoral deformities was associated with increased post-operative contact stress, 20 PAO patients with post-operative increases in maximum contact stress were matched with 20 patients with decreased maximum contact stress. Reoriented CT scan images were used to measure the α-angle for each patient, which was then compared to the change in contact stress.

Some of the dysplastic hips with increased maximum contact stress demonstrated this increase in a non-weight bearing location on the acetabular cartilage, which could be indicative of impingement (Figure 38). Dysplastic hips that had increased maximum contact stress after PAO had significantly (p=0.006) greater α-angles (51°±11.4°) than dysplastic hips with decreased maximum contact stress after PAO (42°±5.1°). The change in contact stress had the best correlations with α-angle (Figure 39; R^2 = 0.091) and post-operative extrusion index (Figure 39; R^2 = 0.098). Interestingly, the change in contact stress was found to be the most variable for the α-angle range of 40°-50° (Figure 39), indicating greater outcome variability for borderline deformity cases. Cam deformity

(defined as α-angle > 50°) was observed in 7/20 (35%) of dysplastic hips with increased contact stress after PAO, compared to only 1/20 (5%) of dysplastic hips with decreased contact stress after PAO. Dysplastic hips with increased contact stress were found to be 10.23 times as likely to have a cam deformity than hips with decreased contact stress (p=0.039). After PAO, all patients had an increased lateral center edge angle and correction of a posterior wall sign (when present), indicating improved radiographic acetabular orientation. These results indicate that a femoral deformity not addressed at the time of PAO may lead to increased post-operative contact stress. Therefore, PAO patients should be assessed pre-operatively for the presence of femoral deformities to ensure that the mechanical environment of the joint is improved post-operatively.

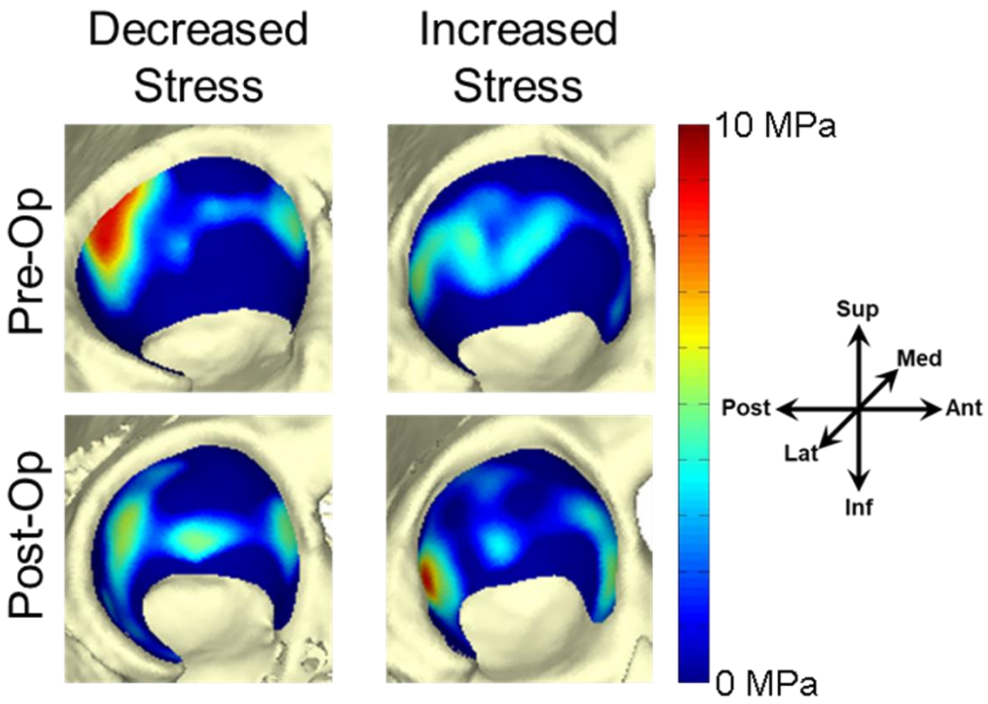

Figure 38. Pre- and post-operative contact stress distributions overlaid on the corresponding hip models for two dysplastic patients. Dark blue color indicates no contact between the acetabular and femoral cartilage surfaces at that location. (Left) A hip model with decreased stress following PAO. (Right) A hip model with increased stress following PAO. This increase in stress occurs in a non-weight bearing location on the acetabular cartilage, which could be indicative of impingement with a femoral cam deformity.

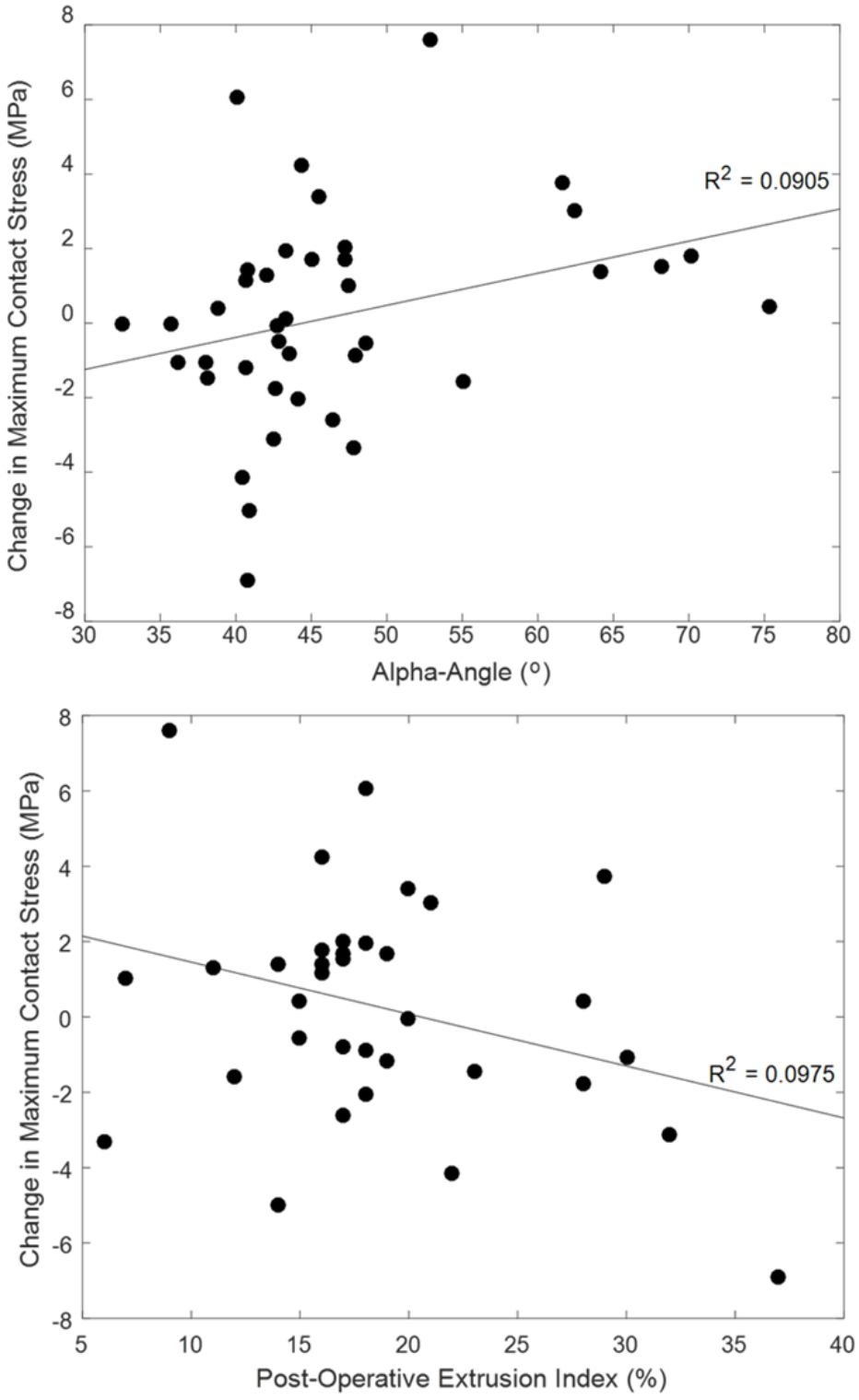

Figure 39. α-angle positively correlates with change in maximum contact stress following PAO (left), while extrusion index negatively correlates with change in maximum contact stress (right). These results demonstrate the potential for unaddressed femoral deformity to impinge on the reoriented acetabulum and increase the stress on the hip joint.

3.4 Contact Stress Correlation to Patient Demographics

While young adults are the typical candidates for PAO, older adults can undergo the procedure to delay total hip arthroplasty. However, there is likely already cumulative damage to the articular cartilage, making clinical outcomes less predictable. To investigate how patient age relates to computed contact stress, hip models of 15 young adults (age = 18.8±4.6 years) and 15 older PAO patients (age = 40.2±6.6 years) were analyzed with DEA. Average maximum pre-operative contact stress was 13.6±0.9 MPa for the older patients, which was significantly (p<0.001) higher than for the younger patients (8.9±0.5 MPa; Figure 40). After PAO, the average maximum contact stress decreased to 7.6±0.6 MPa in the older patients, which was a significant (p<0.001) decrease from the average pre-operative maximum contact stress. Yet, even this significantly decreased contact stress was still significantly (p<0.001) higher than the maximum contact stress for the younger patients (6.8±0.4 MPa; Figure 41).

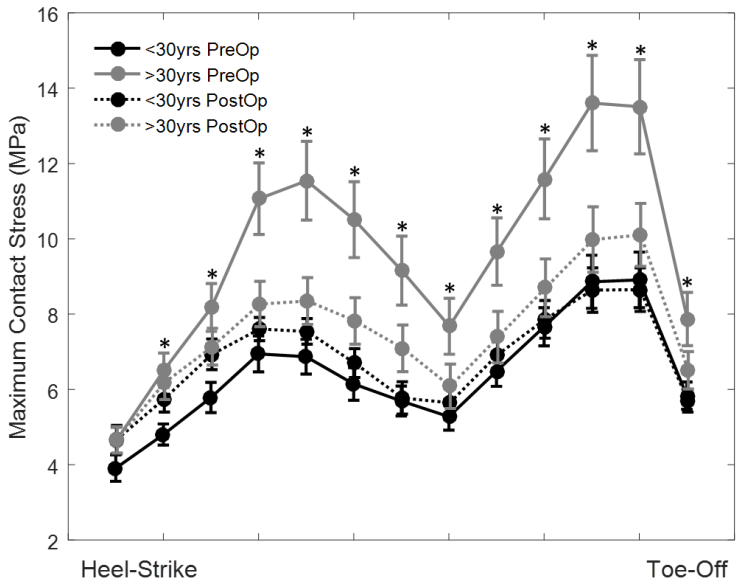

Figure 40. Maximum pre-operative contact stress significantly (*p<0.05) differs between patients <30 yrs and >30 yrs. Maximum post-operative contact stress does not significantly differ between age groups.

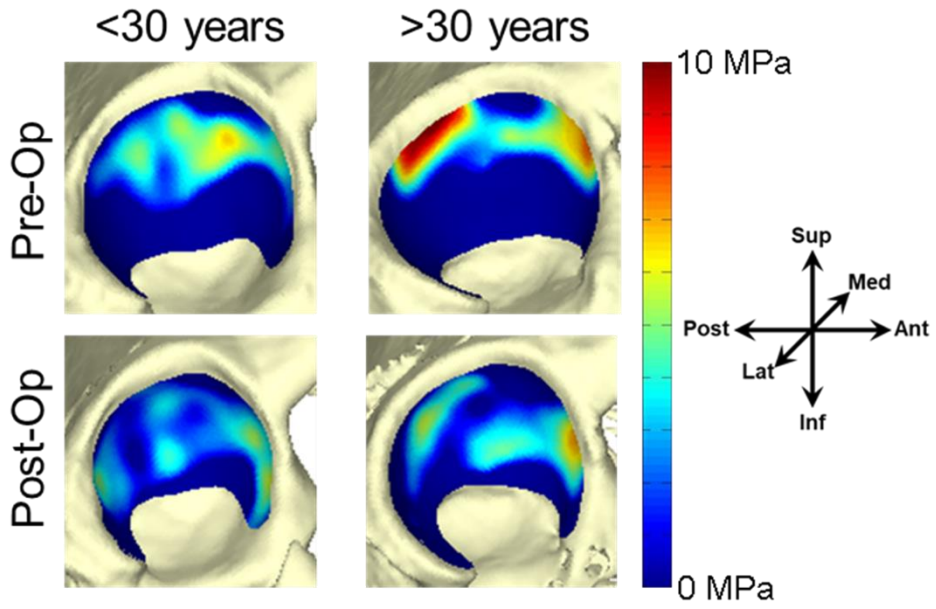

Figure 41. Pre- and post-operative contact stress distributions overlaid on the corresponding hip models for two dysplastic patients. Dark blue color indicates no contact between the acetabular and femoral cartilage surfaces at that location. (Left) A hip model for a patient under the age of 30 years at the time of PAO. (Right) A hip model for a patient over the age of 30 years at the time of PAO. The patient over the age of 30 years had a much higher pre-operative contact stress than the younger patient. PAO decreased the maximum contact stress in the older patient, but this decreased stress was still higher than the maximum contact stress in the younger patient.

The average pre-operative contact area in older patients was 702±83 mm^2, which was significantly ($p<0.001$) lower than that for the younger patients (810±78 mm^2). However, following PAO, the average contact area in the older patients increased significantly ($p<0.001$) to 782±57 mm^2, which was also significantly ($p=0.002$) greater than the average contact area (750±70 mm^2) in the younger patients (Figure 42).

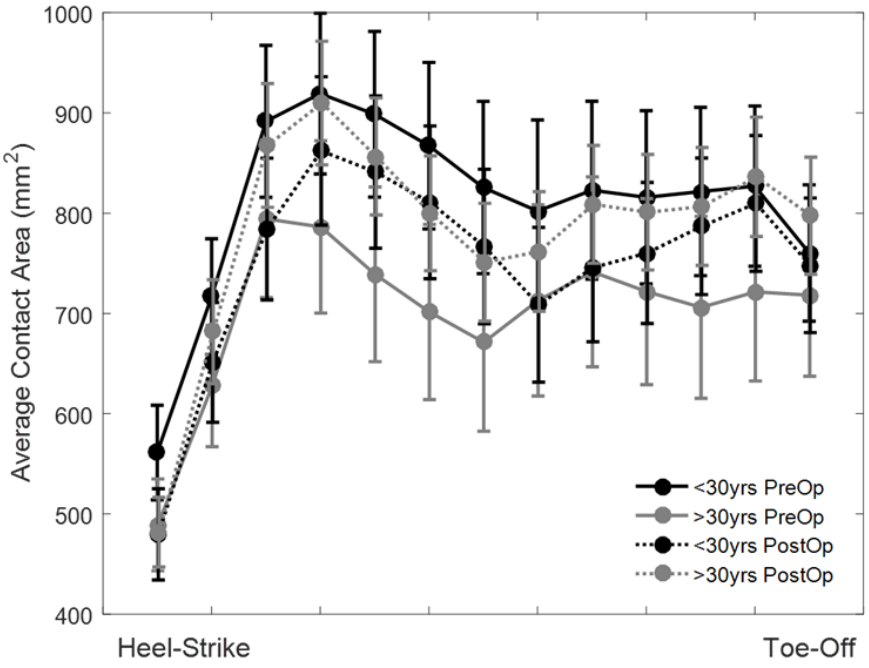

Figure 42. Over the entire stance phase of gait, average pre-operative contact area is significantly ($p<0.001$) greater in patients <30 yrs than patients >30 yrs. After PAO, average contact area is significantly ($p=0.002$) greater in patient >30 yrs than patients <30 yrs over the entire stance phase of gait.

These results indicate that there are significant differences in contact stress associated with the age of the PAO patient. However, other patient factors may also be contributing to these significant differences. Usually, patients that are in their teens weigh less than patients in their forties; thus, it was unknown if the contact stress differences were caused solely by higher applied forces. Additionally, older dysplastic patients have been subjecting their joints to altered loading for a longer period of time, which may have caused bony remodeling to occur. Such remodeling would result in a less spherical acetabulum which could cause focal elevations in contact stress. Therefore, further investigation of the effects of patient weight and deviation from acetabular sphericity on computed contact stress was conducted.

There were significant univariate correlations between maximum pre-operative contact stress and patient weight (p=0.012), deviation from acetabular sphericity (p=0.007), and pre-operative VAS pain score (p=0.02; Figure 43). The deviation from acetabular sphericity was significantly (p=0.023) greater for older patients (0.99 mm) than younger patients (0.78 mm). There were significant correlations between patient age and weight (p=0.04), patient age and deviation from acetabular sphericity (p=0.0014), and patient weight and deviation from acetabular sphericity (p=0.03; Figure 44).

Furthermore, a significant multivariate interaction was found between patient weight and deviation from acetabular sphericity. A significant correlation existed between maximum pre-operative contact stress and the combined metric of patient weight and deviation from acetabular sphericity (p=0.0013). Patient age significantly correlated with the combined metric of patient weight and deviation from acetabular sphericity (p=0.0014).

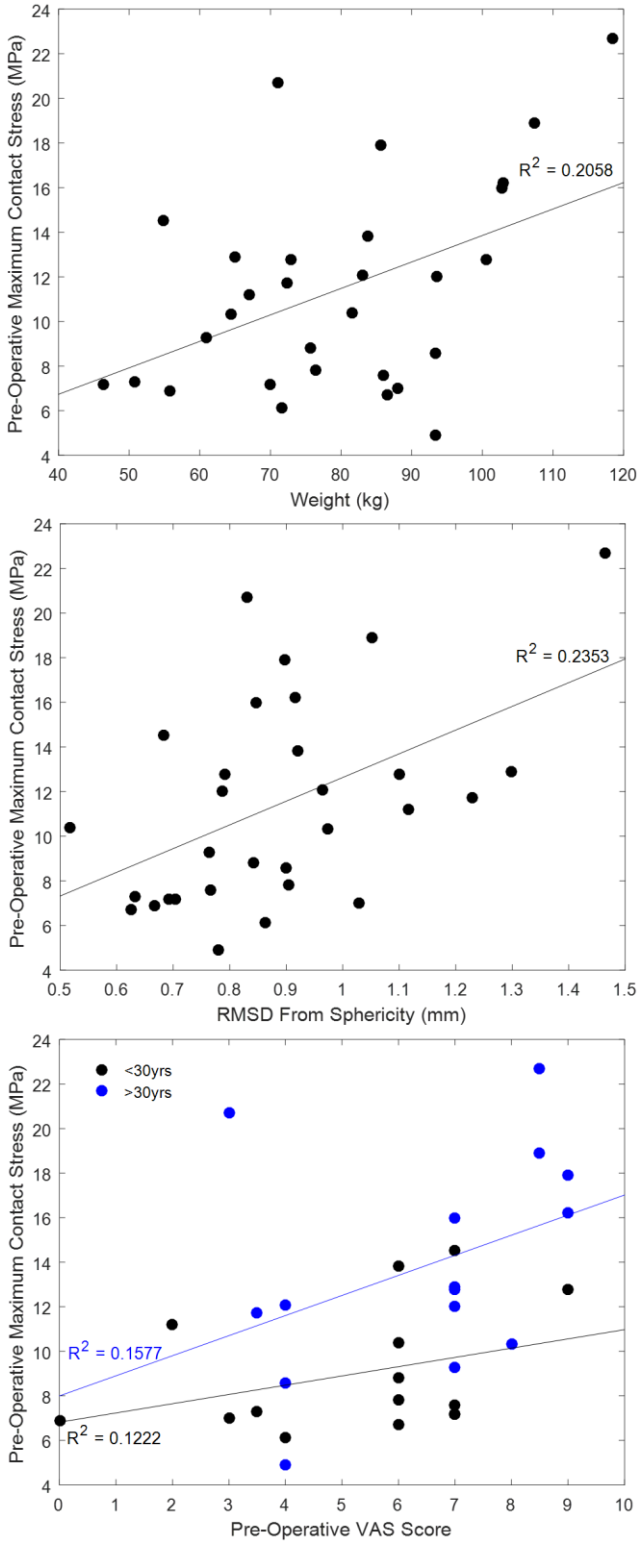

Figure 43. Patient weight (top), deviation from acetabular sphericity (middle) and pre-operative VAS pain scores for both age groups (bottom) significantly (p=0.012, p=0.007, and p=0.02, respectively) correlate with pre-operative maximum contact stress.

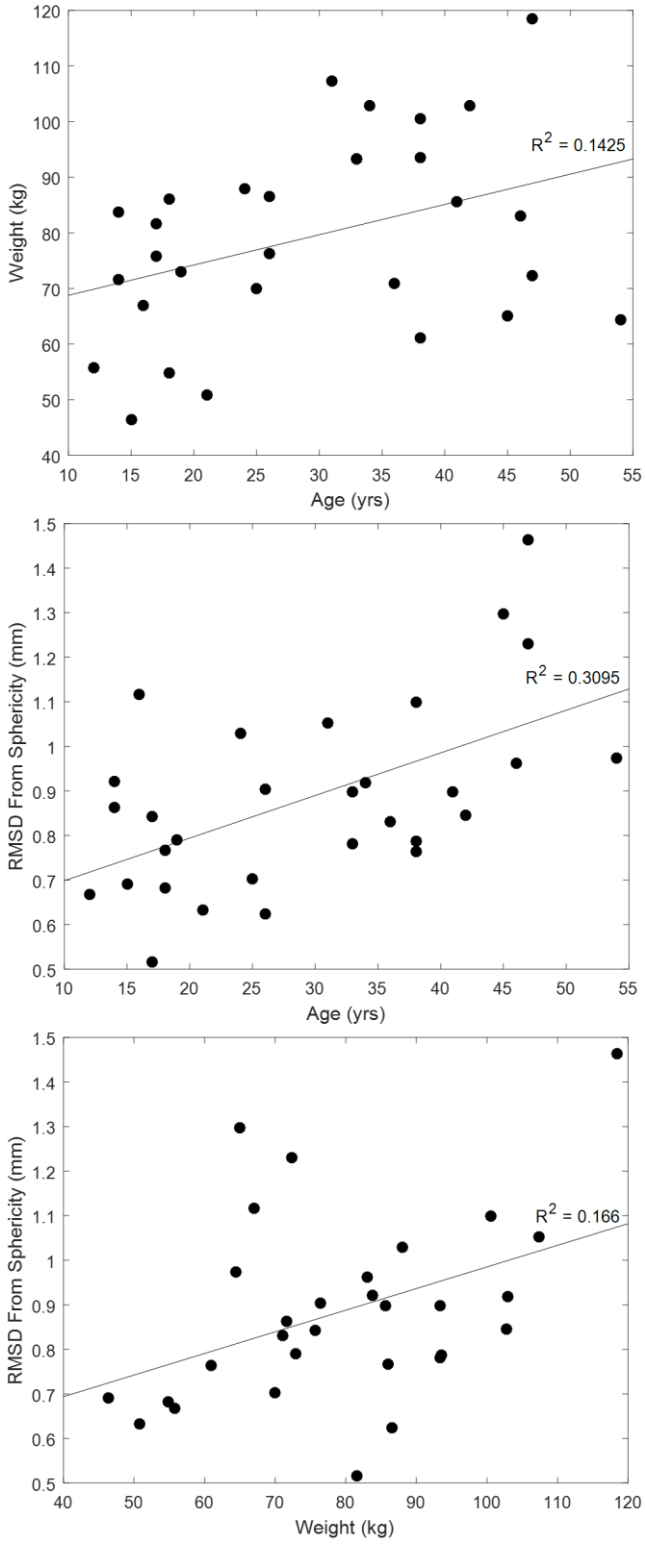

Figure 44. Patient weight (top) and deviation from acetabular sphericity (middle) significantly (p=0.04 and p=0.0014, respectively) correlate with patient age. Patient weight also significantly (p=0.03) correlates with deviation from acetabular sphericity (bottom).

3.5 Contact Stress Comparison to the Healthy Hip Joint

Finally, it was important to compare the computed contact measures in dysplastic hips to those of normal hip joints and evaluate whether contact measures in dysplastic hips normalize post-operatively. To make this comparison, ten normal hips (average age = 31.3±9.2 years; average weight = 103.7±26.6 kg) and ten dysplastic hips (average age = 30.3±7.6 years; average weight = 97.3±26.0 kg) were loaded with the Bergmann gait pattern and analyzed with DEA to obtain contact measures. The maximum contact stress for DEA models of normal hips was 7.2±0.7 MPa, which was significantly (p<0.001) lower than the pre-operative maximum contact stress of 10.0 ±1.1 MPa for DEA models of dysplastic hips. These results are similar in magnitude to previous findings of increased contact stress in dysplastic hips compared to normal hips [108, 109]. Furthermore, the dysplastic hips had on average 28.6% less contact area and 38.2% greater maximum contact stress than normal hips, which is very similar to differences found in a previous study [22]. In addition to the significant difference in magnitude of these contact stresses, the time during stance phase of gait at which the maximum contact stress occurred differed greatly, with the dysplastic hips having much higher stress near toe-off than the normal hips (Figure 45). Mean contact area for DEA models of normal hips was 1184±145 mm^2, which was significantly (p<0.001) greater than that for DEA models of pre-operative dysplastic hips (845±64 mm^2; Figure 46).

When the dysplastic hips were analyzed with DEA post-operatively, the maximum contact stress had actually increased slightly to 10.1±1.6 MPa. However, the increase in pre-operative maximum contact stress near toe-off decreased after PAO (Figure 47), resulting in a normalized timing of maximum contact stress during stance

phase of gait (Figure 45). Mean contact area increased to 906±88 mm^2 after PAO, but this was still significantly (p<0.001) less than contact areas calculated for DEA models of normal hips (Figure 46).

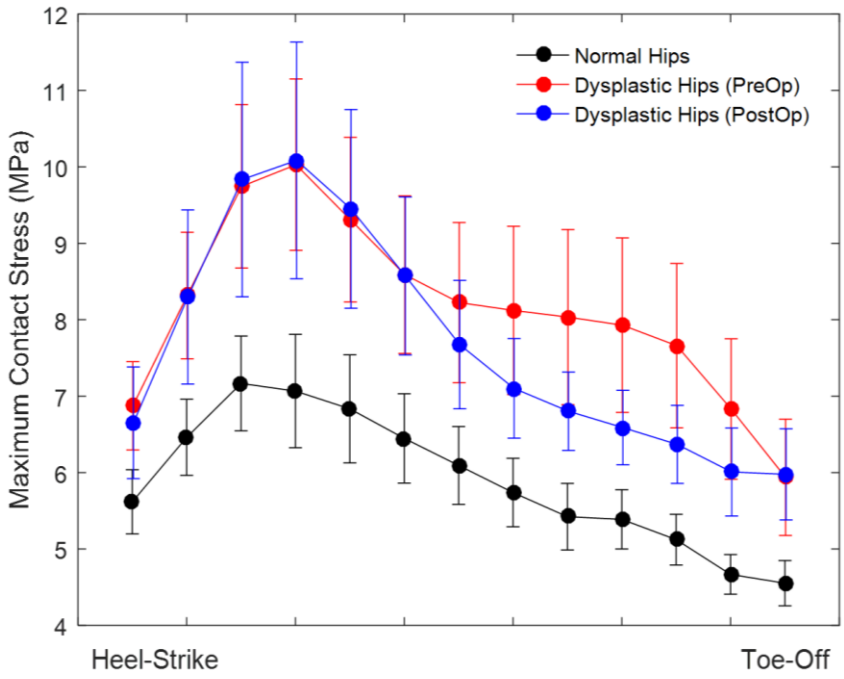

Figure 45. Maximum contact stress throughout stance phase of gait in normal and dysplastic hip models. Pre-operative dysplastic models have increased maximum contact stress near toe-off. Following PAO, this increase in stress is resolved, and the timing of maximum contact stress during stance phase of gait is normalized. Even with this normalization in timing, the magnitude of the maximum contact stress in post-operative dysplastic hips does not return to normal levels.

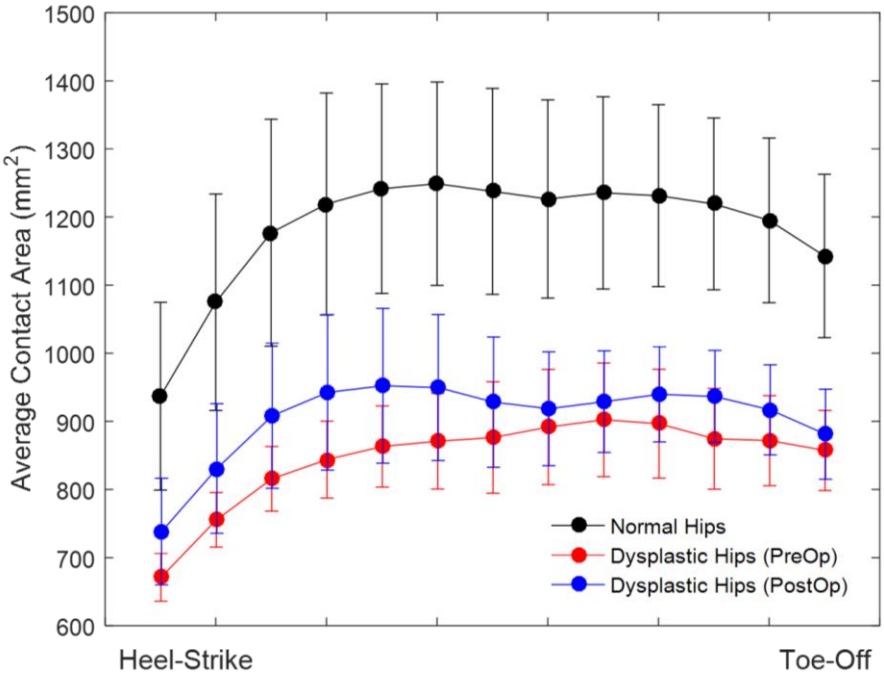

Figure 46. Average contact area throughout stance phase of gait in normal and dysplastic hip models. Even though the average contact area in dysplastic hips increases following PAO, it does not return to normal levels.

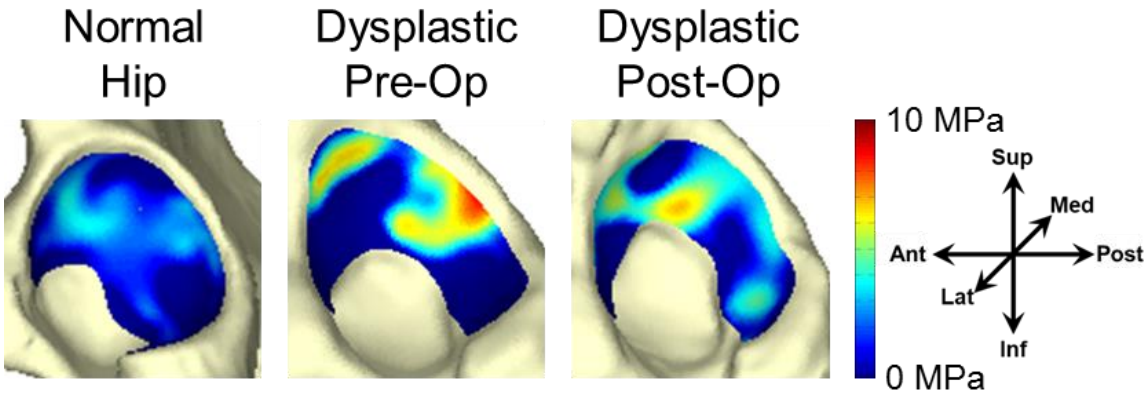

Figure 47. (Left) A contact stress map from a trauma patient's hip with no history of dysplasia, pain, or injury. (Middle) A contact stress map for a hip dysplasia patient pre-operatively (Right) and post-operatively. Dark blue color indicates no contact between the acetabular and femoral cartilage surfaces at that location. The pre-operative dysplastic hip had much greater maximum contact stress than the normal hip. While PAO decreased the maximum contact stress in the dysplastic hip, the contact stress did not return to normal levels.

CHAPTER 4: DISCUSSION

The objective of this thesis was to understand how the gait loading of dysplastic models, as well as patient-specific demographics and anatomic variations, influence the DEA-computed hip joint mechanics. This understanding would constitute an improvement on current DEA modeling methods and further general knowledge of dysplastic joint mechanics in the field of orthopaedic research. The long-term objective of this line of work is to relate this biomechanical data with clinical measures of treatment success (i.e. radiographic measurements, patient-reported outcomes).

It was found that dysplastic loading subjects the hip joint to much higher vertical reaction forces near toe-off compared to the arthritic and normal gait loading, which has serious implications for the mechanical environment in the joint. Abnormal mechanics as a result of deformed anatomy and altered loading can increase the contact stresses on the hip joint, which can lead to early development of osteoarthritis. A better understanding of the mechanics that result from variations in gait loading, patient demographics, and acetabular and femoral anatomy can assist in guiding surgical pre-operative planning and evaluating how the planned acetabular reorientation will affect joint mechanics and patient-reported outcomes.

With the long-term objective of correlating contact mechanics with patient-reported outcomes, this work focused on understanding how model loading parameters and anatomic and demographic factors contributed to the DEA-computed contact stress. It was hypothesized that implementing a gait pattern measured from patients with hip dysplasia would produce contact stress patterns that were more realistic for that patient population. The decision about what is the correct loading was limited by the lack of

ability to directly measure contact stress in living patients. Therefore, the choice of best DEA loading regimen was selected based on obtaining results that best relate to clinical assumptions of improved function and outcomes with a mechanically improved joint. As a followup to this primary investigation, several focused studies on other anatomic and demographic factors contributing to calculation of contact stress were performed. By understanding how these other factors contribute to the computed contact mechanics, the large PAO cohort can be broken down into refined groups based on these factors before performing DEA analysis, thus maximizing the chances of identifying meaningful relationships between surgically altered joint mechanics and patient-reported outcomes.

4.1 Validity of DEA for Contact Stress Assessment

There are several limitations to utilizing DEA for contact stress computations in an articular joint. DEA is only able to provide information on contact stress distributions and the associated reaction forces; it cannot predict internal tissue stresses or strains. This is a limitation since cartilage shear stresses are known to contribute to the development of osteoarthritis. However, in this study, contact stress distributions between cartilage surfaces were evaluated at static loading positions simulating walking gait, making the effects of shear negligible from a modeling standpoint. DEA assumes the contacting surfaces to consist of an isotropic, linearly elastic material. Modeling complex material properties is highly difficult in DEA and problematic for articular cartilage in particular, which exhibits a poroelastic mechanical behavior that is dependent on loading rate. However, in this study, the linearly elastic material property definition of cartilage was thought to be acceptable due to the relatively high cartilage loading rate that occurs

during walking gait [110] that limits fluid exudation. The contact stress results obtained using this DEA methodology have been validated against FEA [79] and experimental measurements in cadaver hips [77], illustrating that DEA produces realistic contact stress distributions. The investigation of cartilage thickness and cartilage modulus further illustrated that the specific modeling parameters used in the DEA validation produce contact stress distributions that correlate well with physical Tekscan measurements.

Despite the relatively simple mechanical data that can be obtained using DEA, the DEA methodology can be very advantageous. The computational time of DEA is greatly reduced from that of FEA due to the absence of a complex mesh generation/refinement procedure and a reduced simulation complexity that eliminates the need to solve complex differential equations. The numerical stability of DEA is useful for assessing articulation between incongruent joints, such as dysplastic deformities, that may have difficulty converging in FEA. The reduced developmental complexity and computational time of DEA permits the evaluation of much larger cohorts than most FEA studies [73, 74], potentially improving the statistical power of correlative studies.

When investigating a hip dysplasia cohort, numerous anatomic variations (i.e. lateral coverage deficiency, acetabular version, femoral deformities) and patient-specific factors influence the computed contact stress, making it difficult to accurately assess these patient cohorts with the limited sample sizes that can realistically be investigated using FEA. Much larger sample sizes are needed to accurately and thoroughly investigate how anatomic and demographic variations affect computed contact stress and its correlation with patient-reported outcomes. Such evaluations would be incredibly difficult if utilizing FEA for all subjects due to the time-intensive, computationally

difficult nature of FEA. In cases were continuum information is necessary, DEA could potentially be used as a screening tool for FEA, where interesting patient cases with non-ideal contact stress changes computed with DEA could be selected for further investigated using FEA. Dysplastic hips indicated to have developed osteoarthritis following PAO could also be studied with FEA to understand the potential effects of shear stresses on the articular cartilage.

4.2 Influence of Gait Loading Pattern on Contact Stress and Patient Outcomes

As detailed above (section 3.1 Influence of Gait Loading Pattern on Calculated Contact Stress and Relationship with Patient-Reported Outcomes), loading the models with the dysplastic gait pattern resulted in calculation of pre-operative maximum contact stresses that were significantly greater than those that were calculated when loading the models with the normal or the arthritic gait pattern. The maximum contact stress values calculated using our DEA methodology were similar in magnitude to those previously reported in DEA and FEA studies of PAO patients [73, 96, 111] and contact stress values from Tekscan sensors in cadaver hips [77], verifying that our methods produce realistic representations of the contact mechanics of the hip joint.

This dysplastic gait pattern in the DEA models of our dysplasia patients prior to PAO resulted in calculation of greatly increased contact stress. This was particularly interesting as this would indicate that the joint stabilization techniques used by hip dysplasia patients during gait may be producing damaging contact stress and contributing to their clinical symptoms. Prolonged exposure to high levels of contact stress can increase the rate of cartilage loss and progression of joint degeneration, thereby resulting

in earlier development of osteoarthritis. With the majority of PAO patients being active individuals in their adolescent to young adult years, development of osteoarthritis at such an early age would have significant negative impacts on their quality of life.

DEA models of post-PAO hips that were loaded with the dysplastic gait pattern had an average decrease in maximum contact stress relative to the preoperative values. While this average decrease was modest, it was significantly different from increases in calculated stresses that occurred when models were loaded with the arthritic or the normal gait patterns. This decrease in maximum contact stress observed when implementing the dysplastic gait loading coincides with the clinical assumption that acetabular reorientation improves the biomechanics of the joint. Furthermore, the utilization of the dysplastic gait pattern improved the correlation of contact stress with the radiographic measures of lateral center edge angle, Tönnis angle, and extrusion index. When loading with the dysplastic gait pattern, more PAO models were found to have decreased stress, decreased pain, increased function, and increased quality-of-life, furthering agreement with clinical findings.

The patients modeled in this work were not assessed with pre- and post-operative gait analysis, meaning that there is no way to verify that the gait loading parameters used in this study were realistic for these patients. Thus, the best option currently available for these patients is to utilize an average gait pattern. This led us to investigate the effects of loading our models with various average gait patterns from relevant patient populations. This work illustrated that the contact stress distributions produced with DEA are highly dependent on the loading parameters used. Additionally, the clinical assumption is that both joint mechanics and patient-reported outcomes improve after PAO, which was only

seen when the models were subjected to dysplastic loading. Therefore, it is critical that dysplastic gait is utilized to load DEA models of this deformed cohort to capture accurate mechanistic outcomes.

While more PAO cases were found to have the combination of decreased contact stress and improved clinical outcomes when the dysplastic gait cycle was implemented in the DEA models, none of the gait loading patterns produced contact stress calculations that showed a strong correlation with patient-reported outcome measures. The lack of strong correlations could be the result of a relatively small sample size of thirty pre- and post-operative cases as well as anatomic and demographical variability. The 30 hip models used in this gait investigation were the first 30 hips of our cohort and thus were not controlled for acetabular deformity type (i.e. lateral coverage deficiencies, acetabular version, etc.), presence of femoral deformity, or patient age and weight. In particular, femoral deformity and patient age and weight were shown in this work to have significant effects on the DEA-computed contact stress (Results sections 3.3 and 3.4). Furthermore, PAO correction of a lateral coverage deformity may be a more straightforward surgery since the deformity is easily visible on a pre-operative scan. With simple radiographs, it is difficult to visualize acetabular version and femoral deformities because they are out-of-plane of the imaging orientation. If version and femoral deformities are not identified during pre-operative planning, they may not be accurately addressed during PAO, resulting in less predictable outcomes.

Only 18 of the 30 patients in this study had pre- and post-operative SF-36 scores, and 12 patients had pre- and post-operative WOMAC scores. The lack of SF-36 and WOMAC data for all patients makes it difficult to accurately assess their correlations to

contact stress measurements. All 30 patients had pre- and post-operative VAS pain scores, but this is a very subjective measure. For example, the older female PAO patients in our cohort may have experienced childbirth, which could greatly increase their pain tolerance. Adolescent PAO patients are still be experiencing growing pains and may not be used to dealing with chronic hip pain. Thus, a VAS score of 10 (i.e. the highest pain possible) for an adolescent patient may be very different than that for a patient who previously gave birth. Bilateral PAO patients may have difficulty distinguishing pain between their hip sides, resulting in a VAS score that does not accurately portray their pain for the hip undergoing surgery. Better correlations may be found with patient-reported outcome scores after longer-term followup or with outcome scores not investigated in this work (e.g. Harris Hip Score, etc.).

Contact stress measurement has the potential to provide valuable clinical information. Contact stress provides a quantitative measure of the whole joint environment rather than a one-dimensional measure from imaging that can vary in accuracy. It can assist in predicting the contact stress distribution in a patient pre-operatively and determining if an orthopaedic surgeon has achieved the biomechanically optimum reorientation to reduce contact stresses and prevent cartilage loss and joint degeneration. Furthermore, DEA-computed contact stress can provide objective mechanical information to the orthopaedic surgeon that subjective patient-reported outcome scores cannot. Therefore, further investigation using this DEA methodology is needed.

There are several limitations to this investigation of gait cycle. The gait data used to load the DEA models were averages from multiple subjects included in each of the

studies. Such measurements are intended to be representative of a given patient population but do not necessarily illustrate how any given PAO patient would walk. Given that no gait data was collected for the thirty PAO subjects modeled in this study, no subject-specific gait patterns exist to be applied to their DEA models. While it is a very gross approximation, an average gait pattern that is representative of gait for individuals with these hip deformities is the best available option for loading DEA models. Prospective studies may include the collection of motion capture data prior to PAO to more accurately assess the patient-specific hip joint biomechanics in these patients.

A similar assumption had to be made when assessing the post-operative changes in contact stress. In this work, the post-operative DEA models were loaded with the same gait pattern as the corresponding pre-operative models, which assumes no change in gait pattern following acetabular reorientation. It is probable that an improved joint alignment would permit the individual to walk in a more efficient manner, and previous findings have illustrated that some, but not all, gait characteristics normalize following PAO [43, 112-114]. The follow-up time for our patients was relatively short, limiting the likelihood that gait adaptations for the newly realigned joints would have occurred. Since post-operative gait does not appear to completely return to normal, and these patients would not have had sufficient time for gait retraining, applying normal gait loading did not seem realistic. Therefore, no change in gait loading was made for the pre-operative models. Collection of motion capture data after PAO would ensure realistic gait loading is applied to accurately assess changes in hip joint biomechanics in these patients.

Finally, the primary outcome measure used in this study was maximum contact stress, which was the largest magnitude contact stress anywhere within the acetabular cartilage. This approach omits the location of that stress. However, different applied loading patterns and the change in acetabular orientation after PAO both alter the DEA-computed contact stress distributions. The findings that maximum contact stress may be similar regardless of gait pattern or acetabular alignment, do not capture the finding that the location of this stress may have changed (Figure 48). Ongoing investigations using DEA assessment of contact stress in the hip as related to PAO must incorporate an evaluation of spatial changes in the contact stress to fully describe the change in joint mechanics associated with this operation.

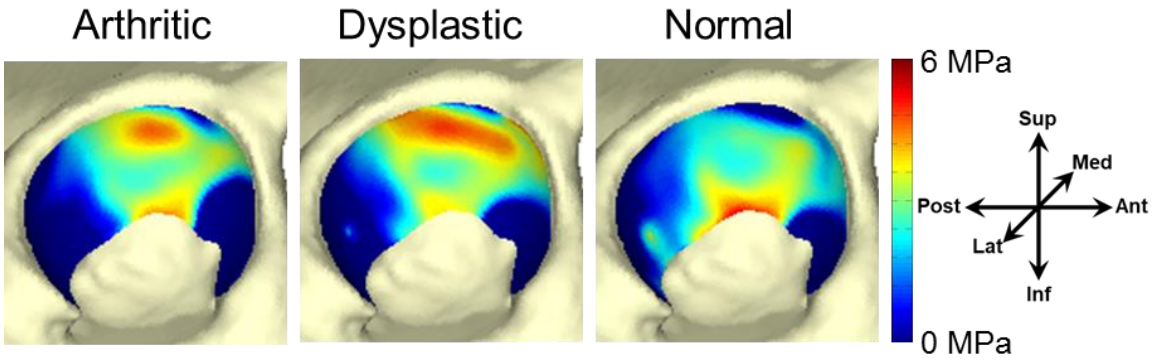

Figure 48. The magnitude of the maximum contact stress is similar regardless of the gait pattern used to load the DEA model. However, the spatial location of the maximum contact stress is very different. Incorporating a spatial measure in future studies is crucial in fully understanding post-operative changes in contact stress distributions.

Despite these limitations, implementation of the dysplastic gait cycle to load DEA models of dysplastic hips produced a contact stress assessment that concurred with clinical expectation. When loaded with the dysplastic gait, more patient cases illustrated improved biomechanics and clinical measures than when loaded with arthritic and normal

gaits. Therefore, the mechanical environment of the dysplastic hip joint is most realistically represented with the implementation of the dysplastic gait cycle in the DEA methodology to assess contact stress. While utilizing an average gait cycle measured in dysplastic patients should be representative of gait in the dysplastic population, it has not been formally validated and does not necessarily illustrate patient-specific gait. However, it is the best available option for loading our DEA models. This methodology will be utilized in further assessment of the larger PAO cohort and in prospective PAO studies to biomechanically optimize acetabular reorientation.

4.3 Factors Influencing Contact Stress Evaluation

In addition to the effects that the applied gait loading has on DEA-calculated contact stress, several patient factors that may also be influencing the contact stress distribution were considered. The shallow nature of the dysplastic acetabulum results in a lateralized acetabular center of rotation, which has been shown to be medialized following PAO. In this work, changes in pre- to post-operative center of rotation of the acetabulum were investigated and correlated with changes in the maximum contact stress (Results section 3.2). The results showed that the acetabular center of rotation in dysplasia patients was medialized by an average of 4 mm following PAO, which correlated with reduced post-operative contact stress. This 4-mm medialization of the center of rotation is similar to previous findings [115], which verifies our results. Interestingly, even though the acetabular center of rotation was significantly anteriorized post-operatively, this anteriorization did not have a meaningful effect on the post-operative maximum contact stress when compared to the effect of medialization. The

correlation between medialization of the acetabular center of rotation and post-operative contact stress indicates that a more medialized center of rotation was associated with a greater reduction in mechanical stress on the joint. These results confirm the clinical expectation that it is the improvement in lateral femoral coverage which reduces the contact stress on the hip joint, despite potential multiplanar changes in acetabular orientation.

While the goal of PAO is to reduce pain and contact stress on the hip joint, some of our models demonstrated increased contact stress after PAO, which could arise from overcorrection, out-of-plane correction, or femoral deformity. All patients had improved radiographic measures for dysplasia, indicating that another factor besides inadequate reorientation or overcorrection may be contributing to the increased contact stress. Further investigation of our patient cases demonstrated significantly greater α-angles and a greater presence of cam deformities in hips with increased post-operative contact stress. Interestingly, the greatest variation in post-operative change in contact stress occurred in cases with an α-angle range of 40°-50°, indicative of borderline cam deformity. This illustrates that the acetabular reorientation in these patients may alter the degree of bony interaction with smaller cams, potentially resulting in impingement. Therefore, it is possible that unaddressed femoral deformities may be impinging on the acetabulum. However, it is unlikely that femoral impingement is the sole factor in increases in contact stress in our models. Our DEA methodology does not model the acetabular labrum, which is the likely location for impingement stresses. Yet, depending on the location of the extra-articular femoral deformity, it is possible that a cam deformity could contribute to the intra-articular cartilage stresses computed in our DEA models. Therefore, pre-

operative planning should include femoral assessment to minimize potentially damaging impingement that could be worsened after PAO.

In addition to evaluating the presence of femoral deformities, relationships between contact stress and patient demographics were investigated. Previous PAO studies that have investigated contact mechanics [73, 96, 111] included subjects of a wide age range. It is unclear how the age of the patient at the time of operation on the biomechanical and clinical outcomes. In this work, the older dysplasia patients were found to have significantly less spherical acetabula and higher pre-operative contact stress, which may indicate that long-term exposure of these patients' hip joints to damaging loads produced locations of high contact stress that have resulted in bony remodeling. A significant interaction between patient weight and acetabular sphericity was found when correlating these factors with patient age and pre-operative contact stress. This interaction indicates that patient age affects both patient weight and acetabular sphericity, and this interplay affects the magnitude of the contact stress. Therefore, it is probable that the age (i.e. duration of exposure to damaging loading) of a dysplasia patient affects the patient weight (i.e. joint loading magnitude) and the acetabular geometry, and both factors contribute to the resulting hip joint mechanics. Orthopaedic surgeons should consider how a patient's age and weight may have affected the shape of the acetabulum in their pre-operative planning to ensure that the planned acetabular reorientation reduces the contact stress on the hip joint.

PAO operations aim to return a deformed joint to functional normalcy. While the above studies (Results sections 3.1-3.4) investigated changes in contact stress due to modeling parameters and patient factors, no comparison of post-operative contact stress

distributions with contact stress distributions in normal hips was made. In this modeling work (Results section 3.5), the magnitude of contact stress for normal hips was very similar to previous findings [74], further supporting the accuracy of our modeling methods. DEA models for normal hips had significantly lower maximum contact stress and greater average contact area than those for dysplastic hips. Dysplastic hips also demonstrated an increased maximum contact stress near toe-off compared to the normal hips. Perhaps most important was that following PAO, dysplastic patients did not have "normal" joint mechanics. Following PAO, the increase in maximum contact stress near toe-off was resolved, and the timing of maximum contact stress during stance phase of gait was normalized. However, the magnitude of the maximum contact stress in post-operative dysplastic hips did not return to normal levels. The higher maximum contact stress in post-operative dysplastic hips likely still produces hip pain, which would explain the maintained relief mechanism of reduced flexion in post-operative gait. Post-operative dysplastic hips had greater contact area than pre-operative hips, but the contact area was still significantly less than that in a normal hip, indicating that acetabular reorientation improves femoral coverage but not to normal levels. The notable differences between normal and post-operative dysplastic hips indicate that PAO improves joint mechanics but does not return a dysplastic hip to a "normal" mechanical state.

The results of these focused patient-based studies provide valuable information regarding the interpretation of contact stress assessments in the dysplastic hip joint. These studies suggest that there are important differences between specific PAO patients that should be considered prior to assessing a cohort. Patient demographics, acetabular and femoral geometry, and osteoarthritic changes all affect the observed contact stress

distributions in the hip joint. Hence, patients should be categorized based on these influential factors in addition to their clinical outcomes and surgical success before attempting to interpret meaningful relationships between biomechanical and clinical measures.

4.4 Future Directions

Future directions for this work include assessment of the entire 139 PAO patient cohort to develop meaningful relationships between contact measures and clinical outcomes. While the cohort of thirty patients that was heavily used in this work is larger than many previous studies, it is not large enough to evaluate subgroups of patients based on anatomic and demographical information. Our full cohort of 139 individual cases will encompass a variety of deformity types and severities, and the factors described in this thesis can be utilized to characterize these subgroups and produce meaningful correlations.

4.5 Conclusions

This thesis has described a set of studies performed to better understand the use of a discrete element analysis methodology for evaluating the joint contact stresses in patients with dysplastic hip joints. The methods focused on systematically assessing how the gait pattern used to load the DEA models and how other anatomic and demographic factors affect the computed contact stress and the correlation of those mechanical data to patient-reported outcomes. Implementing a dysplastic gait pattern to load DEA models

significantly increased the calculated pre-operative maximum contact stress, indicating that dysplastic gait may be producing damaging contact stress in an attempt to maintain hip joint stabilization. More PAO cases were found to have decreased stress, decreased pain, increased function, and increased quality-of-life post-operatively when contact stress was computed utilizing dysplastic loading in the DEA models. These results illustrate that it is crucial to use dysplastic gait when loading models in this cohort to obtain accurate contact stress distributions. It was also demonstrated that patient demographics and acetabular and femoral geometry all affect the contact stress distributions in the hip joint and should be carefully considered when analyzing a dysplastic cohort. These studies have improved the ability to interpret the joint mechanics in computational models of dysplastic hip joints and understand the relationships between these biomechanical data and patient-reported outcome measures.

REFERENCES

1. Levangie, P.K. and C.C. Norkin, *Joint structure and function: a comprehensive analysis (4th ed.)*. 2005, Philadelphia: F.A. Davis Company.
2. Konrath, G.A., et al., *The role of the acetabular labrum and the transverse acetabular ligament in load transmission in the hip.* J Bone Joint Surg Am, 1998. **80**(12): p. 1781-8.
3. Seldes, R.M., et al., *Anatomy, histologic features, and vascularity of the adult acetabular labrum.* Clin Orthop Relat Res, 2001. **382**: p. 232-40.
4. Ferguson, S.J., et al., *An in vitro investigation of the acetabular labral seal in hip joint mechanics.* J Biomech, 2003. **36**(2): p. 171-8.
5. Dwyer, M.K., et al., *The acetabular labrum regulates fluid circulation of the hip joint during functional activities.* Am J Sports Med, 2014. **42**(4): p. 812-9.
6. Ferguson, S.J., et al., *The influence of the acetabular labrum on hip joint cartilage consolidation: a poroelastic finite element model.* J Biomech, 2000. **33**(8): p. 953-60.
7. The General Hospital Corporation. *Hip arthritis treatment: overview*. 2017.
8. Nashville Hip Institute. *Labrum & articular cartilage injury*. 2017.
9. Polkowski, G.G. and J.C. Clohisy, *Hip biomechanics.* Sports Med Arthrosc, 2010. **18**(2): p. 56-62.
10. Correa, T.A., et al., *Contributions of individual muscles to hip joint contact force in normal walking.* J Biomech, 2010. **43**(8): p. 1618-22.
11. Bergmann, G., et al., *Hip contact forces and gait patterns from routine activities.* J Biomech, 2001. **34**(7): p. 859-71.
12. Bergmann, G., F. Graichen, and A. Rohlmann, *Hip joint contact forces during stumbling.* Langenbecks Arch Surg, 2004. **389**(1): p. 53-9.
13. Gu, D.Y., et al., *The shape of the acetabular cartilage surface and its role in hip joint contact stress.* Conf Proc IEEE Eng Med Biol Soc, 2010. **2010**: p. 3934-7.
14. Daniel, M., A. Iglic, and V. Kralj-Iglic, *The shape of acetabular cartilage optimizes hip contact stress distribution.* J Anat, 2005. **207**(1): p. 85-91.
15. Bullough, P., J. Goodfellow, and J. O'Conner, *The relationship between degenerative changes and load-bearing in the human hip.* J Bone Joint Surg Br, 1973. **55**(4): p. 746-58.
16. Brinckmann, P., W. Frobin, and E. Hierholzer, *Stress on the articular surface of the hip joint in healthy adults and persons with idiopathic osteoarthrosis of the hip joint.* J Biomech, 1981. **14**(3): p. 149-56.
17. Aronsson, D.D., et al., *Developmental dysplasia of the hip.* Pediatrics, 1994. **94**(2): p. 201-8.
18. Storer, S.K. and D.L. Skaggs, *Developmental dysplasia of the hip.* Am Fam Physician, 2006. **74**(8): p. 1310-6.
19. Dezateux, C. and K. Rosendahl, *Developmental dysplasia of the hip.* The Lancet, 2007. **369**(9572): p. 1541-1552.
20. Moraleda, L., et al., *Dysplasia in the development of the hip.* Rev Esp Cir Ortop Traumatol, 2013. **57**(1): p. 67-77.
21. Maquet, P., *Biomechanics of hip dysplasia.* Acta Orthop Belgica, 1999. **65**(3).

22. Hipp, J.A., et al., *Planning acetabular redirection osteotomies based on joint contact pressures.* Clin Orthop Relat Res, 1999. **364**(134-43).
23. Tsumura, H., H. Miura, and Y. Iwamoto, *Three-dimensional pressure distribution of the human hip joint--comparison between normal hips and dysplastic hips.* Fukuoka Igaku Zasshi, 1998. **89**(4): p. 109-18.
24. Parvizi, J., et al., *Arthroscopy for Labral Tears in Patients with Developmental Dysplasia of the Hip: A Cautionary Note*. The Journal of Arthroplasty, 2009. **24**(6): p. 110-113.
25. Noguchi, Y., et al., *Cartilage and labrum degeneration in the dysplastic hip generally originates in the anterosuperior weight-bearing area: an arthroscopic observation.* Arthroscopy, 1999. **15**(5): p. 496-506.
26. Mavcic, B., et al., *Cumulative hip contact stress predicts osteoarthritis in DDH.* Clin Orthop Relat Res, 2008. **466**(4): p. 884-91.
27. Clohisy, J.C., et al., *Radiographic structural abnormalities associated with premature, natural hip-joint failure.* J Bone Joint Surg Am, 2011. **93**(Suppl 2): p. 3-9.
28. Mostert, A.K., N.J.A. Tulp, and R.M. Castelein, *Results of Pavlik harness treatment for neonatal hip dislocation as related to Graf's sonographic classification.* J Ped Orthop, 2000. **20**(3): p. 306-10.
29. Böhm, P. and A. Brzuske, *Salter innominate osteotomy for the treatment of developmental dysplasia of the hip in children: results of seventy-three consecutive osteotomies after twenty-six to thirty-five years of follow-up.* J Bone Joint Surg Am, 2002. **84**(2): p. 178-86.
30. Hadley, N.A., T.D. Brown, and S.L. Weinstein, *The effects of contact pressure elevations and aseptic necrosis on the long-term outcome of congenital hip dislocation.* J Orthop Res, 1990. **8**(4): p. 504-13.
31. Gosvig, K.K., et al., *Prevalence of malformations of the hip joint and their relationship to sex, groin pain, and risk of osteoarthritis: a population-based survey.* J Bone Joint Surg Am, 2010. **92**(5): p. 1162-9.
32. Jacobsen, S. and S. Sonne-Holm, *Hip dysplasia: a significant risk factor for the development of hip osteoarthritis. A cross-sectional survey.* Rheumatology (Oxford), 2005. **44**(2): p. 211-8.
33. Wiberg, G., *Shelf operation in congenital dysplasia of the acetabulum and in subluxation and dislocation of the hip.* J Bone Joint Surg Am, 1953. **35**(1): p. 65-80.
34. Fredensborg, N., *The CE Angle of Normal Hips.* Acta Orthopaedica Scandinavica, 2009. **47**(4): p. 403-405.
35. Werner, C.M., et al., *Normal values of Wiberg's lateral center-edge angle and Lequesne's acetabular index--a coxometric update.* Skeletal Radiol, 2012. **41**(10): p. 1273-8.
36. Lequesne, M. and S. de Seze, *Le faux profil du bassin: nouvelle incidence radiographique pour l'étude de la hanche. Son utilitè dans les dysplasies et les differentes coxopathies.* . Rev Rhum Mal Osteoartic, 1961. **28**: p. 643-52.
37. Tönnis, D. and A. Heinecke, *Acetabular and femoral anteversion: relationship with osteoarthritis of the hip.* J Bone Joint Surg Am, 1999. **81**: p. 1747-70.

38. Murphy, S.B., R. Ganz, and M.E. Müller, *The prognosis in untreated dysplasia of the hip. A study of radiographic factors that predict the outcome.* J Bone Joint Surg Am, 1995. **77**(7): p. 985-9.
39. Reynolds, D., J. Lucas, and K. Klaue, *Retroversion of the acetabulum: a cause of hip pain.* J Bone Joint Surg Br, 1999. **81**(2): p. 281-8.
40. Romanò, C.L., et al., *Analysis of the gait of adults who had residua of congenital dysplasia of the hip.* J Bone Joint Surg Am, 1996. **78**(10): p. 1468-79.
41. Endo, H., et al., *Three-dimensional gait analysis of adults with hip dysplasia after rotational acetabular osteotomy.* J Orthop Sci, 2003. **8**(6): p. 762-71.
42. Pedersen, E.N., et al., *Walking pattern in adults with congenital hip dysplasia: 14 women examined by inverse dynamics.* Acta Orthop Scand, 2004. **75**(1): p. 2-9.
43. Pedersen, E.N., et al., *Walking pattern in 9 women with hip dysplasia 18 months after periacetabular osteotomy.* Acta Orthop, 2006. **77**(2): p. 203-8.
44. Jacobsen, J.S., et al., *Changes in walking and running in patients with hip dysplasia.* Acta Orthop, 2013. **84**(3): p. 265-70.
45. Skalshoi, O., et al., *Walking patterns and hip contact forces in patients with hip dysplasia.* Gait Posture, 2015. **42**(4): p. 529-33.
46. Harris, M.D., et al., *Higher medially-directed joint reaction forces are a characteristic of dysplastic hips: A comparative study using subject-specific musculoskeletal models.* J Biomech, 2017. **54**: p. 80-87.
47. Chegini, S., M. Beck, and S.J. Ferguson, *The effects of impingement and dysplasia on stress distributions in the hip joint during sitting and walking: a finite element analysis.* J Orthop Res, 2009. **27**(2): p. 195-201.
48. Anderson, D.D., et al., *Is elevated contact stress predictive of post-traumatic osteoarthritis for imprecisely reduced tibial plafond fractures?* J Orthop Res, 2011. **29**(1): p. 33-9.
49. Segal, N.A., et al., *Baseline articular contact stress levels predict incident symptomatic knee osteoarthritis development in the MOST cohort.* J Orthop Res, 2009. **27**(12): p. 1562-8.
50. Havelin, L.I., et al., *The Norwegian arthroplasty register: a survey of 17,444 hip replacements 1987-1990.* Acta Orthop Scand, 1993. **64**: p. 245-51.
51. Schulte, K.R., et al., *The outcome of Charnley total hip arthroplasty with cement after a minimum twenty-year follow-up. The results of one surgeon.* J Bone Joint Surg Am, 1993. **75**(7): p. 961-75.
52. Salter, R.B., *Innominate osteotomy in the treatment of congenital dislocation and subluxation of the hip.* J Bone Joint Surg Br, 1961. **43B**(3): p. 518-39.
53. Sutherland, D.H. and R. Greenfield, *Double innominate osteotomy.* J Bone Joint Surg Am, 1977. **59**(8): p. 1082-91.
54. Le Coeur, P., *Correction des défauts d'orientation de l'articulation coxo-fémorale par ostéotomie de l'isthme iliaque.* Rev Chir Orthop, 1965. **51**: p. 211-2.
55. Hopf, A., *Hip acetabular displacement by double pelvic osteotomy in the treatment of hip joint dysplasia and subluxation in young people and adults [German].* Z Orthop Ihre Grenzgeb, 1966. **101**: p. 559-86.
56. Steel, H.H., *Triple osteotomy of the innominate bone.* J Bone Joint Surg Am, 1973. **55**(2): p. 343-50.

57. Tönnis, D., *Eine neue Form der Hüftpfannenschwenkung durch Dreifachosteotomie zur Ermöglichung späterer Hüftprothesenversorgung.* Orthoppädische Praxis, 1979. **15**: p. 1003.
58. Carlioz, H., N. Khouri, and P. Hulin, *Triple juxtacotyloud osteotomy [French].* Rev Chir Orthop, 1982. **68**(7): p. 497-501.
59. Ganz, R., et al., *A new periacetabular osteotomy for the treatment of hip dysplasias. Technique and preliminary results.* Clin Orthop Relat Res, 1988. **232**: p. 26-36.
60. Leitz, G. and R. Reck, *Necessarily disappointing results after triple osteotomy in the dysplastic hip joint.* Arch Orthop Trauma Surg, 1979. **95**(4): p. 271-3.
61. Salter, R.B. and J. Dubos, *The first fifteen years' personal experience with innominate osteotomy in the treatment of congenital dislocation and subluxation of the hip.* Clin Orthop Relat Res, 1974. **98**: p. 72-103.
62. Steppacher, S.D., et al., *Mean 20-year followup of Bernese periacetabular osteotomy.* Clin Orthop Relat Res, 2008. **466**(7): p. 1633-44.
63. Haidar, R.K., et al., *Simultaneous open reduction and salter innominate osteotomy for developmental dysplasia of the hip.* J Bone Joint Surg Br, 1996. **78**(3): p. 471-6.
64. Trumble, S.J., K.A. Mayo, and J.W. Mast, *The periacetabular osteotomy. Minimum 2 year followup in more than 100 hips.* Clin Orthop Relat Res, 1999. **363**: p. 54-63.
65. Mechlenburg, I., et al., *Changes in load-bearing area after Ganz periacetabular osteotomy evaluated by multislice CT scanning and stereology.* Acta Orthop Scand, 2004. **75**(2): p. 147-53.
66. Iglic, A., et al., *Effect of the periacetabular osteotomy on the stress on the human hip joint articular surface.* IEEE Trans Rehab Eng, 1993. **1**(4): p. 207-12.
67. Maeyama, A., et al., *Periacetabular osteotomy reduces the dynamic instability of dysplastic hips.* J Bone Joint Surg Br, 2009. **91**(11): p. 1438-42.
68. Millis, M.B., et al., *Periacetabular osteotomy for acetabular dysplasia in patients older than 40 years: a preliminary study.* Clin Orthop Relat Res, 2009. **467**(9): p. 2228-34.
69. Huiskes, R. and E.Y. Chao, *A survey of finite element analysis in orthopedic biomechanics: the first decade.* J Biomech, 1983. **16**(6): p. 385-409.
70. Anderson, A.E., et al., *Effects of idealized joint geometry on finite element predictions of cartilage contact stresses in the hip.* J Biomech, 2010. **43**(7): p. 1351-7.
71. Grosland, N.M., et al., *IA-FEMesh: an open-source, interactive, multiblock approach to anatomic finite element model development.* Comput Methods Programs Biomed, 2009. **94**(1): p. 96-107.
72. Abraham, C.L., et al., *A new discrete element analysis method for predicting hip joint contact stresses.* J Biomech, 2013. **46**(6): p. 1121-7.
73. Zou, Z., et al., *Optimization of the position of the acetabulum in a ganz periacetabular osteotomy by finite element analysis.* J Orthop Res, 2013. **31**(3): p. 472-9.
74. Harris, M.D., et al., *Finite element prediction of cartilage contact stresses in normal human hips.* J Orthop Res, 2012. **30**(7): p. 1133-9.

75. Schuind, F., et al., *Force and pressure transmission through the normal wrist. A theoretical two-dimensional study in the posteroanterior plane.* J Biomech, 1995. **28**(5): p. 587-601.
76. An, K.N., et al., *Pressure distribution on articular surfaces: Application to joint stability evaluation.* J Biomech, 1990. **23**(10): p. 1013-20.
77. Townsend, K.C., et al., *Discrete element analysis is a valid method for computing joint contact stresses in the hip before and after acetabular fracture.* J Biomech, (Accepted 11/13/17).
78. Li, G., M. Sakamoto, and E.Y. Chao, *A comparison of different methods in predicting static pressure distribution in articulating joints.* J Biomech, 1997. **30**(6): p. 635-8.
79. Kern, A.M. and D.D. Anderson, *Expedited patient-specific assessment of contact stress exposure in the ankle joint following definitive articular fracture reduction.* J Biomech, 2015. **48**(12): p. 3427-32.
80. Anderson, D.D., et al., *Implementation of discrete element analysis for subject-specific, population-wide investigations of habitual contact stress exposure.* J Appl Biomech, 2010. **26**(2): p. 215-23.
81. Chao, E.Y., et al., *Discrete element analysis in musculoskeletal biomechanics.* Mol Cell Biomech, 2010. **7**(3): p. 175-92.
82. Rudert, M.J., et al., *A new sensor for measurement of dynamic contact stress in the hip.* J Biomech Eng, 2014. **136**(3): p. 035001.
83. Kern, A.M., *Large population evaluation of contact stress exposure in articular joints for prediction of osteoarthritis onset and progression.* MS (Master of Science) thesis, University of Iowa, 2011.
84. Shivanna, K.H., et al., *Diarthrodial joint contact models: finite element model development of the human hip.* Engineering with Computers, 2007. **24**(2): p. 155-163.
85. Townsend, K.C., *Validation and applications of discrete element analysis in the hip joint.* MS (Master of Science) thesis, University of Iowa, 2015.
86. Thomas, T.P., et al., *ASB Clinical Biomechanics Award Paper 2010 Virtual pre-operative reconstruction planning for comminuted articular fractures.* Clin Biomech (Bristol, Avon), 2011. **26**(2): p. 109-15.
87. Eckstein, F., et al., *Quantitative analysis of incongruity, contact areas and cartilage thickness in the human hip joint.* Acta Anat (Basel), 1997. **158**(3): p. 192-204.
88. Shepherd, D.E.T. and B.B. Seedhom, *Thickness of human articular cartilage in joints of the lower limb.* Ann Rheum Dis, 1999. **58**(1): p. 27-34.
89. Li, W., et al., *Human hip joint cartilage: MRI quantitative thickness and volume measurements discriminating acetabulum and femoral head.* IEEE Trans Biomed Eng, 2008. **55**(12): p. 2731-40.
90. Mechlenburg, I., et al., *Cartilage thickness in the hip measured by MRI and stereology before and after periacetabular osteotomy.* Clin Orthop Relat Res, 2010. **468**(7): p. 1884-90.
91. Shepherd, D.E.T. and B.B. Seedhom, *The 'instantaneous' compressive modulus of human articular cartilage in joints of the lower limb.* Rheumatology (Oxford), 1999. **38**(2): p. 124-32.

92. Hori, R.Y. and L.F. Mockros, *Indentation tests of human articular cartilage.* J Biomech, 1976. **9**: p. 259-268.
93. Yoshida, H., et al., *Three-dimensional dynamic hip contact area and pressure distribution during activities of daily living.* J Biomech, 2006. **39**(11): p. 1996-2004.
94. Phillips, A.T., et al., *Finite element modelling of the pelvis: inclusion of muscular and ligamentous boundary conditions.* Med Eng Phys, 2007. **29**(7): p. 739-48.
95. Anderson, A.E., et al., *Validation of finite element predictions of cartilage contact pressure in the human hip joint.* J Biomech Eng, 2008. **130**(5): p. 051008.
96. Abraham, C.L., et al., *Patient-specific chondrolabral contact mechanics in patients with acetabular dysplasia following treatment with peri-acetabular osteotomy.* Osteoarthritis Cartilage, 2017. **25**(5): p. 676-684.
97. Perron, M., et al., *Three-dimensional gait analysis in women with a total hip arthroplasty.* Clin Biomech, 2000. **15**(7): p. 504-15.
98. Mont, M.A., et al., *Gait analysis of patients with resurfacing hip arthroplasty compared with hip osteoarthritis and standard total hip arthroplasty.* J Arthroplasty, 2007. **22**(1): p. 100-8.
99. Kang, H.G. and J.B. Dingwell, *Separating the effects of age and walking speed on gait variability.* Gait Posture, 2008. **27**(4): p. 572-7.
100. Jordan, K., J.H. Challis, and K.M. Newell, *Walking speed influences on gait cycle variability.* Gait Posture, 2007. **26**(1): p. 128-34.
101. Delp, S.L., et al., *OpenSim: open-source software to create and analyze dynamic simulations of movement.* IEEE Trans Biomed Eng, 2007. **54**(11): p. 1940-50.
102. Cappozzo, A., et al., *Position and orientation in space of bones during movement: anatomic frame definition and determination.* Clin Biomech, 1995. **10**(4): p. 171-8.
103. Anderson, F.C. and M.G. Pandy, *Dynamic optimization of human walking.* J Biomech Eng, 2001. **123**(5): p. 381-90.
104. Clohisy, J.C., et al., *Medial translation of the hip joint center associated with the Bernese periacetabular osteotomy.* Iowa Orthop J, 2004. **24**: p. 43-48.
105. Pompe, B., et al., *Gradient of contact stress in normal and dysplastic human hips.* Medical Engineering & Physics, 2003. **25**(5): p. 379-385.
106. Nötzli, H.P., et al., *The contour of the femoral head-neck junction as a predictor for the risk of anterior impingement.* J Bone Joint Surg Br, 2002. **84**(4): p. 556-60.
107. Clohisy, J.C., et al., *Periacetabular osteotomy for the treatment of severe acetabular dysplasia.* J Bone Joint Surg Am, 2005. **87**(2): p. 254-9.
108. Mavcic, B., et al., *Mathematical estimation of stress distribution in normal and dysplastic human hips.* J Orthop Res, 2002. **20**(5): p. 1025-30.
109. Genda, E., et al., *A computer simulation study of normal and abnormal hip joint contact pressure.* Arch Orthop Trauma Surg, 1995. **114**: p. 202-206.
110. Johnson, G.R. and V.W. Dowson, *The elastic behaviour of articular cartilage under a sinusoidally varying compressive stress.* Int J Mech Sci, 1977. **19**(5): p. 301-8.
111. Armiger, R.S., et al., *Three-dimensional mechanical evaluation of joint contact pressure in 12 periacetabular osteotomy patients with 10-year follow-up.* Acta Orthop, 2009. **80**(2): p. 155-61.

112. Gahramanov, A., et al., *Functional results in periacetabular osteotomy: is it possible to obtain a normal gait after the surgery?* Hip Int, 2017. **27**(5): p. 449-454.
113. Sucato, D.J., et al., *Gait, hip strength, and functional outcomes after a Ganz periacetabular osteotomy for adolescent hip dysplasia.* J Pediatr Orthop, 2010. **30**(4): p. 344-350.
114. Jacobsen, J.S., et al., *Joint kinematics and kinetics during walking and running in 32 patients with hip dysplasia 1 year after periacetabular osteotomy.* Acta Orthop, 2014. **85**(6): p. 592-9.
115. Trousdale, R.T., et al., *Magnetic resonance imaging pelvimetry before and after a periacetabular osteotomy.* J Bone Joint Surg Am, 2002. **84**(4): p. 552-56.